Neural architecture
underlying thirst regulation

Thesis by

Vineet Augustine

In Partial Fulfillment of the Requirements for

the degree of

Doctor of Philosophy

Caltech

CALIFORNIA INSTITUTE OF TECHNOLOGY

Pasadena, California

2019

(Defended 13th February 2019)

© 2019

Vineet Augustine
ORCID: 0000-0003-4431-1663

ACKNOWLEDGEMENTS

The successful completion of any project requires many hands, and this is a PhD. I have numerous people to thank without whose help this would not have been possible.

I would like to express my heartfelt gratitude to my advisor, Prof. Yuki Oka, for giving me the opportunity to work in his lab. His enthusiasm for science and the ability to work hard is infectious. More importantly, the freedom which he gave me allowed me to explore areas that in the end turned out to be very rewarding. Being his first graduate student, I got the invaluable opportunity to learn the ropes of setting up a new lab- buying equipment, setting up protocols, and most importantly hiring new members. This is one of the most valuable things I have learned and will forever be grateful. I could not have asked for a more productive graduate school experience.

I would like to thank my thesis committee members, Prof. Thanos Siapas, Prof. David Anderson, and Prof. Viviana Gradinaru, for their invaluable input that forced me to go back to the drawing board and think. They were always available to answer my queries and provide advice. I hope to stay in touch and keep on learning from them. A special word of thanks to my program chairs, Profs. Siapas and Pietro Perona, for having faith in me and being supportive throughout. Without their guidance and support, this thesis would not have seen the light of the day.

A special shoutout to Prof. K VijayRaghavan who is probably the busiest person in Indian science, but has always made time for me. His humility and passion is something I wish I could emulate. My high school teacher, Madam Sandipa Bhattacharjee, deserves a special mention. It was because of her help that I got through my graduate applications in the first place and has been a constant source of encouragement throughout.

I would like to thank other lab members: Sangjun, Brittany, Kutal, Haruka, Takako, Yuan, Bo, and Allan, for being co-travelers along this journey. Though small, the Oka Lab has a very conducive environment for carrying out science and it is largely because of the lab members.

Prof. Ralph Adolphs has been one of my greatest inspirations to pursue neuroscience. Since the time I was an undergraduate researcher in his lab till now, he has been there always. He is the reason why I got into Caltech. No words can express the gratitude I feel.

One of the greatest gifts that I have received from Caltech are a bunch of friends whom I cherish dearly and will maintain for a lifetime. My cohort: Janis, Ryan, Gabi, Juri, and Mason. We lived together, danced on pool-tables, had crazy parties, did homework, egged each other on, and are now a family. My brothers from different mothers, Sangjun and Dhruv, were my pillars of support at Caltech. To literally ensuring I would have food every day to doing experiments together, from disappearing from lab all together midweek for roadtrips to waiting for hours at the emergency room, we did it all. Their company is what I will miss the most. Thanks folks!

ABSTRACT

An important aspect of thirst is its quick quenching. When thirsty, you drink a glass of water for a few seconds; the water travels from the mouth to the stomach and you are satiated. The water has not yet been absorbed into the blood, so the brain needs to have mechanisms to signal stopping of drinking. It cannot simply depend on the body, as the body takes a good 15 - 30 minutes to even start absorption.

In this dissertation, I describe dynamic thirst circuits that integrate the homeostatic-instinctive requirement for fluids, the consequent drinking behavior, and reward processing to maintain internal water balance.

In Chapter 1, I show how neural populations in the lamina terminalis, a forebrain structure, form a hierarchical circuit architecture to regulate thirst. Among them, excitatory neurons in the median preoptic nucleus (MnPO) are essential for the integration of signals from the thirst-driving neurons of the subfornical organ (SFO). Thirst-driving neurons in the SFO receive temporarily distinct preabsorptive inhibition by drinking action and gastrointestinal osmolality sensing. A distinct inhibitory circuit, involving MnPO GABAergic neurons that express glucagon-like peptide 1 receptor (GLP1R), is activated immediately upon drinking and monosynaptically inhibits SFO thirst neurons. These responses are induced by the ingestion of fluids but not solids, and are time-locked to the onset and offset of drinking. Furthermore, loss-of-function manipulations of these neurons lead to a polydipsic, overdrinking phenotype. These neurons therefore facilitate rapid satiety of thirst by monitoring real-time fluid ingestion.

In Chapters 2 and 3, I talk about how thirst triggers a strong motivational state that drives animals toward drinking behavior. The consequent fluid intake provides both satiation and pleasure of drinking to animals. However, how these two factors are processed and represented by the brain remains poorly understood. Here I will use in vivo optical recording, genetics, and intragastric infusion approaches to dissect thirst satiation circuits and their contribution to reward signals. Thirst-driving neurons in the subfornical organ (SFO) receive multiple temporally-distinct satiation signals prior to the homeostatic

recovery: oropharyngeal stimuli induced by drinking action and gastrointestinal sensing of osmolality changes. In chapter 1, I have shown that drinking action is represented by inhibitory neurons in the median preoptic nucleus (MnPO). Here, I demonstrate that gut osmolality signals are mediated by specific GABAergic neurons in the SFO. These neurons were selectively activated by hypo-osmotic stimuli in the gut independent of drinking action. Optogenetic gain- and loss-of-function of this inhibitory population suppressed and increased water intake in thirsty animals, respectively. These results indicate that oropharyngeal- and gastrointestinal-driven satiation signals are transmitted to thirst neurons through different neural pathways. Furthermore, I investigated the contribution of thirst satiation signals to the reward circuit using a genetically-encoded ultrafast dopamine (DA) sensor. Interestingly, oral ingestion but not gut osmolality changes triggered robust DA release. Importantly, chemogenetic activation of thirst-quenching neurons did not induce DA release in water-deprived animals. Together, this dissected genetically-defined thirst satiation circuits, the activity of which are functionally separable from reward-related brain activity. Taken together, these finding provide answers to some longstanding questions in the neural control of fluid intake, and appetite in general.

PUBLISHED CONTENT AND CONTRIBUTIONS

Augustine, V. et al. (2018). "Hierarchical neural architecture underlying thirst regulation". In: Nature 555, pp. 204-209. doi: 10.1038/nature25488.

    V.A. conceived the research program, designed and carried out experiments, analyzed data and wrote the paper.

Augustine, V. et al. (2018). "Peripheral and Central Nutrient Sensing Underlying Appetite Regulation". In: *Trends in Neurosciences* 41, pp. 526–539. doi: 10.1016/j.tins.2018.05.003

    V.A. conceived the manuscript outline, designed and made figures, and wrote the review.

Augustine, V. et al. (2019). "Temporally-and spatially-distinct thirst satiation signals". In: *Neuron.* doi:10.1016/ j.neuron.2019.04.039

    V.A. conceived the research program, designed and carried out experiments, analyzed data and wrote the paper.

Lee, S., Augustine, V. et al. (2019). "Chemosensory modulation of neural circuits for sodium appetite". In: *Nature* 41, pp. 93–97. doi: 10.1038/s41586-019-1053-2.

    V.A. designed and carried out experiments and analyzed data

Ichiki, T., Augustine, V. et al. (2019). "Neural populations for maintaining body fluid balance". In: *Current Opinion of Neurobiology* 57, pp. 134–140. doi: 10.1016/j.conb.2019.01.014

    V.A. conceived the manuscript outline, designed figures, and wrote the review.

TABLE OF CONTENTS

LIST OF ILLUSTRATIONS AND/OR TABLES

Chapter 1

HIERARCHICAL NEURAL ARCHITECTURE UNDERLYING THIRST REGULATION

SUMMARY

Neural circuits for appetites are regulated by both homeostatic perturbations and ingestive behavior. However, the circuit organization that integrates these internal and external stimuli is unclear. Here we show in mice that excitatory neural populations in the lamina terminalis form a hierarchical circuit architecture to regulate thirst. Among them, nitric oxide synthase-expressing neurons in the median preoptic nucleus (MnPO) are essential for the integration of signals from the thirst-driving neurons of the subfornical organ (SFO). Conversely, a distinct inhibitory circuit, involving MnPO GABAergic neurons that express glucagon-like peptide 1 receptor (GLP1R), is activated immediately upon drinking and monosynaptically inhibits SFO thirst neurons. These responses are induced by the ingestion of fluids but not solids, and are time-locked to the onset and offset of drinking. Furthermore, loss-of-function manipulations of GLP1R-expressing MnPO neurons lead to a polydipsic, overdrinking phenotype. These neurons therefore facilitate rapid satiety of thirst by monitoring real-time fluid ingestion. Our study reveals dynamic thirst circuits that integrate the homeostatic-instinctive requirement for fluids and the consequent drinking behavior to maintain internal water balance.

INTRODUCTION

The precise regulation of water intake is critical to the maintenance of fluid homeostasis in the body. The initiation of drinking in animals is triggered by internal fluid imbalance, such as water depletion[1,2,3,4]. By contrast, drinking is terminated rapidly when animals have ingested a sufficient amount of water, which generally precedes the absorption of the ingested fluid[5,6,7,8,9,10]. To achieve such accurate fluid regulation, the brain needs to monitor both internal water balance and fluid ingestion on a real-time basis[11,12]. How the brain integrates homeostatic and behavioral inputs to coordinate drinking behavior is an unsolved question. As such, uncovering the neural circuits that process these regulatory signals is a critical step in understanding the neural logic of thirst regulation[13,14,15].

The lamina terminalis is the principal brain structure responsible for sensing and regulating internal water balance[3,5,16,17]. It contains three main nuclei: the SFO, the organum vasculosum lamina terminalis (OVLT), and the MnPO, all of which are anatomically interconnected[17,18,19,20,21]. The SFO and the OVLT in particular are two major osmosensory sites in the brain because they lack the normal blood–brain barrier. Recent studies have shown that specific neural populations in the lamina terminalis have a causal role in the regulation of drinking behavior. For instance, optogenetic and chemogenetic activation of excitatory SFO neurons co-expressing a transcription factor, ETV1, and nitric oxide synthase (SFO^{nNOS} neurons) drives immediate and robust drinking behavior[19,22,23]. Conversely, stimulation of inhibitory populations of lamina terminalis nuclei suppresses water intake[19,24]. Although these studies pinpointed the neural substrates that regulate thirst, the circuit organization that mediates drinking behavior remains poorly understood, owing to anatomical complexity and the lack of genetic handles.

Here we focused on the neural architecture of the lamina terminalis, and investigated genetically defined thirst circuits using neural manipulation, tracing, and *in vivo* optical recording approaches.

HIERARCHICAL CIRCUIT FOR THIRST

SFO[nNOS] neurons project their axons to other nuclei of the lamina terminalis (OVLT and MnPO)[10,25], as well as to the paraventricular and supraoptic nuclei, which contain vasopressin-expressing neurons[19]. These axonal projections and the downstream neurons define a framework of circuit elements that control thirst-related behaviours and hormonal outputs[26]. To identify genetically defined SFO[nNOS] downstream populations that regulate drinking, we used optogenetics along with monosynaptic rabies tracing. Water restriction induces robust c-Fos expression in the SFO and putative downstream regions (Extended Data Fig. 1a). In the MnPO and OVLT, essentially all of the c-Fos signals were found in nNOS-expressing excitatory neurons (MnPO[nNOS] and OVLT[nNOS]; Extended Data Fig. 1a top, b). Similar results were obtained when we photostimulated SFOnNOS neurons by expressing channelrhodopsin (ChR2)[27] using adeno-associated virus (AAV-DIO-ChR2) in nNOS-cre (also known as Nos1-cre) mice (Extended Data Fig. 1a, bottom). These data suggest that MnPO[nNOS] and OVLT[nNOS] neurons are putative downstream populations of SFO[nNOS] neurons. Retrograde monosynaptic rabies tracing[28] from MnPO[nNOS] and OVLT[nNOS] neurons confirmed direct connections with the SFO[nNOS] population (Fig. 1a, b and Extended Data Fig. 1c). Moreover, photostimulation of ChR2-expressing MnPO[nNOS] or OVLT[nNOS] neurons selectively induced water drinking in satiated mice (Extended Data Fig. 1d). These studies demonstrated that SFO[nNOS] neurons send monosynaptic excitatory inputs to the MnPO[nNOS] and OVLT[nNOS] populations, each of which is sufficient to trigger water drinking.

To further investigate the circuit architecture that processes the internal need for water, we performed neural epistasis analysis for the circuits of the lamina terminalis by loss-of-function manipulation (Fig. 1c). We reasoned that if SFO[nNOS] and its downstream populations redundantly encode thirst in parallel, the ablation of one population should have only minor effects on drinking. Alternatively, if the circuit is organized in a hierarchical fashion in which a specific population has a critical role, the elimination of such a downstream population should abolish SFO[nNOS]-stimulated drinking. To test these

ideas, we expressed caspase (AAV-flex-Casp3)[29] in the MnPO, OVLT or SFO of nNOS-cre mice (Fig. 1c). The expression of Casp3 resulted in the specific and near-complete elimination of nNOS-expressing neurons of a given nucleus (Fig. 1d and Extended Data Fig. 2a). In OVLT^{nNOS}-ablated and control mice, photostimulation of SFO^{nNOS} neurons triggered robust drinking (Fig. 1e and Extended Data Fig. 2b). By sharp contrast, the ablation of MnPO^{nNOS} neurons markedly suppressed SFO^{nNOS}-stimulated water intake (Fig. 1e and Extended Data Fig. 2b, MnPOx). We also found that MnPO^{nNOS} neurons have an important role in the drinking behaviour evoked by OVLT^{nNOS} neurons. Water intake induced by photostimulation of OVLT^{nNOS} neurons was significantly attenuated after ablating MnPO^{nNOS}, but not SFO^{nNOS} neurons (Extended Data Fig. 2c). These results suggest that MnPO^{nNOS} neurons are essential neural substrates of the lamina terminalis for the behavioural output. If this model is correct, stimulating the MnPO^{nNOS} population without the inputs from their upstream SFO^{nNOS}, or both SFO^{nNOS} and OVLT^{nNOS}, neurons should still trigger robust drinking (Fig. 1c). As hypothesized, the elimination of these populations had no impact on drinking when MnPO^{nNOS} neurons were directly photostimulated (Fig. 1e and Extended Data Fig. 2b, SFOx, SFOx and OVLTx). Similar results were obtained by chemogenetic acute silencing using hM4Di (ref. 30) (Fig. 1f). In awake mice, acute inhibition of MnPO^{nNOS} neurons by clozapine N-oxide (CNO) severely suppressed water consumption in both water-restricted and SFO^{nNOS}-stimulated mice (Fig. 1g and Extended Data Fig. 2d, e). However, the same manipulation did not decrease sugar consumption in food-restricted mice (Fig. 1g and Extended Data Fig. 2d, e).

Importantly, the silencing of MnPO^{nNOS} neurons did not compromise the osmosensory function of the SFO^{nNOS} population. We used fibre photometry[31] in awake-behaving mice that expressed the calcium indicator GCaMP6s in the SFOnNOS, and the neuronal silencer hM4Di in MnPO^{nNOS} neurons (Fig. 1h). We showed that the activation of SFO^{nNOS} neurons by osmotic stress was unaffected in the absence of functioning MnPO^{nNOS} neurons (Fig. 1i and Extended Data Fig. 2f). These results were supported by our electrophysiological recordings: only a minor fraction of SFO neurons received monosynaptic input from MnPO^{nNOS} neurons (Extended Data Fig. 3), demonstrating the unidirectional connection

from SFO[nNOS] to MnPO[nNOS] neurons. Taken together, our results demonstrate that thirst neurons in the lamina terminalis form a hierarchical circuit organization, and that the MnPO[nNOS] population is required to process signals from SFO[nNOS] neurons to coordinate drinking.

MNPO[GLP1R] → SFO[nNOS] INHIBITORY INPUT

The thirst neurons of the lamina terminalis also receive negative feedback regulation upon drinking itself[1,8,10]. It has been shown that water intake rapidly suppresses the activity of thirst neurons in the lamina terminalis[10,18] (Extended Data Fig. 4). It is suggested that this quick regulation of thirst circuits optimizes fluid ingestion[8,9]. To examine the neural basis of drinking-induced thirst inhibition, we functionally mapped the upstream inhibitory circuits of SFO[nNOS] neurons using two neural tracing approaches. First, we retrogradely labelled inhibitory neurons that project to the SFO by injecting herpes simplex virus conjugated with mCherry (HSV-mCherry) into the SFO of Vgat-cre mice (Fig. 2a, left). Among the putative upstream structures (Extended Data Fig. 5a), the MnPO contained the strongest HSV signals (Fig. 2a, right). Next, we performed monosynaptic rabies tracing from SFO[nNOS] neurons (Extended Data Fig. 5b). Consistent with the results of the HSV tracing, the MnPO contained the greatest number of rabies-virus-positive neurons that minimally overlapped with excitatory neurons (Extended Data Fig. 5b). These complementary tracing results suggest that GABAergic neurons in the MnPO are a major source of inhibitory input to the SFO[24].

To gain a more specific genetic handle on these neurons, we performed RNA sequencing analysis of the inhibitory population of the dorsal lamina terminalis (containing the MnPO and SFO) and the cortex. We found that GLP1R transcripts were highly enriched in the inhibitory neurons from the lamina terminalis, by a factor of 100 compared to the cortex (Fig. 2b). In situ hybridization and immunohistochemical studies in Glp1r-cre mice[32] confirmed that GABAergic MnPO neurons expressed GLP1R (Fig. 2c and Extended Data Fig. 6a, b). As predicted from our tracing results, ChR2-assisted circuit mapping[33] revealed

that all recorded SFO^{nNOS} neurons (16 out of 16 cells) received robust monosynaptic inhibitory input from GLP1R-expressing MnPO (MnPO^{GLP1R}) neurons, with an inhibitory postsynaptic current latency of 8.4 ms (Fig. 2d). However, SFO$^{non-nNOS}$ neurons received such input rarely (4 out of 15 cells with small inhibitory postsynaptic currents, Fig. 2d), showing that inhibitory input from MnPO^{GLP1R} neurons is specific to excitatory neurons in the SFO. Furthermore, photostimulation of MnPO^{GLP1R} neurons selectively suppressed water intake in thirsty mice (Fig. 2e and Extended Data Fig. 6c), although this acute inhibition was not observed upon the application of a GLP1R agonist[34] (Extended Data Fig. 6d–f). Collectively, our findings suggest that the MnPO^{GLP1R} population has a key modulatory role in thirst.

MNPO^{GLP1R} NEURONS MONITOR LIQUID INTAKE

Next, we measured the in vivo calcium dynamics of MnPO^{GLP1R} neurons expressing GCaMP6s in Glp1r-cre mice (Fig. 3a). In freely moving mice, MnPO^{GLP1R} neurons were acutely activated during water drinking, and their activity returned to the basal level when they stopped drinking (Fig. 3a, red trace). These neurons responded equally when thirsty mice licked either water or isotonic saline, but not when they licked an empty spout (Fig. 3b and Extended Data Fig. 7c–e). Notably, the neuronal responses were also observed when the mice licked non-aqueous silicone oil, which showed that the activation of MnPO^{GLP1R} neurons is independent of fluid composition. Under food-restricted conditions, we found that MnPO^{GLP1R} neurons still responded upon licking sucrose solution (300 mM, Fig. 3c and Extended Data Fig. 7c, d). However, solid peanut butter evoked no response despite its high palatability (Fig. 3c). These optical recording studies indicate that MnPO^{GLP1R} neurons are activated purely by fluid consumption and not by reward-seeking behavior or licking action per se. Consistent with the connection from MnPO^{GLP1R} to SFO^{nNOS} neurons, the activity of the SFO^{nNOS} population mirrored precisely the calcium dynamics of MnPO^{GLP1R} neurons, except that water intake evoked an additional persistent inhibition (Extended Data Fig. 7a, b). This water-specific inhibition of SFO^{nNOS} neurons is probably due to osmolality sensing or water absorption in the gastrointestinal tract as

proposed previously[1,9]. These results demonstrate two important properties of thirst circuits. First, MnPO^{GLP1R} neurons are activated upon fluid ingestion; this activation is independent of fluid composition and the internal state of the animal. Second, this neural population transmits inhibitory signals to SFO^{nNOS} neurons, in a manner that is time-locked to drinking.

EFFECT OF EATING AND DRINKING

We investigated the mechanisms by which MnPO^{GLP1R} neurons exclusively represent fluid intake. To this end, we provided water-restricted mice with water in two different forms— liquid and gel (HydroGel: 98% water + hydrocolloids)—while recording MnPO^{GLP1R} activity (Fig. 4a). In either form, the mice ingested a similar amount of water within the 30-min session (Fig. 4b). Notably, compared to the robust activation of MnPO^{GLP1R} neurons upon drinking water, gel-eating behavior did not elicit any response (Fig. 4a, c). Similarly, eating normal chow did not stimulate this neural population (Fig. 4d). Therefore, MnPO^{GLP1R} neurons are able to distinguish between drinking and eating behavior even if an animal consumes essentially the same substance. These results suggest that the MnPO^{GLP1R} population facilitates satiety, which is induced by drinking behavior and not specifically by water.

Because the rate of ingestion differed considerably between the drinking of water and the eating of HydroGel (Fig. 4b), we speculated that MnPO^{GLP1R} neurons may monitor the pattern of ingestion in order to distinguish the mode of consumption. To examine this possibility, mice were given access to water for 30 s in total at two different rates: 2 s × 15 times and 30 s × 1 time (Fig. 4e). As hypothesized, concentrated periods of drinking evoked significantly greater responses in the MnPO^{GLP1R} neurons than did sparse periods of drinking, regardless of the total amount of water consumed (Fig. 4e). We note that the temperature of the fluid did not affect the response (Fig. 4f). Because animals can ingest fluids much faster than they can ingest solid substances, these data strongly support the idea that the MnPO^{GLP1R} population distinguishes between drinking and eating on the basis

of ingestion speed. Consequently, concentrated (that is, rapid) fluid intake recruits MnPO^{GLP1R}-mediated inhibition signals, which in turn suppress the activity of SFO^{nNOS} neurons. These findings provide key mechanistic insight into rapid thirst alleviation as a result of drinking behavior.

MNPO^{GLP1R} NEURONS HELP THIRST SATIETY

In view of the function of the MnPO^{GLP1R} population in the monitoring of fluid intake, we next considered its physiological importance in the regulation of drinking using chemogenetic loss-of-function manipulation (Fig. 5a). Whereas any fluid elicits transient MnPO$^{GLP1R} \rightarrow$SFO^{nNOS} inhibition, water evokes an additional inhibitory effect that persists after drinking episodes (Extended Data Fig. 7a). Owing to this water-specific signal, inhibition of MnPO^{GLP1R} neurons by CNO had only a minor effect on the total water intake of water-restricted mice during a 30-minute period (Extended Data Fig. 8a, b, d). By contrast, marked effects were observed for isotonic saline, in which MnPO^{GLP1R}-independent inhibitory signals are absent (Fig. 5b). Compared to the vehicle control, inhibition of MnPO^{GLP1R} neurons robustly increased both the total amount and the duration of saline intake (Fig. 5c and Extended Data Fig. 8c). However, under satiated conditions, the same manipulation did not increase water or saline intake, which excludes the possibility that inhibiting MnPO^{GLP1R} neurons stimulates appetite directly (Fig. 5c). We observed the same overdrinking phenotype in mice in which MnPO^{GLP1R} neurons were ablated by Casp3 (Extended Data Fig. 8e, f). Our functional manipulation studies demonstrate that MnPO^{GLP1R} neurons promote satiety of thirst by monitoring real-time fluid intake, and that the malfunction of this neuronal regulation leads to polydipsic overdrinking, especially in the case of non-hypoosmotic fluids such as saline.

DISCUSSION

In this study, we identified genetically defined thirst circuits in the lamina terminalis that integrate the instinctive need for water with the consequent drinking behavior to maintain internal water balance (Fig. 5d). We showed that multiple downstream populations of

SFO[nNOS] neurons are individually sufficient to induce water intake. These data are reminiscent of the circuit organization for hunger, in which eating behavior is redundantly encoded by multiple output projections of AgRP neurons in the arcuate nucleus[35]. However, we showed that individual thirst-related neuronal populations of the lamina terminalis are hierarchically organized, and that MnPO[nNOS] neurons are the behavioral output neurons. Previous lesion studies in rats and sheep have proposed a model in which the MnPO serves as a critical site that integrates inputs from osmosensory neurons of the SFO and the OVLT[36,37,38]. Our findings well explain and further advance the concept of this model with cell-type-specific precision. Whereas the necessity of the SFO may vary among species[10], the MnPO appears to consistently function as the key centre for drinking across species[38]. In our analysis, MnPO[nNOS] neurons project to various areas including the hypothalamus and the midbrain (Extended Data Fig. 9a; see also ref. 18). These results reveal a neural logic to thirst processing in the lamina terminalis circuit, and provide a platform for investigation into how the appetite for water is integrated at downstream sites of MnPO[nNOS] neurons.

Notably, MnPO[GLP1R] neurons responded selectively to the ingestion of fluids but not solids. These inhibitory neurons provide rapid monosynaptic inhibition to thirst-driving SFO[nNOS] neurons. Our results indicate strongly that the MnPO[GLP1R] population facilitates thirst satiation upon drinking rather than upon water absorption. At a psychophysical level, these findings provide an explanation for the long-standing observation that thirst is quickly alleviated at the onset of drinking[6,9]. At a physiological level, these results reveal a neural interface that adjusts the activity of thirst neurons on the basis of real-time drinking behavior. Although systemic recovery of fluid balance relies on water absorption into the blood, thirst is modulated by multiple preabsorptive factors including oral, oropharyngeal and gastrointestinal signals[1]. It is unlikely that the MnPO[GLP1R] $\rightarrow$ SFO[nNOS] circuit mediates oral sensory information such as taste[39,40,41] because it responds to any fluid, including silicone oil. Instead, MnPO[GLP1R] neurons may function as a flow-meter by sensing gulping actions in the oropharyngeal area, and provide rapid, liquid-specific inhibition to thirst circuits. This idea is consistent with previous findings that drinking hyperosmotic saline[7],

but not eating food[42], transiently suppressed vasopressin secretion. In this model, MnPO^{GLP1R} neurons serve as a central detector that discriminates fluid ingestion from solid ingestion, which promotes acute satiation of thirst through the SFO and other downstream targets (Extended Data Fig. 9b). Subsequently, gastrointestinal mechanisms may selectively detect water over other fluids that induce persistent inhibitory effects on SFO^{nNOS} neurons (Extended Data Fig. 7a). Although fluid-sensing mechanisms at each peripheral area are poorly understood, further molecular and cellular studies should help to reveal complex regulatory signals that maintain body-fluid homeostasis.

METHODS

Animals

All animal procedures were performed in accordance with the US NIH guidance for the care and use of laboratory animals and were approved by the Institutional Animal Care and Use Committee (protocol no: 1694-14, California Institute of Technology). Mice used for data collection were both males and females, at least eight weeks of age. The following mice were purchased from the Jackson Laboratory: C57BL/6J, stock number 000664; Slc32a1-cre (also known as Vgat-cre), stock number 016962; Ai9, stock number 007909; Ai3, stock number 007903; Slc17a6-cre (also known as Vglut2-cre), stock number 016963 and Nos1-cre, stock number 017526. Glp1r-cre and Ai110 lines were provided by F. Gribble (Cambridge) and D. Anderson (Caltech), respectively. Mice were housed in temperature- and humidity-controlled rooms with a 13 h:11 h light:dark cycle with ad libitum access to chow and water.

Viral constructs

The following AAVs were purchased from the UNC Vector Core: AAV1-CA-FLEX-RG, 4×10^{12} copies per ml; AAV1-EF1a-FLEX-TVA-mCherry, 6×10^{12} copies per ml; AAV2-EF1a-DIO-hChR2-eYFP, 5.6×10^{12} copies per ml; AAV2-hSyn-DIO-hM4D(Gi)-mCherry, 3.7×10^{12} copies per ml; AAV2-EF1a-DIO-mCherry, 5.7×10^{12} copies per ml; AAV5-CamKIIa-hM4D(Gi)-mCherry, 4.3×10^{12} copies per ml; AAV5-CamKIIa-hM3D(Gq)-mCherry, 1.7×10^{12} copies per ml; AAV5-FLEX-taCasp3-TEVp, 5.3×10^{12} copies per ml. The following AAVs were purchased from the UPenn Vector Core: AAV1-Syn-FLEX-GCaMP6s-WPRE-SV40, 2.9×10^{13} genome copies per ml; AAV1-Syn-GCaMP6s-WPRE-SV40, 2.28×10^{13} genome copies per ml; AAV1-CamKII-eYFP-WPRE-hGH, 1.86×10^{13} genome copies per ml; AAV2-EF1a-DIO-eYFP-WPRE-hGH, 3.05×10^{12} genome copies per ml. EnvA G-deleted Rabies-eGFP (1.6×10^{8} transduction units per ml) was purchased from the Salk Institute. Herpes simplex virus (hEF1a-LS1L-mCherry HT) was purchased from the Vector Core Facility at the Massachusetts Institute of Technology.

Surgery

All procedures were adopted from a previous report[19]. Mice were anaesthetized with a mixture of ketamine (1 mg ml^{-1}) and xylazine (10 mg ml^{-1}) in isotonic saline, injected intraperitoneally (i.p.) at 10 µl g^{-1} bodyweight. The mice were then placed in a stereotaxic apparatus (Narishige Apparatus) on a heating pad. An incision was made to expose the skull. The three-dimensional magnetic resonance imaging coordinate system was used to align the skull reference. A small craniotomy, less than 1 mm, was made using a hand drill at the regions of interest. Viral constructs were injected using a pressure injection system (Nanoliter 2000) using a pulled glass capillary at 100 nl min^{-1}. The coordinates were: anteroposterior −4,030, mediolateral 0, dorsoventral −2,550 (200-nl injection) for the SFO; anteroposterior −3,100, mediolateral 0, dorsoventral −4,080 (100-nl injection) and −3,800 (50–100-nl injection) for the MnPO; and anteroposterior −2,700, mediolateral 0, dorsoventral −4,900 (75-nl injection) for the OVLT. For optogenetic implants, a 200-µm fiber bundle (FT200EMT, Thorlabs) glued to a ceramic ferrule (Thorlabs) with epoxy was used. For photometry implants, a 400-µm fiber bundle (BFH48-400, Thorlabs) glued to a ceramic ferrule with low autofluorescence epoxy (EPO-TEK301) or a custom-made implant (Doric Lenses) was used. A fiber was implanted 200–300 µm (for photostimulation) or 0–50 µm (for photometry) above the virus injection site. After the application of a local anesthetic to the sides of the skin incision, the implants were permanently fixed to the skull using dental cement. Cannulated mice were placed in a clean cage on a heating pad to recover from anesthesia. Mice were kept in their home cage for at least ten days before any behavioral tests.

Photostimulation

For optogenetic experiments, photostimulation was performed using 473-nm laser pulses: 20 ms, 5 Hz (for OVLT) or 20 Hz (for SFO and MnPO) delivered via a custom-made optic cable using a pulse generator (World Precision Instruments). The laser intensity was maintained at 5 mW (for OVLT) or 10 mW (for SFO and MnPO) at the tip of the fiber.

Behavioral assays

For water-restriction experiments, mice were provided with 1 ml of water daily. For food-restriction experiments, mice were provided with 0.5 pellets per 20 grams of body weight daily. All assays were performed in a modified lickometer as described previously[39] or a Biodaq monitoring system (Research Diets Inc.). For all photometry assays, mice were acclimatized for 10–15 min in the lickometer cage before stimuli were given.

Long-term access assays

For optogenetic testing (Fig. 1g and Extended Data Fig. 2c, e), satiated mice were given ad libitum access to water with photostimulation. Photostimulation was delivered for 1 s at 3-s intervals throughout the behavioral sessions. For Fig. 2e and Extended Data Fig. 6c, mice were given access to water for 20 min after 24-h water restriction, and photostimulation was delivered for the first 10 min. For feeding assays (Fig. 2e), mice were single-housed in Biodaq cages after 24-h food restriction, and chow intake was measured for 20 min with or without light stimulation. For acute inhibition experiments, mice were given access to 150 mM NaCl (Fig. 5b and Extended Data Fig. 8c) or water (Fig. 1g and Extended Data Figs 2e, 8a, b, d) for 20–30 min after 24 h water restriction, or 300 mM sucrose (Fig. 1g and Extended Data Fig. 2e) after food restriction. For all acute inhibition experiments, CNO was injected at 10 mg kg^{-1} body weight, 30 min before the start of the behavior session. For acute activation experiments, CNO was injected at 1 mg kg^{-1} body weight (Extended Data Fig. 7e), 30 min before the start of the behavior session. For Fig. 3a and Extended Data Figs 4a and 8f, access to water or saline was provided for 30 min after 24 h of water restriction. For Fig. 4a, water or HydroGel (ClearH2O) in a cup was provided for 30 min after 24 and 36 h of water restriction, respectively. The weight of the cup was measured before and after the behavior session. For Fig. 4d, 0.5 pellets of chow was provided for 30 min after 24 h of food restriction. The entire session was recorded using a camera at 30 frames per second, and ingestion episodes were manually annotated.

Salt- or mannitol-loading experiments

150 µl or 300 µl of 2 M NaCl, or 300 µL of 2 M mannitol, was injected intraperitoneally at the end of the acclimatization period. For Fig. 1i and Extended Data Fig. 2f, CNO or vehicle (water) was injected 10 min before the injection of NaCl or mannitol.

Brief access assays

For optogenetic experiments, behavioral assays were performed essentially as previously described[19]. Satiated mice were tested in a gustometer for 10–15 trials (Fig. 1e and Extended Data Fig. 1d). The laser pulses were delivered for 20 s of the 40-s trial. After the first lick, mice were given access to a water spout for 5 s. For photometry recording (Fig. 3b and Extended Data Fig. 7a), water-restricted mice were presented with one of the following four stimuli for 30 s: water, isotonic saline, silicone oil or empty bottle (control). Under food-restricted conditions (Fig. 3c and Extended Data Fig. 7b), a bottle containing 300 mM sucrose, peanut butter coated on a spout, or an empty bottle was presented for 30 s. To avoid the effect of internal state changes, we used the data from the first stimulus presentation in each session. To test the effect of temperature (Fig. 4f), three bottles of water at 4 °C, room temperature (25 °C) or 37 °C were placed at the start of the acclimatization period (10 min). Each trial was 30 s long with an inter-trial interval of 2 min. For Fig. 4e, water-restricted mice had access to water for 2 s repeated 15 times or for one 30-s period. Each presentation was followed by a 30-s interval.

Fiber photometry

We measured bulk fluorescence signals using fiber photometry as previously described[31]. In brief, 490 nm and 405 nm light-emitting diodes (Thorlabs, M490F1 and M405F1) were collimated and delivered to the brain. The light intensity was maintained at less than 100 µW during all recordings. The fluorescence signal was then focused onto a femtowatt photoreceiver (Newport, Model 2151). The modulation and demodulation were performed with an RP2.1 real time processor (Tucker-Davis Technologies) running custom software. The licks from the lickometer were simultaneously recorded as real-time transistor–transistor logic signals to the RP2.1. Fluorescence changes were analyzed using custom

MATLAB (MathWorks) code as described previously[31]. Data were extracted and subjected to a low-pass filter at 1.8 Hz. A linear function was used to scale up the 405-nm channel signal to the 490-nm channel signal to obtain the fitted 405-nm signal. The resultant $\Delta F/F$ was calculated as (raw 490 nm signal – fitted 405 nm signal)/(fitted 405 nm signal). For brief access tests, the area under the curve ($\Sigma\Delta F_{during}$) was quantified by integrating the fluorescence signals during the bout. For all bouts, the mean fluorescence for 30 s before the first lick was calculated and subtracted from the entire session. ΔF changes ($\Delta F_{post} - \Delta F_{pre}$) were calculated by subtracting the mean fluorescence signal during the 2-s period before the first lick from the mean signal during the 2-s period at 1 min after the bout. To display traces, the fluorescence data was time-binned by a factor of 2.5× the sampling frequency and down-sampled to 1 Hz. For long-term tests, the area under the curve was calculated for 2.5 min after the start of the bout. Changes in ΔF were calculated by subtracting the mean signal during the 2-s period before the first lick or NaCl injection from the mean signal during the 2-s period at 5 or 10 min after the bout (Extended Data Fig. 4). For peristimulus time histograms (Fig. 4c, d), the first bout at the start of the session and the last bout within 10 min of access were used. The areas under the curve for the peristimulus time histograms were calculated during the first or the last 15 s.

Viral tracing

Monosynaptic rabies tracing

150 nl of a mixture of AAV1-CA-FLEX-RG and AAV1-EF1a-FLEX-TVA-mCherry (4:1 ratio) was injected to the target area. Two weeks later, 200 nl of EnvA G-deleted Rabies-eGFP was injected into the same area. The mice were euthanized a week later and their brains collected.

HSV tracing

200 nl of a mixture of AAV1-Syn-GCaMP6s-WPRE-SV40 and hEF1-LS1L-mCherry HT (2:5 ratio) was injected to the SFO of Vgat-cre mice. The GCaMP virus was used to mark

the injection site. The mice were euthanized three weeks later and their brains collected. The sections were imaged using a confocal microscope (TCS SP8, Leica) or a slide scanner (VS120, BX61VS, Olympus) at 20×. The slide scanner images were used to count cells using ImageJ. Representative images in Figs 1a, 2a and Extended Data Fig. 5 are from the confocal microscope. Regions with an average greater than 10 rabies-virus-positive cells were included in the analysis.

Histology

Mice were deeply anaesthetized with carbon dioxide and then transcardially perfused with PBS followed by 4% paraformaldehyde in PBS (pH 7.4) at 4 °C. The brains were extracted and fixed in 4% paraformaldehyde at 4 °C overnight. 100 μm coronal sections were prepared using a vibratome (Leica, VT-1000 s) for antibody staining. The primary antibodies (1:500 dilution) used were: goat anti-c-Fos (Santa Cruz, SC-52G), rabbit anti-NOS1 (Santa Cruz, sc-648), rabbit anti-GAD65+GAD67 (Abcam, ab183999), chicken anti-GFP (Abcam, ab13970) and rat anti-mCherry (Thermo Fisher, M11217). After washing three times with PBS, the sections were incubated with secondary antibodies (1:500 dilution) in blocking buffer for 4 h. The GAD65/67 primary/secondary antibody incubation solution was prepared without detergent. Fluorescence in situ hybridization was carried out using the RNAscope fluorescent multiplex kit (Advanced Cell Diagnostics) in accordance with the manufacturer's instructions. Glp1r-cre/Ai9 mice were used with probes targeted to tdTomato and GLP1R.

RNA sequencing analysis

The dorsal lamina terminalis in Vgat-cre/Ai9 mice were dissected under a fluorescence microscope. To minimize contamination from other tissues, the lamina terminalis tissue containing the SFO and dorsal MnPO were peeled off. For non-lamina-terminalis control, we dissected small tissues of the cortex from the same mice. These samples were dissociated into single cells using the Papain Dissociation System (Worthington), labelled with 4′,6-diamidino-2-phenylindole (DAPI) and the tdTomato-positive neurons were sorted

using a flow cytometer (MoFlo Astrios, Beckman Coulter). RNA was extracted using a PicoPure RNA isolation kit (Applied Biosystems) and complementary DNA was prepared using an Ovation RNA-seq V2 kit (Nugen). Relative gene expression (Fig. 2b) was calculated as a ratio of fragments per kilobase million of the dorsal lamina terminalis to that of the cortex. The genes with fragments per kilobase million < 0.1 in the cortex were omitted from the plot.

Slice electrophysiology

Procedures for the preparation of acute brain slices and recordings with optogenetic stimulations were similar to those described previously[19,43]. After decapitation, the brain was removed and immersed in ice-cold solution. Coronal slices (300 mm) were cut using a vibratome (VT-1200 s, Leica) and moved into HEPES holding solution (in mM: NaCl 92, KCl 2.5, NaH2PO4 1.2, NaHCO3 30, HEPES 20, glucose 25, Na-ascorbate 5, thiourea 2, Na-pyruvate 3, MgSO4 2, CaCl2 2, at pH 7.35). The slices were allowed to recover at 33 °C for 30 min and then held at room temperature (around 25 °C) until use.

While recording, slices were perfused continuously (around 2 ml min^{-1}) with artificial cerebrospinal fluid (in mM: NaCl 124, KCl 2.5, NaH2PO4 1.2, NaHCO3 24, glucose 25, MgSO4 1, CaCl2 2) at 25 °C. Neurons were visualized and targeted using an upright infrared differential interference contrast microscope (BX51WI, Olympus). Whole-cell recordings were achieved using glass pipettes with an impedance of 4–6 MΩ when filled with intracellular solution (for voltage clamp, in mM: CsCl 145, NaCl 2, HEPES 10, EGTA 0.2, QX-314 Chloride 5, Mg-ATP 4, Na-GTP 0.3, at pH 7.25; for current clamp, in mM: K-gluconate 145, NaCl 2, KCl 4, HEPES 10, EGTA 0.2, Mg-ATP 4, Na-GTP 0.3, at pH 7.25). Electrical signals were sampled at 20 kHz and filtered at 2.9 kHz using an EPC 10 system (HEKA Elektronik). To evaluate postsynaptic currents evoked by light pulses, the membrane potential of SFO^{nNOS} (transduced with CamKII-mCherry/eYFP) or SFO$^{non-nNOS}$ neurons was held at −60 mV. Light pulses were generated by a mercury lamp, filtered by an optical filter (Chroma) and controlled by an electronic shutter driver (VCM-D1, UNIBLITZ). 2-ms light pulses were delivered at 1 Hz four times, followed by a 4-s

interval. We repeated this stimulus cycle 20 times. To confirm that the postsynaptic currents recorded were GABAergic, picrotoxin (150 µM) was applied through the bath for part of the experiments. To confirm glutamatergic postsynaptic currents, 6-cyano-7-nitroquinoxaline-2,3-dione (CNQX, 10 µM) and 2-amino-5-phosphonovaleric acid (DL-APV, 25 µM) were applied through the bath. Monosynaptic connection was defined by synaptic inhibitory or excitatory postsynaptic currents with latencies less than 16.4 ms. For hM4Di experiments, current-clamp recordings were performed by applying a constant supra-threshold current injection to produce tonic action potentials. CNO (around 6 µM) was applied using a puff (30 s) from another glass pipette placed approximately 50 µm from the recorded cell.

Plasma Na^+ and osmolality measurements

After the injection of 150 µl of 2 M NaCl or 300 µl of 2 M mannitol, trunk blood was collected from wild-type mice. Plasma was then extracted after centrifugation at 1500g for 20 min. Plasma osmolality was measured using a vapour pressure osmometer (Vapro 5520). Plasma Na+ concentration was measured using Dionex (Thermo) ICS 2000.

Intra-cranial drug delivery

100 ng of exendin-4 (Sigma Aldrich) dissolved in 1 µl of artificial cerebrospinal fluid was delivered using a custom-made cannula and tubing (PlasticsOne) connected to a Hamilton syringe driven by a pump (NewEra PumpSystems) at 100 nl min^{-1} into the MnPO of water-deprived mice under head-fixed conditions. Two minutes after infusion, freely moving mice were given access to water for the next 45 min. The cannula position was verified by infusing exendin-4-FAM (Anaspec) conjugate before euthanasia.

Enzyme-linked immunosorbent assay

Total plasma GLP1 was measured using EZGLP1T-36k kit (Millipore) as described previously[44]. In brief, after blood was collected in EDTA-coated tubes, plasma was isolated by centrifugation at 1500g for 20 min. Samples were then kept at −80 °C until

measurement. For food-repleted (FD + F) and water-repleted (WD + W) conditions, mice were given access to Ensure for 30 min or water for 5 min, respectively.

Statistics

All statistical analyses were carried out using Prism (GraphPad). We used a two-tailed Mann–Whitney U test, a paired t-test or a Kruskal–Wallis one-way ANOVA, depending on the experimental paradigm. $*P < 0.05$, $**P < 0.01$, $***P < 0.001$. No statistics to determine sample size, blinding, or randomization methods were used. Viral expression and implant placement was verified by histology before mice were included in the analysis. These criteria were pre-established.

Acknowledgements

a

eGFP+
Starter cells

SFO
MnPO
OVLT
3V

AAV-flex-
TVA + RG

SAD-ΔG-eGFP
(EnvA)

nNOS-Cre

Starter cells
SAD
TVA
MnPO
OVLT

SFO

SAD-ΔG-eGFP   nNOS

b

No. of eGFP+ cells in the SFO

nNOS+/eGFP+ (%)

Starter cells
MnPO OVLT   MnPO OVLT

c

MnPOx/OVLTx

AAV-DIO-hChR2
SFO
MnPO
OVLT
3V
nNOS+

AAV-flex-Casp3

SFOx

AAV-flex-Casp3
SFO
MnPO
OVLT
3V
nNOS+

AAV-DIO-hChR2

d

MnPO   OVLT
MnPOx
OVLTx

nNOS   cFos

e

Water intake (licks)

Control MnPOx OVLTx   SFOx SFOx/
                                OVLTx
SFO stim   MnPO stim

f

MnPO^nNOS/
hM4Di-mCherry

CNO

−50 mV   100 s

AAV-DIO-hChR2
SFO
MnPO
3V
nNOS+

AAV-DIO-hM4Di

g

SFO stim

Water intake (licks)

−Water

−Food

Sugar intake (licks)

Time (min)

Vehicle
CNO

h

Fibre photometry

SFO
MnPO
3V
nNOS+

AAV-flex
-GCaMP6s

AAV-DIO
-hM4Di

i

CNO/
Vehicle   NaCl   Water
               access

ΔF/F_0
(10%)

Vehicle
CNO

Lick rate
(2/s)

100 s   Time (s)

SFO activity

ΔF/F_0 (%)

CNO Vehicle

Drinking

Water intake (licks)

CNO Vehicle

Plasma osmolality (mOsm kg^{-1})

Plasma Na+ (mM)
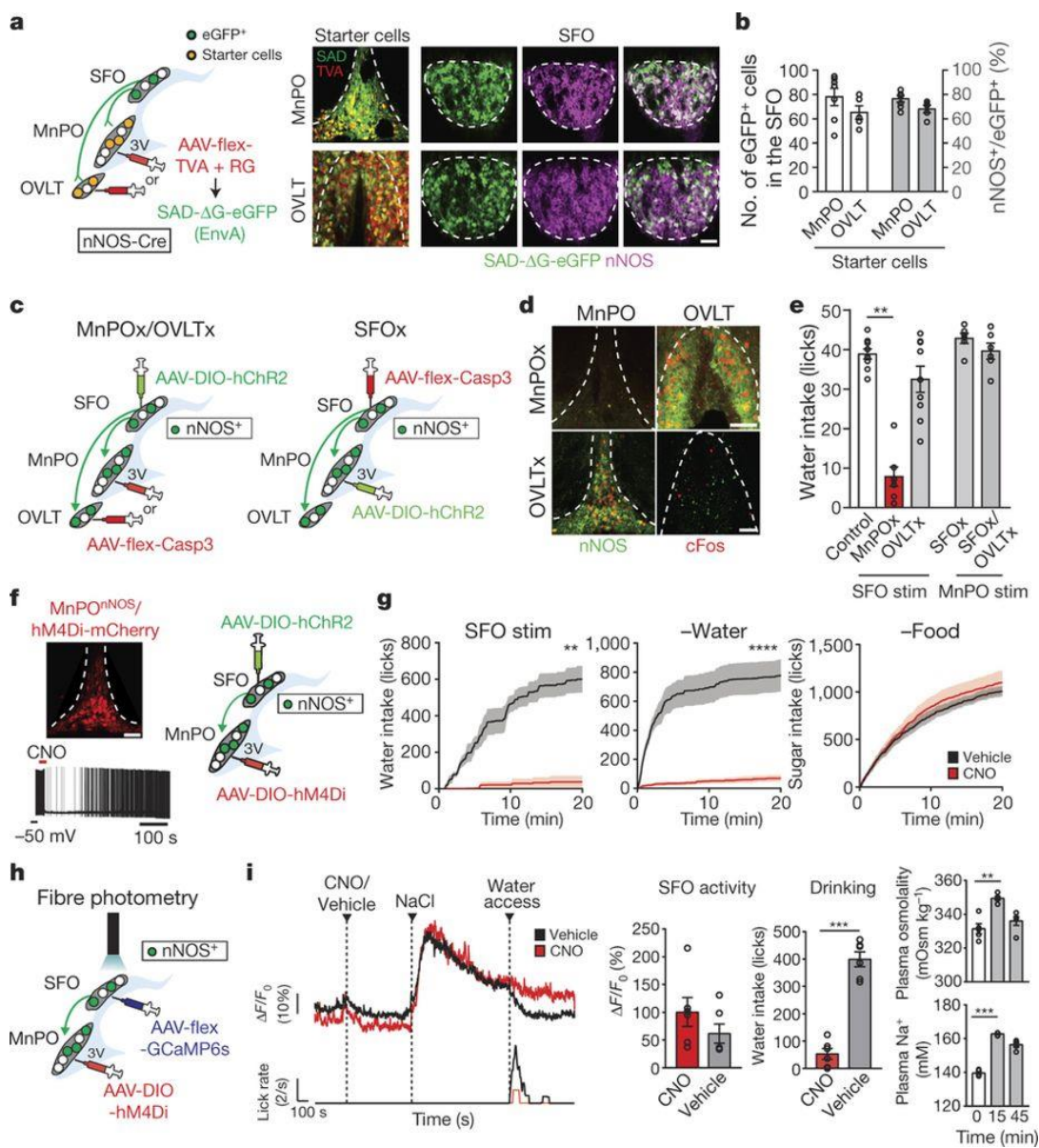
0 15 45
Time (min)

Fig. 1

Figure 1: Thirst-driving neurons are organized hierarchically in the lamina terminalis. a, Schematic of monosynaptic rabies tracing (left). Representative images of the MnPO (top right, one of seven mice) and OVLT (bottom right, one of five mice) of an nNOS-cre mouse transduced with AAV-CA-flex-RG and AAV-EF1a-flex-TVA-mCherry (red) followed by RV-SAD-ΔG-eGFP (green). 3V, third ventricle. **b,** Quantification of eGFP$^+$ neurons in the SFO (n = 7 and 5 mice for MnPO and OVLT, respectively). **c,** Neural epistasis analysis of the circuits of the lamina terminalis by loss-of-function manipulation. Caspase expression is induced in the MnPO, OVLT (left) or SFO (right) of nNOS-cre mice. **d,** Casp3-TEVp efficiently eliminates nNOS-expressing neurons (green) in the MnPO (93.2 ± 2.5%, n = 4 mice) and OVLT (90.6 ± 1.4%, n = 6 mice). c-Fos expression (red) upon the stimulation of SFO^{nNOS} neurons is shown. **e,** Number of licks during the 5-s session (n = 9 mice for controls and OVLTx, n = 7 mice for MnPOx, n = 6 mice for SFOx and SFOx/OVLTx). **f,** Chemogenetic inhibition of MnPO^{nNOS} neurons by CNO (left, six out of six neurons), and a diagram of photostimulation of SFO^{nNOS} and chemogenetic inhibition of MnPO^{nNOS} neurons (right). **g,** Cumulative water intake in SFO^{nNOS}-stimulated mice (left, n = 5 mice) or water-restricted mice (middle, n = 10 mice for CNO and n = 9 mice for vehicle), and sucrose (300 mM) intake in food-restricted mice (right, n = 10 mice for CNO and n = 9 mice for vehicle). **h,** Fiber photometry of SFO^{nNOS} neurons while MnPO^{nNOS} neurons are inhibited by hM4Di-mCherry. **i,** Intraperitoneal NaCl injection robustly activates SFO^{nNOS} neurons with (red trace) or without (black trace) CNO injection (left and middle left). By contrast, CNO injection drastically suppressed drinking behavior (middle right, n = 6 mice). Plasma osmolality (top right) and Na+ concentration (bottom right) were measured after NaCl injection (n = 5 mice). **P < 0.01, ***P < 0.001, ****P < 0.0001, by Mann–Whitney U test, paired two-tailed t-test or Kruskal–Wallis one-way analysis of variance (ANOVA) test. All error bars and shaded areas show mean ± s.e.m. Scale bars, 50 μm.
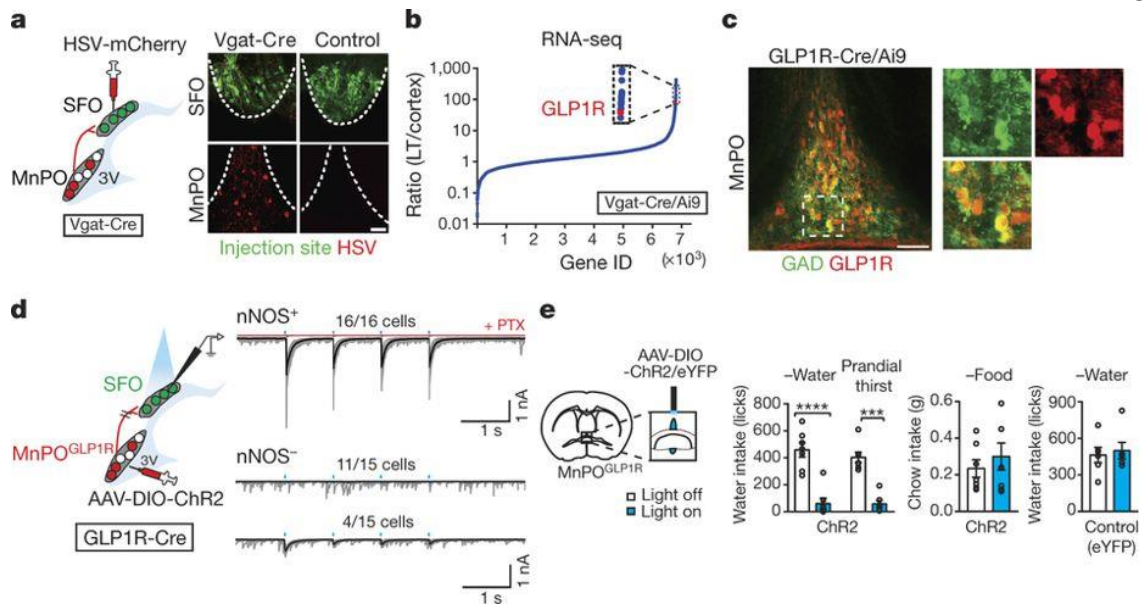
Fig. 2

Figure 2: GLP1R-expressing GABAergic neurons in the MnPO are a major source of inhibitory input to the SFO. a, GABAergic input to the SFO. Representative image of the SFO and MnPO after co-injection of AAV-Syn-GCaMP6s (green) and HSV-mCherry (red) in the SFO (one out of four mice). **b,** GLP1R expression is enriched in inhibitory neurons from the lamina terminalis (LT) relative to the cortex. **c,** MnPO^{GLP1R} neurons are GABAergic ($84.7 \pm 3.4\%$ of GAD+ neurons are tdTomato+, n = 3 mice, representative images are from one out of three mice). These neurons did not overlap with glutamatergic neurons ($4.3 \pm 0.9\%$ overlap, n = 3 mice, Extended Data Fig. 6a). **d,** The MnPO$^{GLP1R} \rightarrow$ SFO monosynaptic connection. MnPO^{GLP1R} neurons send monosynaptic inhibitory input to SFO^{nNOS} neurons. **e,** Optogenetic stimulation of MnPO^{GLP1R} neurons selectively suppresses water intake (n = 7 mice for ChR2 and n = 6 mice for control). ***P < 0.001, ****P < 0.0001, by paired two-tailed t-test. All error bars show mean $\pm$ s.e.m. Scale bars, 50 µm.
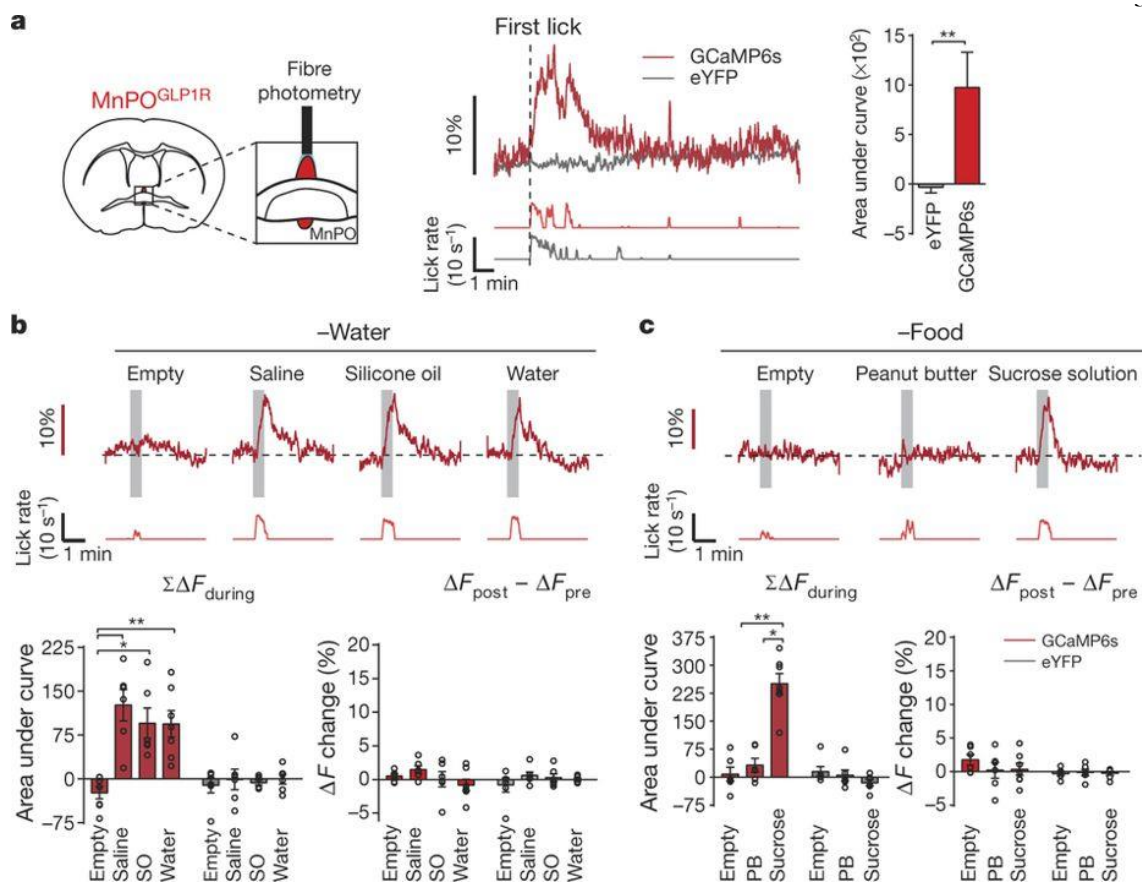
Fig. 3

Figure 3: Rapid and transient activation of MnPO$^{\text{GLP1R}}$ neurons during drinking behaviour. a, Fibre photometry recording from MnPO$^{\text{GLP1R}}$ neurons (left). MnPO$^{\text{GLP1R}}$ neurons are activated upon drinking behaviour (right). Representative traces are from GCaMP6s and enhanced yellow fluorescent protein (eYFP) (one out of six mice). **b,** Responses of MnPO$^{\text{GLP1R}}$ neurons under water-restricted conditions towards different types of liquid. Transient activation (bottom left, $\Sigma\Delta F_{\text{during}}$) and baseline activity shift (bottom right, $\Delta F_{\text{post}} - \Delta F_{\text{pre}}$) were quantified ($n = 6$ mice for saline and silicone oil (SO), $n = 7$ mice for empty and water, $n = 6$ mice for all eYFP controls). **c,** Representative responses of MnPO$^{\text{GLP1R}}$ neurons under food-restricted conditions. Transient activation (bottom left, $\Sigma\Delta F_{\text{during}}$) and baseline activity shift (bottom right, $\Delta F_{\text{post}} - \Delta F_{\text{pre}}$) were quantified ($n = 6$ mice for empty and peanut butter (PB), $n = 7$ mice for sucrose, $n = 6$ mice for all eYFP controls). *$P < 0.05$, **$P < 0.01$, by two-tailed Mann–Whitney U test or Kruskal–Wallis one-way ANOVA test. All error bars show mean ± s.e.m.
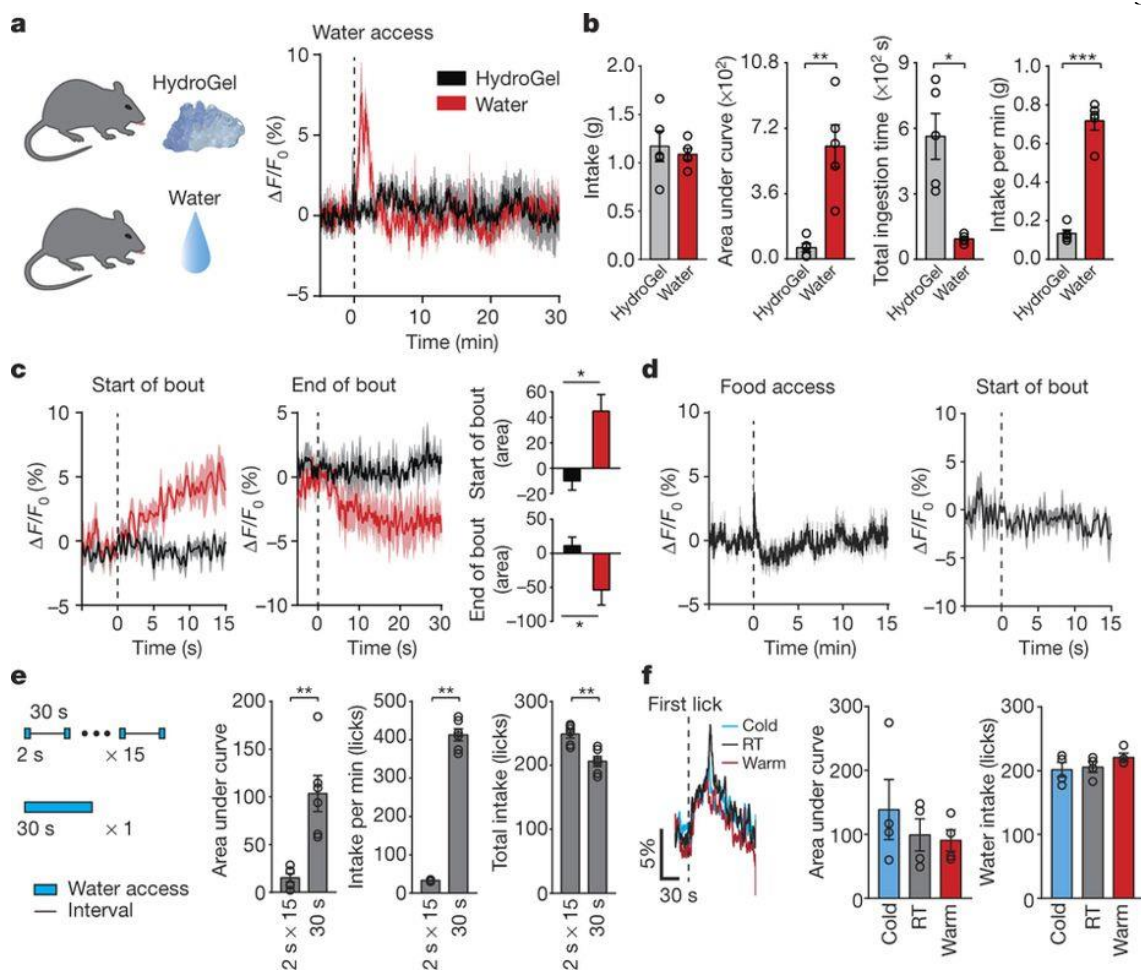
Fig. 4

Figure 4: MnPO^{GLP1R} neurons distinguish between drinking and eating behavior based on ingestive speed. a, MnPO^{GLP1R} neurons respond to the intake of liquid water (red) but not HydroGel (black). **b,** Quantification of neural activity and drinking behavior for the ingestion of HydroGel or water (n = 5 mice). **c,** Peristimulus time histogram around the start (left) and the end (middle) of water and gel intake (n = 5 mice); quantified data are shown on the right. **d,** Eating solid chow does not stimulate MnPO^{GLP1R} neurons (n = 5 mice). **e,** MnPO^{GLP1R} neurons are stimulated to a greater extent during periods of concentrated drinking compared with sparse drinking (n = 6 mice). **f,** The temperature of the ingested fluid has no effect on MnPO^{GLP1R} activity. Total responses (middle) and the number of licks (right) were quantified (n = 4 mice). *$P < 0.05$, **$P < 0.01$, ***$P < 0.001$, by two-tailed Mann–Whitney U test or paired two-tailed t-test. All error bars and shaded areas show mean ± s.e.m.

a

AAV-DIO-hM4Di

MnPO^GLP1R

MnPO^GLP1R/hM4Di-mCherry

CNO

−40 mV
−60 mV

100 s

b

■ Vehicle
■ CNO

Number of licks

Time (min)

5 min

c

Number of licks

−Water   Sated

Licking time (s)

−Water

d

Osmotic/hypovolemic stress

SFO

3V

Drinking inhibition

MnPO

● nNOS+ (excitatory)
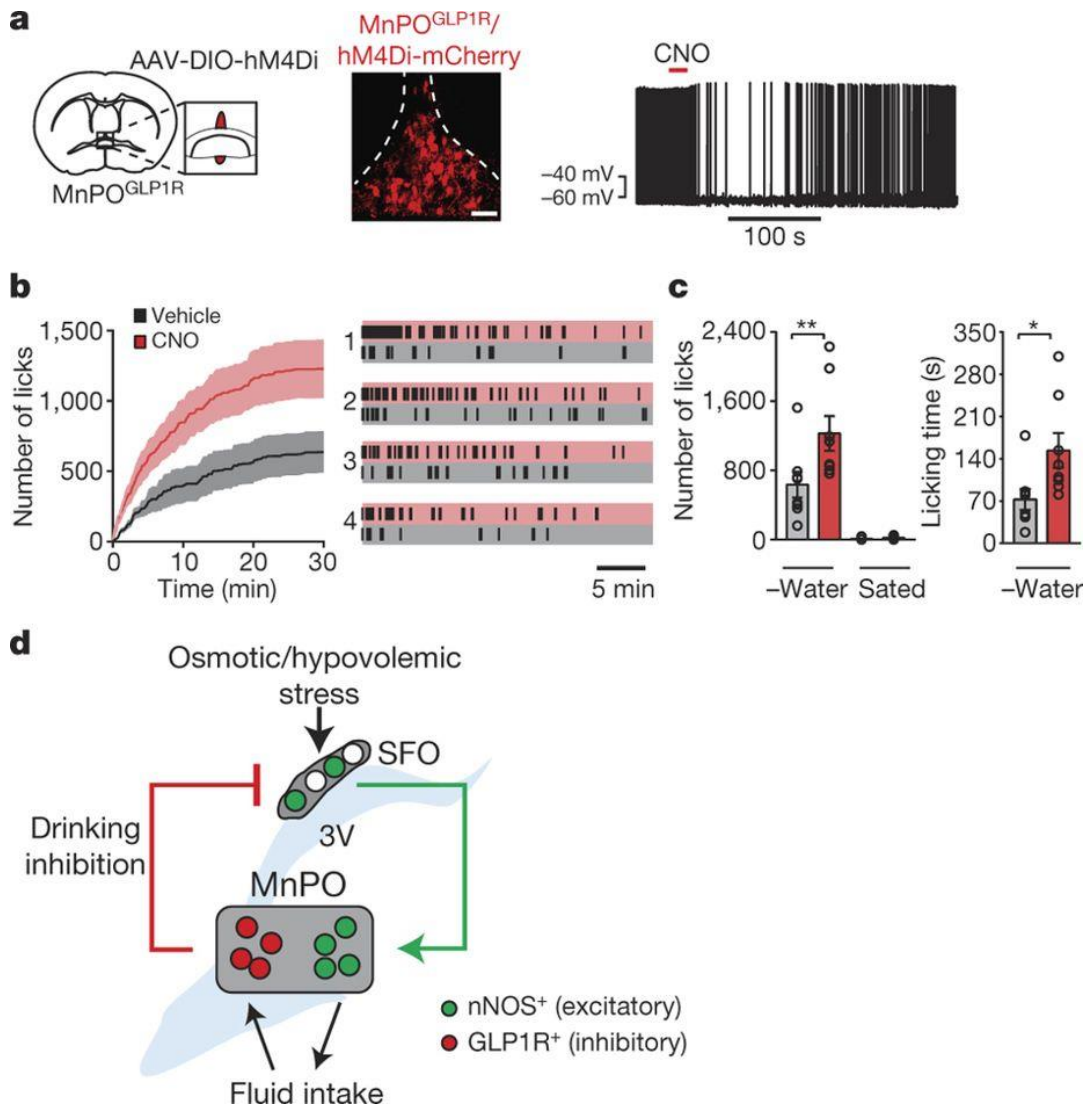● GLP1R+ (inhibitory)

Fluid intake

Fig. 5

Figure 5: Inhibition of MnPO^{GLP1R} neurons leads to overdrinking. a, Treatment with CNO inhibits firing in hM4Di-expressing MnPO^{GLP1R} neurons (right, 6 out of 7 neurons). **b,** Acute inhibition of MnPO^{GLP1R} neurons by CNO results in the overdrinking of isotonic saline in water-restricted mice (n = 8 mice). Representative lick patterns from four out of eight mice are shown (right). **c,** The total amount of saline intake and the time spent drinking (n = 8 mice). **d,** A schematic summarizing thirst genesis, detection of fluid intake and drinking-induced feedback inhibition in the lamina terminalis circuit. *P < 0.05, **P < 0.01, by paired two-tailed t-test. All error bars and shaded areas show mean ± s.e.m. Scale bar, 50 μm.
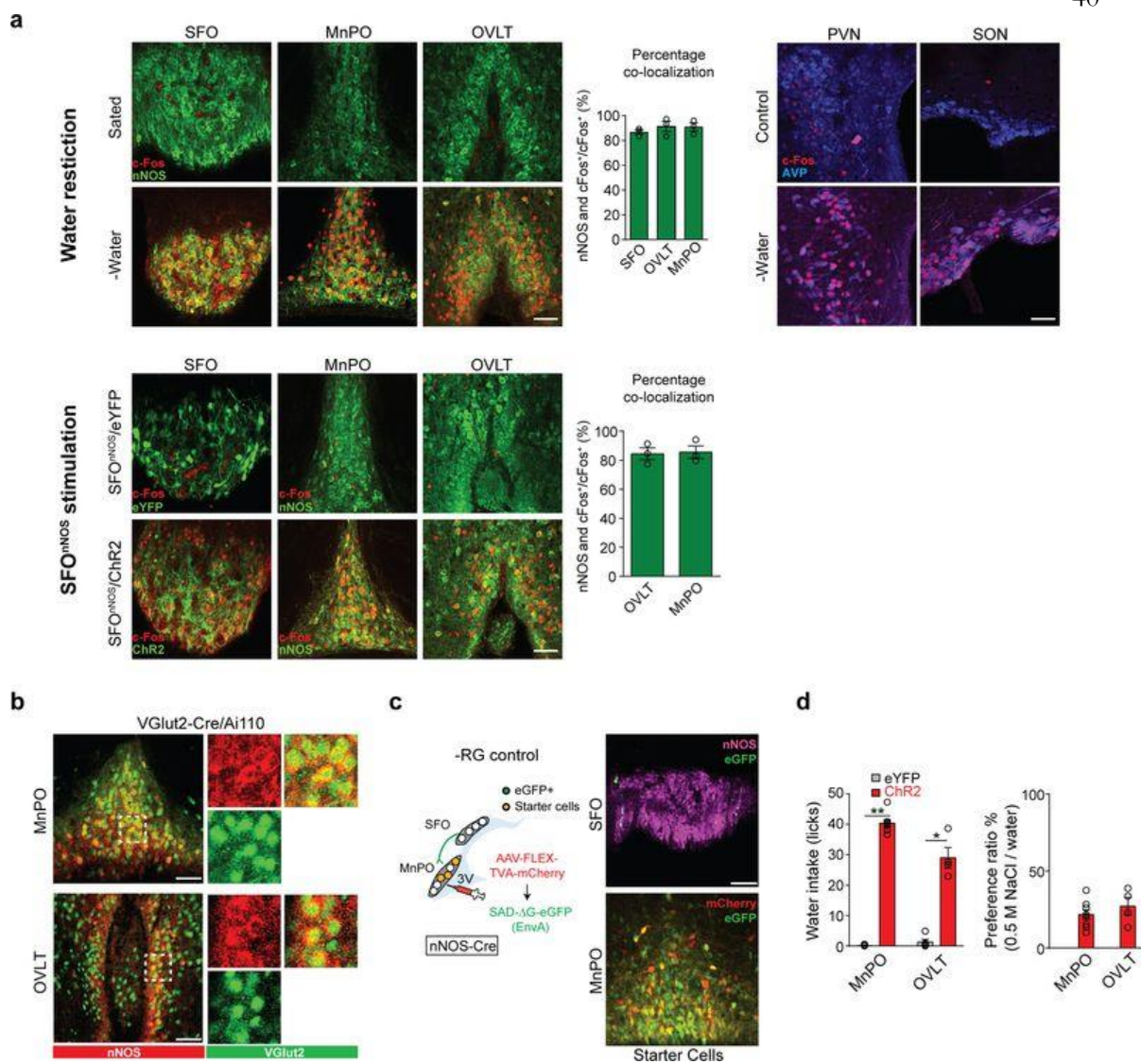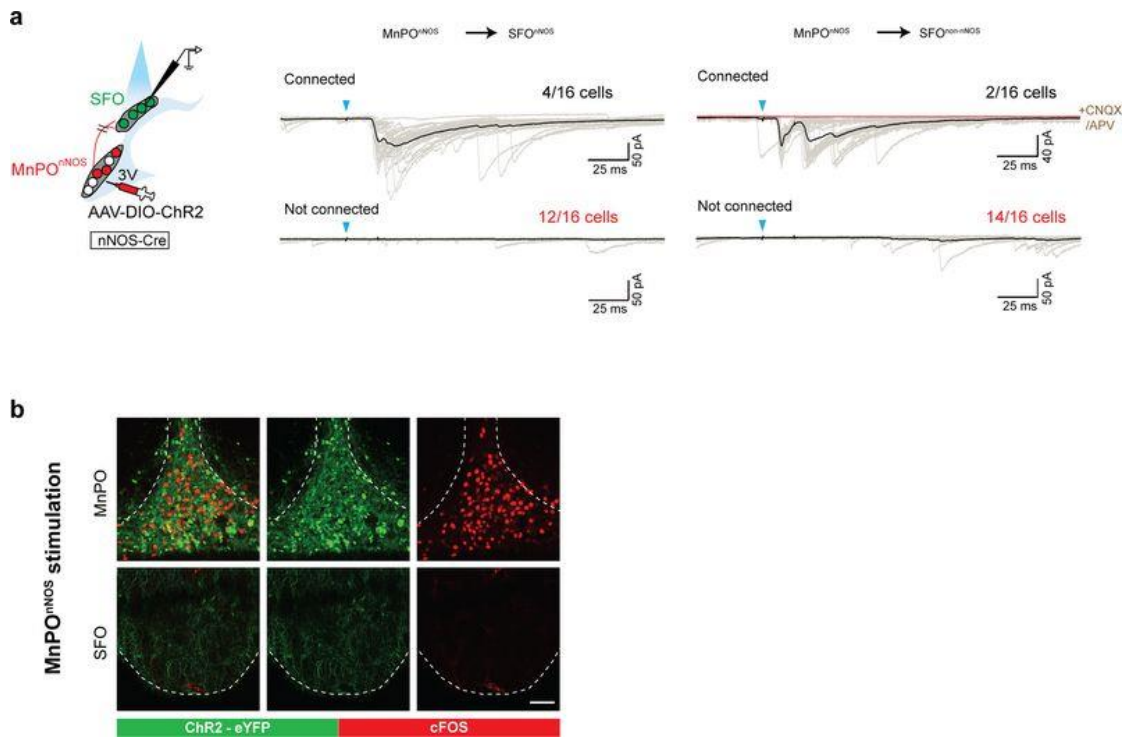
Extended Data Fig. 1

Extended Data Figure 1 : Optogenetic activation MnPO^{nNOS} and OVLT^{nNOS} neurons induces robust water intake in satiated mice. a, Water restriction (top) and SFO^{nNOS} photostimulation (bottom) induces robust c-Fos expression in the SFO, MnPO and OVLT, compared to control conditions. A majority of c-Fos signals in these areas overlapped with nNOS-expressing neurons. The graph shows the quantification of the overlap between nNOS and c-Fos signals (n = 3 mice). c-Fos signals in the paraventricular nucleus (PVN) and supraoptic nucleus (SON) overlapped with vasopressin (AVP)-expressing neurons. **b,** MnPO (top) and OVLT (bottom) excitatory neurons visualized in VGlut2/Ai110 transgenic mice co-stained with nNOS (red, antibody staining). MnPO^{nNOS} and OVLT^{nNOS} neurons co-express a glutamatergic marker. $92.2 \pm 4.9\%$ of nNOS-expressing neurons were excitatory, and $80.9 \pm 2.6\%$ of excitatory neurons are nNOS-expressing in the MnPO (n = 3 mice). Magnified images are shown on the right. **c,** Left, scheme of the control experiments for monosynaptic rabies tracing. Right, a representative image of the MnPO of an nNOS-cre mouse transduced with AAV-EF1a-FLEX-TVA-mCherry (red) followed by EnvA G-deleted Rabies-eGFP (bottom). No eGFP+ cells were present in the SFO (top, one of two mice) **d,** Photostimulation of ChR2-expressing MnPO^{nNOS} and OVLT^{nNOS} neurons (red bars, n = 8 and 4 mice for MnPO and OVLT respectively) triggered intense drinking; control mice infected with AAV-DIO-eYFP showed no such response (grey bars, n = 5 mice). Photostimulated mice showed a strong preference for water over a highly concentrated NaCl solution (500 mM, right panel). $*P < 0.05$, $**P < 0.01$; by two-tailed Mann–Whitney U test. All error bars show mean $\pm$ s.e.m. Scale bars, 50 μm.
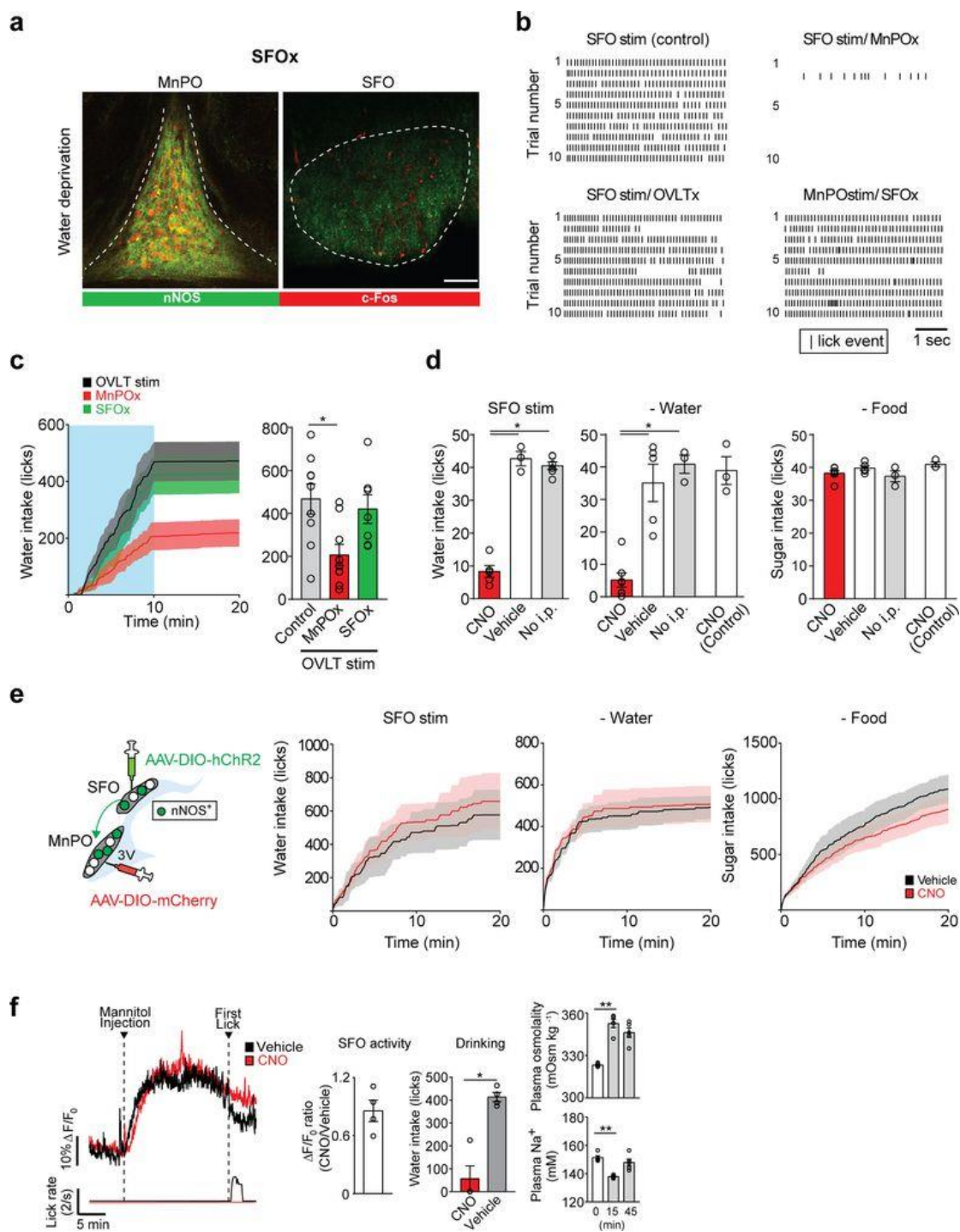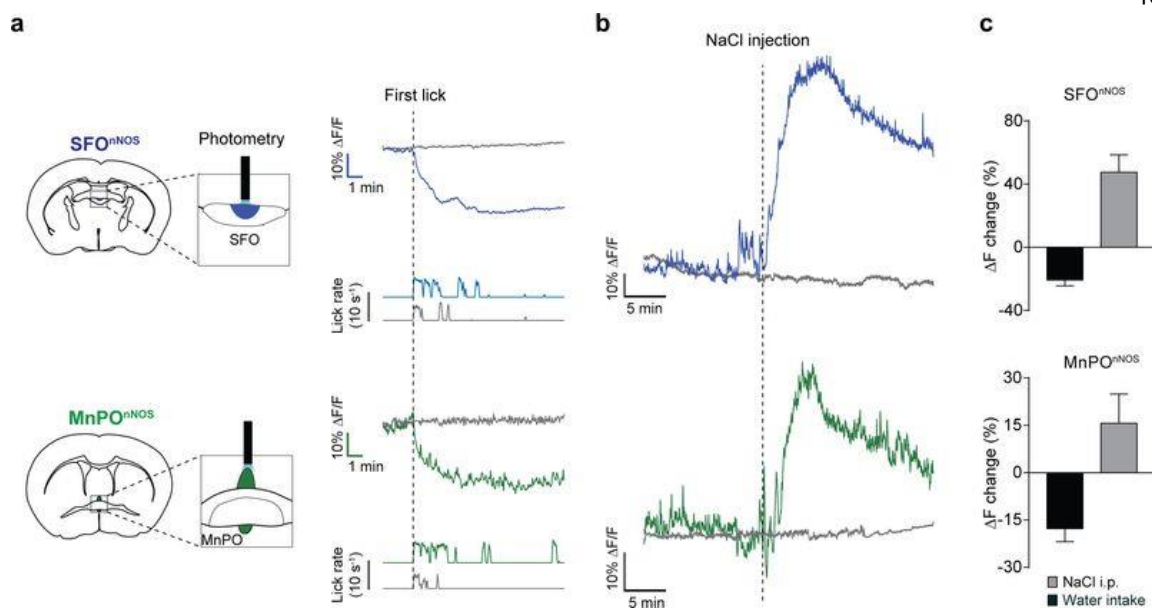
Extended Data Fig. 2

Extended Data Figure 2 : MnPO^{nNOS} neurons are necessary for the induction of drinking by SFO^{nNOS} photostimulation. a, Casp3-TEVp efficiently eliminates SFO^{nNOS} neurons (right) without affecting MnPO^{nNOS} neurons (left). c-Fos expression pattern is shown after water-restriction (red). **b,** Rastor plots representing licking events during the 5-s session with photostimulation. **c,** Ablation of MnPO^{nNOS} (MnPOx) but not SFO^{nNOS} (SFOx) neurons attenuated the drinking response to OVLT^{nNOS} photostimulation (left, 10 min, blue box). Quantification of the number of licks during the 10-min light-on period (right, $n = 9$ mice for controls and MnPOx and $n = 7$ mice for SFOx). **d,** 5-s brief-access assays to examine the necessity of MnPO^{nNOS} neurons. Acute inhibition of MnPO^{nNOS} neurons by CNO injection severely reduced SFO^{nNOS}-stimulated (left, $n = 5$ mice for CNO, $n = 3$ mice for vehicle, and $n = 6$ mice for no i.p.) and dehydration-induced water intake (middle, $n = 7$ mice for CNO, $n = 5$ mice for vehicle, and $n = 3$ mice for no i.p.). However, the same treatment did not suppress sucrose consumption (300 mM, right, $n = 6$ mice for CNO, $n = 5$ mice for vehicle, and $n = 3$ mice for no i.p.). Control mice transduced by AAV-DIO-mCherry in the MnPO showed no reduction after water or food-restriction ($n = 3$ mice). **e,** mCherry control for Fig. 1g. Cumulative water intake in nNOS-cre mice transduced with AAV-DIO-mCherry in the MnPO, AAV-DIO-ChR2-eYFP in the SFO under photostimulated (left, $n = 5$ mice) or water-restricted conditions (middle, $n = 6$ mice), and sucrose (300 mM) intake under food-restricted conditions (right, $n = 5$ mice). **f,** Intraperitoneal injection of mannitol robustly activated SFO^{nNOS} neurons with (red trace) or without (black trace) CNO injection (left). CNO injection drastically suppressed drinking behavior without changing the activity of SFO^{nNOS} neurons (middle, $n = 4$ mice). Plasma osmolality was increased by the injection of mannitol (right, $n = 5$ mice). $*P < 0.05$, $**P < 0.01$, by paired two-tailed t-test or Kruskal–Wallis one-way ANOVA test with Dunn's correction for multiple comparisons. All error bars and shaded areas show mean ± s.e.m. Scale bar, 50 μm.
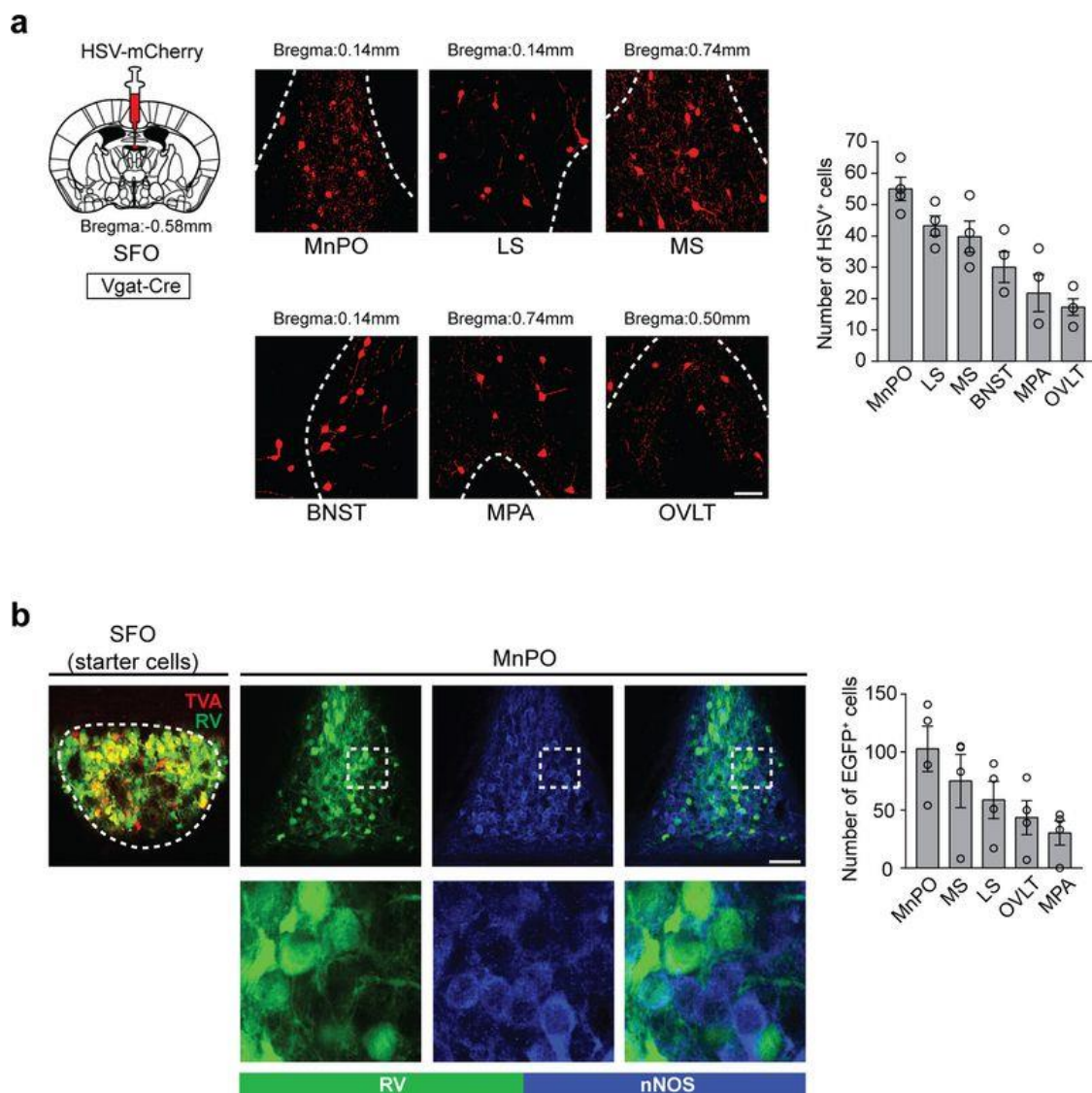
Extended Data Fig. 3

Extended Data Figure 3 : The SFO receives sparse monosynaptic input from MnPO^{nNOS} neurons. a, Left, schematic for the assessment of the MnPO^{nNOS} → SFO monosynaptic connection (left). Right, whole-cell patch-clamp recording from SFO neurons was performed with optogenetic stimulation of MnPO^{nNOS} → SFO projections. Excitatory synaptic currents were measured in the presence (red trace) or absence (black trace) of CNQX (10 μM) + DL-APV (25 μM) after photostimulation (2 ms, blue arrowheads). Most SFO^{nNOS} neurons (12 out of 16 cells, labelled with mCherry, middle panel) or SFO$^{non-nNOS}$ neurons (14 out of 16 cells, right panel) did not receive monosynaptic input from MnPO^{nNOS} neurons. **b,** Representative image (one out of three mice) of robust c-Fos expression (red) in the MnPO (top) but not in the SFO (bottom) by photostimulation of ChR2 expressing MnPO^{nNOS} neurons. Scale bar, 50 μm.
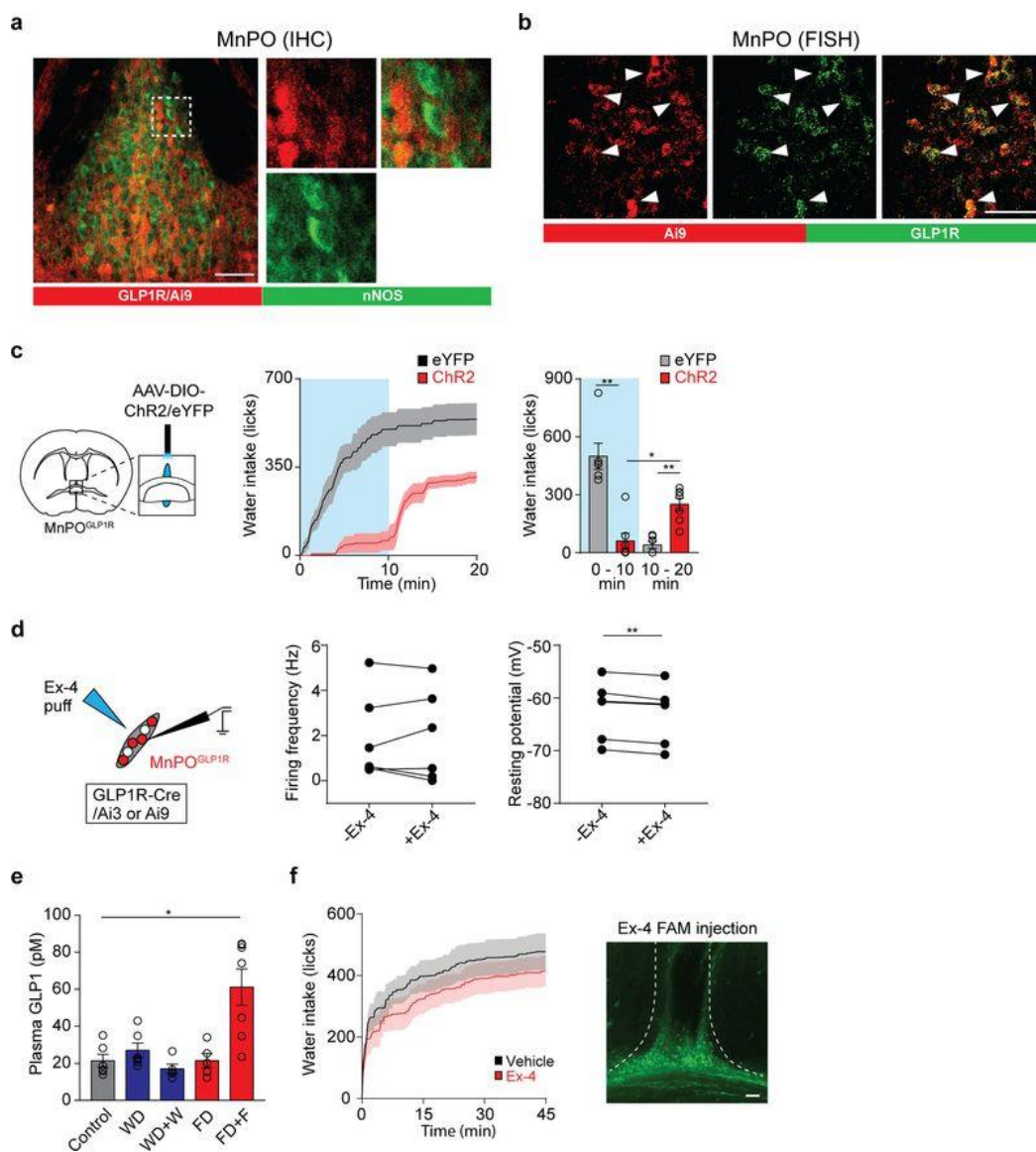
Extended Data Fig. 4

Extended Data Figure 4 : Neural dynamics of SFO^{nNOS} and MnPO^{nNOS} neurons. a, Left, Schematic of fiber photometry experiments from SFO^{nNOS} (top) and MnPO^{nNOS} (bottom) neurons. nNOS-cre mice were injected with AAV-FLEX-GCaMP6s or eYFP into the SFO and MnPO. Right, representative traces showing the real-time activity of the SFO^{nNOS} (blue trace) and MnPO^{nNOS} (green trace) populations with water intake in water-restricted mice. Grey traces show the activity of eYFP control mice. Corresponding lick patterns are also shown (lower traces). SFO^{nNOS} and MnPO^{nNOS} neurons are rapidly and persistently inhibited by water drinking. **b,** SFO^{nNOS} and MnPO^{nNOS} neurons are sensitive to thirst-inducing stimuli. Intraperitoneal injection of NaCl (2 M, 300 µl) in a water-satiated animal robustly activated SFO^{nNOS} (blue) and MnPO^{nNOS} (green) neurons. **c,** Quantification of the neuronal responses. During liquid intake (black bars, n = 4 mice for SFO, n = 6 mice for MnPO) and sodium loading (grey bars, n = 5 mice), both SFO^{nNOS} and MnPO^{nNOS} neurons showed opposite activity changes. All error bars show mean ± s.e.m.

Extended Data Fig. 5

Extended Data Figure 5 : Mapping of inhibitory inputs to the SFO. a, Left, a schematic for retrograde tracing of inhibitory inputs to the SFO by HSV-mCherry. Shown are the major inhibitory inputs to the SFO. Right, quantification of HSV-positive neurons (n = 4 mice). LS, lateral septum; MS, medial septum; BNST, bed nucleus of the stria terminalis; MPA, medial preoptic area. **b,** Monosynaptic retrograde rabies tracing of SFO[nNOS] neurons. Left, a representative image of the SFO of an nNOS-cre mouse transduced with AAV-CA-FLEX-RG and AAV-EF1a-FLEX-TVA-mCherry followed by EnvA G-deleted Rabies-eGFP. Right, almost no eGFP-positive neurons in the MnPO (green, $5.4 \pm 1.3\%$, n = 4 mice) overlapped with excitatory nNOS-expressing neurons (blue). Maximum inputs to the SFO[nNOS] neurons are from the MnPO, followed by the MS, LS, MPA and OVLT (n = 4 mice). All error bars show mean ± s.e.m. Scale bars, 50 μm. The mouse brain in this figure has been reproduced from the mouse brain atlas[45].

Extended Data Fig. 6

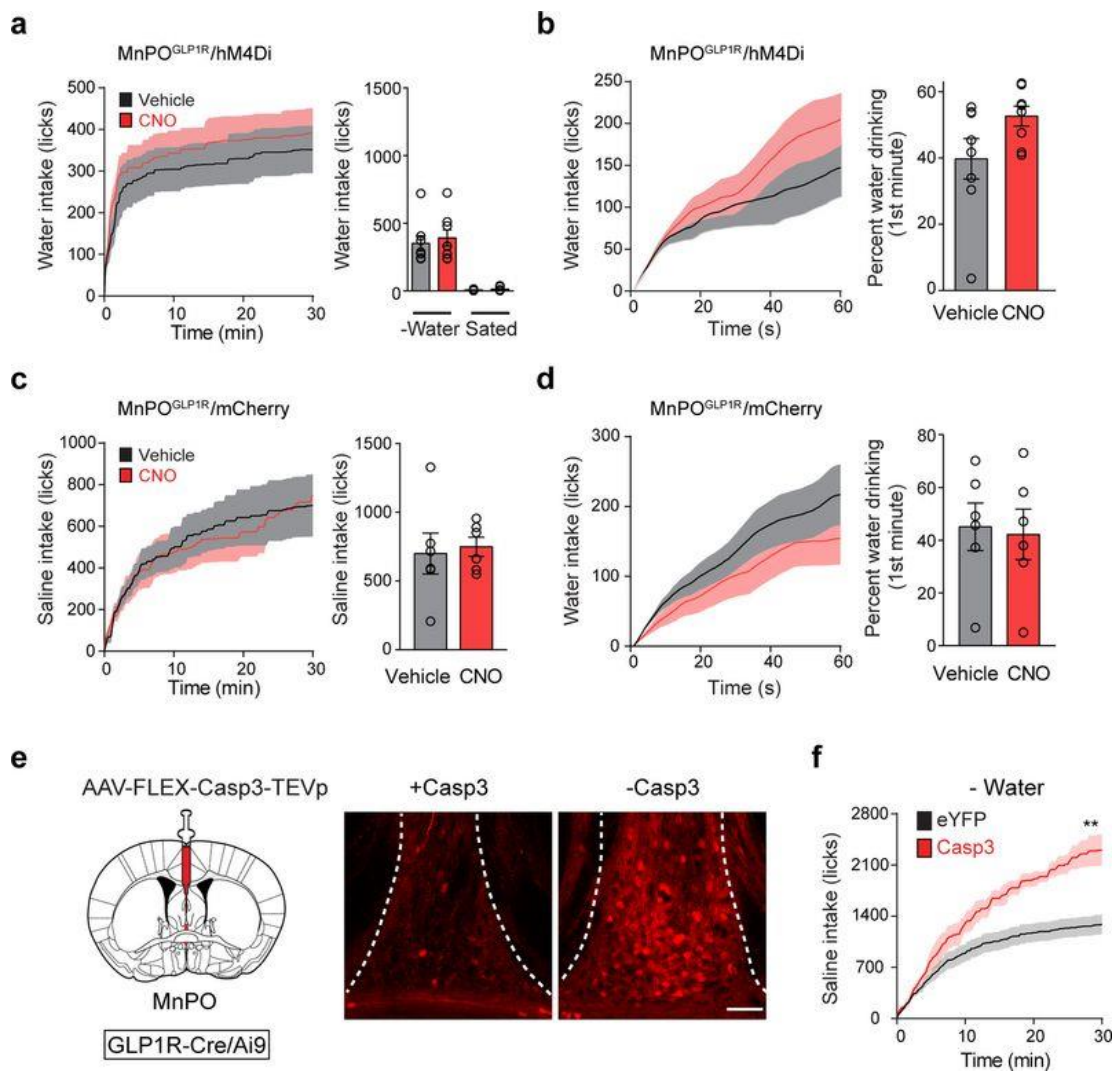**Extended Data Figure 6 : The MnPO^{GLP1R} population does not overlap with nNOS-expressing neurons. a,** nNOS antibody staining (green) of the MnPO from a Glp1r-cre/Ai9 transgenic mouse expressing tdTomato in MnPO^{GLP1R}neurons (red). No substantial overlap was observed between these populations ($4.3 \pm 0.9\%$ of GLP1R-expressing neurons, n = 3 mice). **b,** Fluorescence in situ hybridization (FISH) shows that a majority of Ai9 expression (red, $91.9 \pm 2.4\%$, n = 3 mice) closely overlaps with endogenous GLP1R expression (green). **c,** Left, a diagram showing optogenetic stimulation of MnPO^{GLP1R} neurons transduced with AAV-DIO-ChR2-eYFP or AAV-DIO-eYFP. Right, stimulation of ChR2-expressing MnPO^{GLP1R} neurons inhibited drinking after water restriction as compared to eYFP controls (n = 7 mice for ChR2, n = 6 mice for controls, blue box indicates the Light-ON period). For statistical analysis, we used the same dataset as for 0–10 min from Fig. 2e. **d,** GLP1 has minor effects on acute drinking behavior. A diagram of whole-cell recording from MnPO^{GLP1R} neurons is shown on the left. A GLP1 agonist, exendin-4 (Ex-4), had no effect on the firing frequency of MnPO^{GLP1R} neurons in brain slice preparation (middle, n = 6 neurons). However, there was a small decrease in the resting membrane potential (right, n = 6 neurons). **e,** Enzyme-linked immunosorbent assay analysis of plasma GLP1 levels. Feeding behavior induced robust plasma GLP1 secretion whereas water intake did not (n = 5 mice for WD + W and FD, n = 6 mice for control and WD, and n = 7 mice for FD + F). **f,** Left, intra-cranial injection of Ex-4 (red trace, n = 7 mice) into the MnPO had no effect on water intake after water deprivation as compared to vehicle injection (artificial cerebrospinal fluid, black trace, n = 7 mice). Right, a representative injection pattern visualized with fluorescent Ex-4 FAM. $*P < 0.05$, $**P < 0.01$, two-tailed Mann–Whitney Utest or paired t-test or Kruskal–Wallis one-way ANOVA test with Dunn's correction for multiple comparisons. All error bars and shaded areas show mean $\pm$ s.e.m. Scale bars, 50 μm.
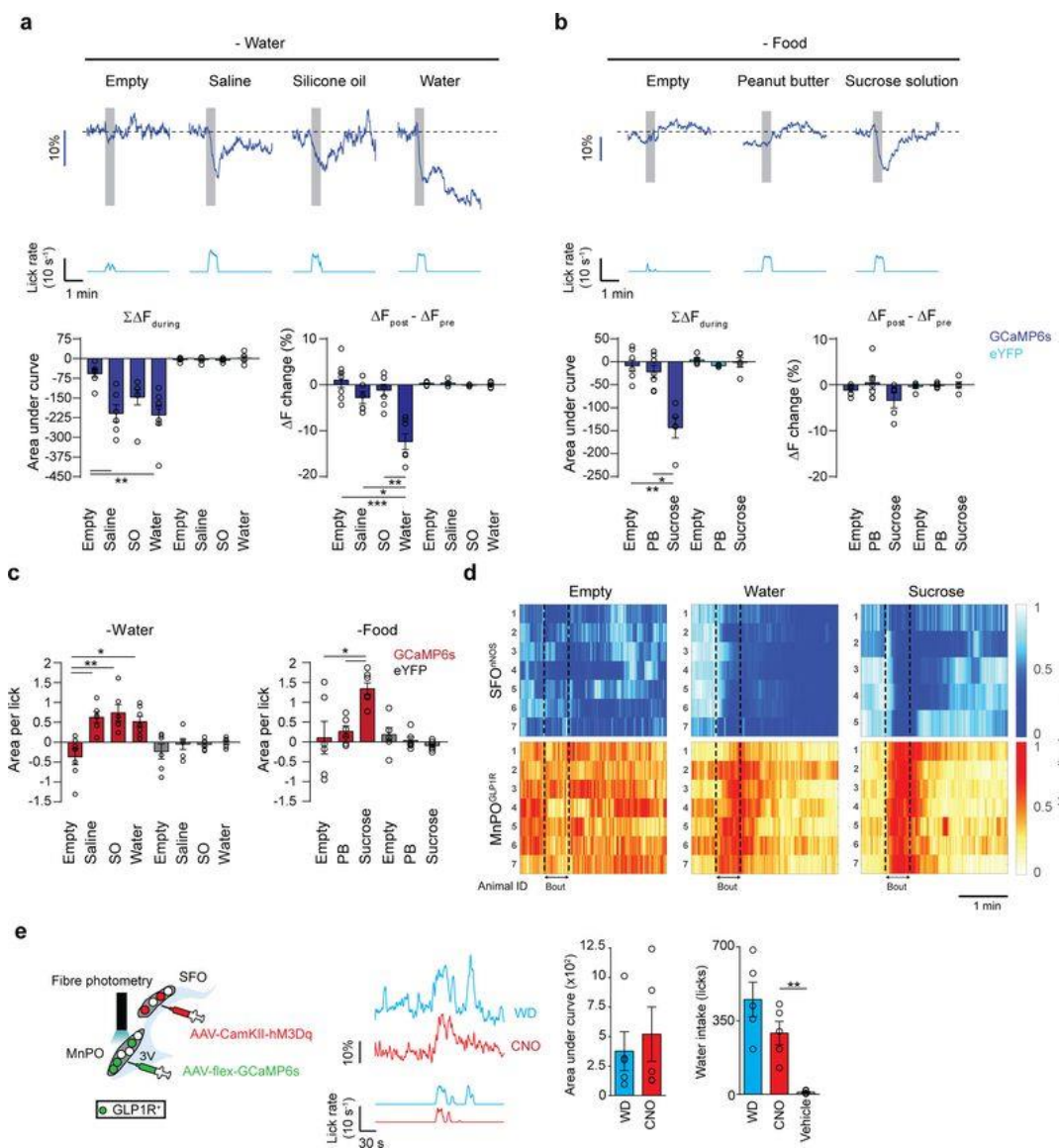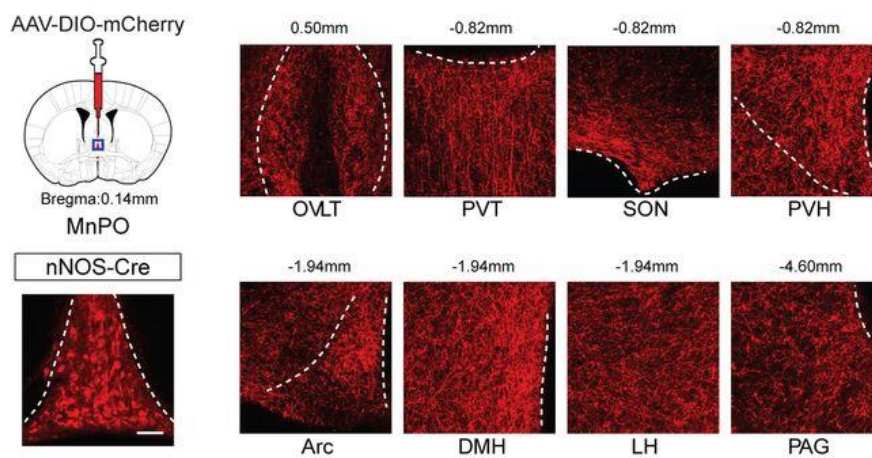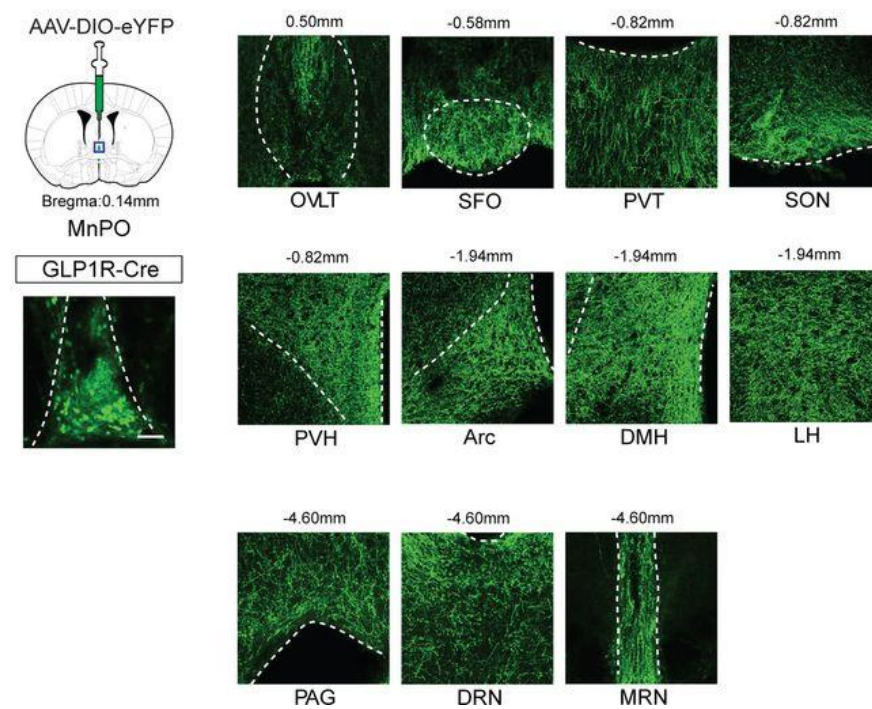
Extended Data Fig. 7

Extended Data Figure 7 : In vivo activation patterns of MnPO^{GLP1R} and SFO^{nNOS} neurons upon ingestion. a, SFO^{nNOS} neurons are negatively and chronically regulated by water drinking. Representative responses of SFO^{nNOS} (blue traces) to different types of liquids under water-restricted conditions: a control empty bottle, isotonic saline, silicone oil and water. Each stimulus was presented for 30 s (shaded box). Quantification of the responses is shown in the bottom panel. Activity change (left, area under curve) and baseline activity shift (right, ΔF change) were quantified for SFO^{nNOS} neurons (GCaMP6s, dark blue bars; control, light blue bars). A significant shift in the baseline activity (ΔF change) was observed only in response to water ingestion (n = 6 mice for saline, n = 7 mice for empty, silicone oil and water, n = 5 mice for eYFP). **b,** Shown are representative responses of SFO^{nNOS} neurons (blue traces) to an empty bottle, peanut butter, and 300 mM sucrose solution under food-restricted conditions (n = 7 mice for empty and peanut butter, n = 5 mice for sucrose, n = 5 mice for all eYFP recordings). **c,** Activity change per lick was quantified for MnPO^{GLP1R} neurons (GCaMP6s, red bars; eYFP, grey bars) under water-restricted conditions (left, n = 6 mice for saline and silicone oil, n = 7 mice for empty and water, n = 6 mice for all eYFP controls) and food-restricted conditions (right, n = 6 mice for empty and peanut butter, n = 7 mice for sucrose, n = 6 mice for all eYFP controls). All data were reanalyzed from Fig. 3b, c. **d,** Normalized fluorescence change of SFO^{nNOS} (top) and MnPO^{GLP1R} (bottom) neurons from individual mice during licking an empty bottle and water under water-restricted, or sucrose under food-restricted conditions. **e,** MnPO^{GLP1R} activation is independent of instinctive need. Left, fiber photometry recording of MnPO^{GLP1R} neurons while activating the SFO^{nNOS} neurons. GCaMP6s was virally expressed in MnPO^{GLP1R} neurons for recording calcium dynamics while activating SFO^{nNOS} neurons by hM3Dq-mCherry under the CamKII promoter. Middle, intraperitoneal CNO injection and water deprivation induce water drinking, which robustly activates MnPO^{GLP1R} neurons (red and blue traces respectively). Right, activity change (area under the curve) and licks were quantified for natural thirst and CNO activation (n = 5 mice). *$P < 0.05$, **$P < 0.01$, ***$P < 0.001$, paired two-tailed t-test or Kruskal–Wallis one-way ANOVA test with Dunn's correction for multiple comparisons. All error bars show mean ± s.e.m.

Extended Data Fig. 8

Extended Data Figure 8 : Acute inhibition or chronic ablation of MnPO^{GLP1R} neurons causes overdrinking. a, b, Acute inhibition of hM4Di-expressing MnPO^{GLP1R} neurons by CNO modestly increases water consumption at the onset of drinking. Drinking behaviour was monitored for 30 min after the injection of CNO (a); magnified data (0–1 min) is shown in b (n = 8 mice). **c, d,** mCherry controls for acute inhibition of MnPO^{GLP1R} neurons. Drinking behaviour was monitored for 30 min after the injection of CNO or vehicle under water-deprived conditions with free access to saline (c) or water (d). No significant difference was found between mice injected with CNO and vehicle (n = 6 mice). **e,** Schematic for the genetic ablation of MnPO^{GLP1R} neurons with AAV-flex-Casp3-TEVp (left) in Glp1r-cre/Ai9 mice. Compared to a control animal (right), a Casp3-injected animal displayed almost no GLP1R-expressing neurons in the MnPO (middle, representative image from one out of four mice). In both cases, GLP1R-expressing neurons were labelled using Glp1r-cre/Ai9 transgenic mice. **f,** Genetic ablation of MnPO^{GLP1R} neurons (red trace, n = 4 mice) recapitulates the overdrinking phenotype similar to the acute inhibition by hM4Di (Fig. 5b), compared to control eYFP group (black trace, n = 6 mice). **P < 0.01, by two-tailed Mann–Whitney U test. All error bars and shaded areas show mean ± s.e.m. Scale bar, 50 μm. The mouse brain in this figure has been reproduced from the mouse brain atlas[45].

a

AAV-DIO-mCherry

Bregma:0.14mm

MnPO

nNOS-Cre

0.50mm OVLT · -0.82mm PVT · -0.82mm SON · -0.82mm PVH

-1.94mm Arc · -1.94mm DMH · -1.94mm LH · -4.60mm PAG

b

AAV-DIO-eYFP

Bregma:0.14mm

MnPO

GLP1R-Cre

0.50mm OVLT · -0.58mm SFO · -0.82mm PVT · -0.82mm SON

-0.82mm PVH · -1.94mm Arc · -1.94mm DMH · -1.94mm LH

-4.60mm PAG · -4.60mm DRN · -4.60mm MRN

Extended Data Fig. 9

Extended Data Figure 9 : Neural projections from nNOS[+] and GLP1R^{+} MnPO neurons. a, b, Left, schematics for mapping downstream targets of MnPO neurons using AAV-DIO-mCherry **(a)** or AAV-DIO-eYFP **(b)**. Right, the major outputs from MnPO neurons. nNOS-cre **(a)** and Glp1r-cre **(b)** mice were injected with AAV-DIO-mCherry and AAV-DIO-eYFP in the MnPO respectively, and the axon projections were examined using reporter expression. Shown are the injection sites and main representative downstream targets (one out of three mice). Arc, Arcuate Nucleus; DMH, dorsomedial hypothalamic nucleus; DRN, dorsal raphe nucleus; LH, lateral hypothalamus; MRN, median raphe nucleus; PAG, periaqueductal gray; PVH, paraventricular hypothalamic nucleus; PVT, paraventricular thalamic nucleus; SON, supraoptic nucleus. Scale bars, 50 μm. The mouse brain in this figure has been reproduced from the mouse brain atlas[45].

REFERENCES

1   Ramsay, D. J. and Booth, D. Thirst: Physiological and Psychological Aspects. Chapters 5, 6, 9-12, and 19 (Springer-Verlog, 1991).

2   Bourque, C. W. Central mechanisms of osmosensation and systemic osmoregulation. Nature reviews. Neuroscience 9, 519-531, doi:10.1038/nrn2400 (2008).

3   Fitzsimons, J. Angiotensin, thirst, and sodium appetite. Physiological reviews 78, 583-686 (1998).

4   McKinley, M. J. & Johnson, A. K. The physiological regulation of thirst and fluid intake. News Physiol Sci 19, 1-6 (2004).

5   Johnson, A. K. & Gross, P. M. Sensory circumventricular organs and brain homeostatic pathways. FASEB journal : official publication of the Federation of American Societies for Experimental Biology 7, 678-686 (1993).

6   Saker, P. et al. Regional brain responses associated with drinking water during thirst and after its satiation. Proceedings of the National Academy of Sciences 111, 5379-5384 (2014).

7   Seckl, J. R., Williams, T. D. & Lightman, S. L. Oral hypertonic saline causes transient fall of vasopressin in humans. Am J Physiol 251, R214-217 (1986).

8   Stricker, E. M. & Hoffmann, M. L. Presystemic signals in the control of thirst, salt appetite, and vasopressin secretion. Physiology & behavior 91, 404-412, doi:10.1016/j.physbeh.2007.04.007 (2007).

9   Thrasher, T. N., Nistal-Herrera, J. F., Keil, L. C. & Ramsay, D. J. Satiety and inhibition of vasopressin secretion after drinking in dehydrated dogs. Am J Physiol 240, E394-401 (1981).

10   Zimmerman, C. A. et al. Thirst neurons anticipate the homeostatic consequences of eating and drinking. Nature 537, 680-684 (2016).

11   Farrell, M. J. et al. Cortical activation and lamina terminalis functional connectivity during thirst and drinking in humans. Am J Physiol-Reg I 301, R623-R631, doi:10.1152/ajpregu.00817.2010 (2011).

12   Gizowski, C. & Bourque, C. W. The neural basis of homeostatic and anticipatory thirst. Nat Rev Nephrol, doi:10.1038/nrneph.2017.149 (2017).

13   Andermann, M. L. & Lowell, B. B. Toward a Wiring Diagram Understanding of Appetite Control. Neuron 95, 757-778, doi:10.1016/j.neuron.2017.06.014 (2017).

14   Sternson, S. M. Hypothalamic survival circuits: blueprints for purposive behaviors. Neuron 77, 810-824 (2013).

15   Zimmerman, C. A., Leib, D. E. & Knight, Z. A. Neural circuits underlying thirst and fluid homeostasis. Nature reviews. Neuroscience 18, 459-469, doi:10.1038/nrn.2017.71 (2017).

16   Denton, D. A., McKinley, M. J. & Weisinger, R. S. Hypothalamic integration of body fluid regulation. Proc Natl Acad Sci U S A 93, 7397-7404 (1996).

17   McKinley, M. J. et al. The sensory circumventricular organs of the mammalian brain. Advances in anatomy, embryology, and cell biology 172, 1-122 (2003).

18   Allen, W. E. et al. Thirst-associated preoptic neurons encode an aversive motivational drive. Science 357, 1149-1155, doi:10.1126/science.aan6747 (2017).

19   Oka, Y., Ye, M. & Zuker, C. S. Thirst driving and suppressing signals encoded by distinct neural populations in the brain. Nature, doi:10.1038/nature14108 (2015).

20   Simpson, J. B. & Routtenberg, A. Subfornical organ: site of drinking elicitation by angiotensin II. Science 181, 1172-1175 (1973).

21   Smith, P. M., Beninger, R. J. & Ferguson, A. V. Subfornical organ stimulation elicits drinking. Brain research bulletin 38, 209-213 (1995).

22   Betley, J. N. et al. Neurons for hunger and thirst transmit a negative-valence teaching signal. Nature 521, 180-185, doi:10.1038/nature14416 (2015).

23   Nation, H. L., Nicoleau, M., Kinsman, B. J., Browning, K. N. & Stocker, S. D. DREADD-induced activation of subfornical organ neurons stimulates thirst and salt appetite. Journal of neurophysiology 115, 3123-3129 (2016).

24   Abbott, S. B., Machado, N. L., Geerling, J. C. & Saper, C. B. Reciprocal Control of Drinking Behavior by Median Preoptic Neurons in Mice. J Neurosci 36, 8228-8237, doi:10.1523/JNEUROSCI.1244-16.2016 (2016).

25   Matsuda, T. et al. Distinct neural mechanisms for the control of thirst and salt appetite in the subfornical organ. Nature neuroscience 20, 230-241, doi:10.1038/nn.4463 (2017).

26   Miselis, R. R., Shapiro, R. E. & Hand, P. J. Subfornical organ efferents to neural systems for control of body water. Science 205, 1022-1025 (1979).

27   Boyden, E. S., Zhang, F., Bamberg, E., Nagel, G. & Deisseroth, K. Millisecond-timescale, genetically targeted optical control of neural activity. Nature neuroscience 8, 1263-1268 (2005).

28   Wickersham, I. R. et al. Monosynaptic restriction of transsynaptic tracing from single, genetically targeted neurons. Neuron 53, 639-647, doi:10.1016/j.neuron.2007.01.033 (2007).

29   Yang, C. F. et al. Sexually dimorphic neurons in the ventromedial hypothalamus govern mating in both sexes and aggression in males. Cell 153, 896-909, doi:10.1016/j.cell.2013.04.017 (2013).

30   Roth, B. L. DREADDs for Neuroscientists. Neuron 89, 683-694, doi:10.1016/j.neuron.2016.01.040 (2016).

31   Lerner, T. N. et al. Intact-brain analyses reveal distinct information carried by SNc dopamine subcircuits. Cell 162, 635-647 (2015).

32   Richards, P. et al. Identification and characterization of GLP-1 receptor-expressing cells using a new transgenic mouse model. Diabetes 63, 1224-1233, doi:10.2337/db13-1440 (2014).

33   Petreanu, L., Huber, D., Sobczyk, A. & Svoboda, K. Channelrhodopsin-2-assisted circuit mapping of long-range callosal projections. Nature neuroscience 10, 663-668, doi:10.1038/nn1891 (2007).

34   McKay, N. J., Galante, D. L. & Daniels, D. Endogenous glucagon-like peptide-1 reduces drinking behavior and is differentially engaged by water and food intakes in rats. Journal of Neuroscience 34, 16417-16423 (2014).

35   Betley, J. N., Cao, Z. F., Ritola, K. D. & Sternson, S. M. Parallel, redundant circuit organization for homeostatic control of feeding behavior. Cell 155, 1337-1350, doi:10.1016/j.cell.2013.11.002 (2013).

36   Cunningham, J. T., Beltz, T., Johnson, R. F. & Johnson, A. K. The effects of ibotenate lesions of the median preoptic nucleus on experimentally-induced and circadian drinking behavior in rats. Brain research 580, 325-330 (1992).

37   McKinley, M., Mathai, M., Pennington, G., Rundgren, M. & Vivas, L. Effect of individual or combined ablation of the nuclear groups of the lamina terminalis on water drinking in sheep. American Journal of Physiology-Regulatory, Integrative and Comparative Physiology 276, R673-R683 (1999).

38   McKinley, M. J. et al. The median preoptic nucleus: front and centre for the regulation of body fluid, sodium, temperature, sleep and cardiovascular homeostasis. Acta physiologica 214, 8-32, doi:10.1111/apha.12487 (2015).

39   Oka, Y., Butnaru, M., von Buchholtz, L., Ryba, N. J. & Zuker, C. S. High salt recruits aversive taste pathways. Nature 494, 472-475 (2013).

40   Yarmolinsky, D. A., Zuker, C. S. & Ryba, N. J. Common sense about taste: from mammals to insects. Cell 139, 234-244, doi:10.1016/j.cell.2009.10.001 (2009).

41   Zocchi, D., Wennemuth, G. & Oka, Y. The cellular mechanism for water detection in the mammalian taste system. Nature neuroscience (2017).

42   Thrasher, T. N., Keil, L. C. & Ramsay, D. J. Drinking, oropharyngeal signals, and inhibition of vasopressin secretion in dogs. American Journal of Physiology-Regulatory, Integrative and Comparative Physiology 253, R509-R515 (1987).

43   Krashes, M. J. et al. An excitatory paraventricular nucleus to AgRP neuron circuit that drives hunger. Nature 507, 238-242, doi:10.1038/nature12956 (2014).

44   Kahles, F. et al. GLP-1 secretion is increased by inflammatory stimuli in an IL-6-dependent manner, leading to hyperinsulinemia and blood glucose lowering. Diabetes 63, 3221-3229, doi:10.2337/db14-0100 (2014).

45   Paxinos, George, and Keith BJ Franklin. The mouse brain in stereotaxic coordinates. Second edition, Academic Press (2001).

Chapter 2

PERIPHERAL AND CENTRAL NUTRIENT SENSING UNDERLYING APPETITE REGULATION

SUMMARY

The precise regulation of fluid and energy homeostasis is essential for survival. It is well appreciated that ingestive behaviors are tightly regulated by both peripheral sensory inputs and central appetite signals. With recent neurogenetic technologies, considerable progress has been made in our understanding of basic taste qualities, the molecular and/or cellular basis of taste sensing, and the central circuits for thirst and hunger. In this chapter, I first highlight the functional similarities and differences between mammalian and invertebrate taste processing. I then discuss how central thirst and hunger signals interact with peripheral sensory signals to regulate ingestive behaviors. I finally indicate some of the directions for future research.

HIGHLIGHTS

Vertebrates and invertebrates use similar cellular logic for taste detection. Cells and receptors for most individual taste qualities have been discovered, but mechanisms of sour taste are not yet fully understood.

Interoceptive neurons for hunger and thirst receive extensive modulation by both internal state and peripheral sensory cues.

The valence of sensory stimuli is modulated by the internal body environment. Recent studies have begun to dissect the underlying neural circuits, which involve the thalamus, the amygdala, and the insular cortex.

Multiple motivational drives are processed in the brain, resulting in the selection of the final behavioral path. Emerging anatomical evidence indicates potential sites of this interaction, including (but not limited to) the parabrachial nucleus and periaqueductal gray.

SENSING INTERNAL AND EXTERNAL NUTRIENT FACTORS

Animals continuously lose water and energy by various physiological processes, such as sweating, urination, and basal metabolic activity[1, 2, 3]. To compensate for such losses, animals must ingest sufficient water and food from external sources at appropriate times[1, 4]. The maintenance of this in-and-out balance represents a key homeostatic function for survival in all organisms. After several decades of studies, it is now evident that this homeostatic regulation is finely controlled at the entire organism level, including the peripheral sensory system, brain appetite circuits, the autonomic nervous system, and the endocrine system (Box 1)[4, 5, 6, 7]. Clarifying the interactions between each of the regulatory systems remains an active research area. The initiation of consummatory behaviors relies heavily on two major sensory mechanisms, that is, peripheral taste system[6, 8], and central interoceptive system[4]. In this chapter, I describe recent progress in peripheral and central nutrient-sensing mechanisms, focusing on functional similarities between invertebrate and vertebrate systems. I also discuss potential mechanisms by which central appetite circuits modulate sensory valence.

VERTEBRATE AND INVERTEBRATE TASTE SYSTEMS: FUNCTIONAL SIMILARITIES AND DISSIMILARITIES

Sweet, Umami, and Bitter: Taste Qualities Hardwired to Attractive and Aversive Behaviors

Sweet and umami tastes are associated with sugars and L-amino acids, respectively, both of which are palatable taste qualities for animals. Conversely, the aversive bitter taste is generally evoked by toxic chemicals that are hazardous to animals [6, 8.] The receptors, cells, and signaling cascades for these three taste qualities have been well studied (for the relevant receptors of these and the other taste qualities, see Figure 1). In vertebrates, sweet and umami compounds are sensed by specific sets of G-protein-coupled receptors (GPCRs), called T1Rs (see Glossary)[9, 10, 11, 12, 13]. A combination of T1R2 and T1R3

subunits detects sugars, whereas T1R1 and T1R3 subunits function as the receptor for L-amino acids. Genetic studies support these findings. For instance, knocking out the T1R2 gene selectively abolishes taste responses in the chorda tympani nerves as well as behavioral attraction toward sweet substances[12]. By contrast, T1R3 knockout (KO) animals show drastically reduced sensitivity to both sweet and umami[12]. These studies demonstrated that T1R3 functions as a co-receptor for sweet and umami tastes.

Bitter taste is recognized by T2Rs that belong to another GPCR family[14, 15, 16, 17]. Unlike T1Rs, individual bitter-sensing taste receptor cells (TRCs) express multiple T2Rs, each of which recognizes a unique set of bitter compounds. This multiplex receptor expression pattern allows animals to detect a variety of bitter compounds through a single type of taste receptor cell. While the functions of T1Rs and T2Rs are widely accepted, there are significant genetic variations across animal species. For instance, T1R2 is pseudogenized in cats, which may be causally linked to their inability to taste sweet stimuli[18]. Dolphins and whales have a premature stop codon in all T1R1s and some T2Rs, resulting in a loss of functional taste receptors[19, 20]. These genomic data suggest that taste receptor genes in each species have evolved to adapt to their specific environments.

At the cellular level, sweet (T1R2+3), umami (T1R1+3), and bitter taste receptors (T2Rs) are expressed in distinct TRC populations on the tongue[6, 21]. Because of this anatomical segregation, each taste quality is mediated by distinct types of TRC. An elegant study using synthetic ligand–receptor pair (RASSL) demonstrated that the taste quality is encoded by the activity of TRCs, but not by taste compounds or receptor activity[12].

Studies in invertebrate species, mainly Drosophila melanogaster, have revealed a similar coding logic of the taste system between vertebrates and invertebrates (Figure 1)[22, 23]. Taste receptors in insects are expressed in the proboscis, an organ equivalent to the tongue in mammals, as well as in multiple body parts, including the wings and legs[24, 25]. In individual sensilla, generally one to four gustatory receptor (GR) neurons (GRNs) are housed, each specialized to detect one basic taste quality, as in mammals. The insect taste receptors

belong to the GR and ionotoropic receptor (IR) families[26, 27]. Sweet and bitter tastes are mainly detected by distinct sets of GR expressed in sweet- and bitter-sensing neurons[6, 23]. Interestingly, multiple Grs are expressed by sugar- and bitter-sensing neurons, and individual Grs recognize different sugars and bitter compounds. For instance, sweet receptors Gr5a and Gr64a are co-expressed in a subset of gustatory neurons that are distinct from Gr66a-expressing bitter-sensing neurons[28]. Gain-of-function studies for individual neural populations have shown that the stimulation of $Gr5^+$ sweet neurons induces appetitive behaviors, whereas activation of $Gr66a^+$ bitter neurons drives avoidance[29, 30]. These results suggest that, as in the mammalian taste system, the sweet (attractive) and bitter (aversive) tastes in invertebrates are hardwired to anatomically distinct neurons. A recent study using behavioral and optical imaging showed that a combination of Ir76b and Ir20a is involved in amino acid sensing[31]. Intriguingly, Ir76b alone has been indicated as a salt taste receptor, as discussed below[32].

Salt and Water Tastes for Body Fluid Homeostasis

Salt and water tastes have essential roles in body fluid homeostasis by providing the ability to detect external sodium and water. These two taste qualities are fundamentally different from other tastes, such as sweet, umami, and bitter, in that the valence of salt and water alters based on internal state. For example, sodium strongly attracts salt-seeking (i.e., sodium deprived) animals, but the same stimuli have little attractive effect on sodium-satiated animals[33, 34]. Recent studies have unveiled the sensing mechanisms of salt and water tastes in both mammals and insects (Figure 1).

Salt Taste

There are two important characteristics of salt taste. First, behavioral preference to salt is a bell-shaped curve depending on its concentration[35]. Second, salt attraction is specific towards sodium salts, while aversion is induced by any salts[36]. Generally, moderate concentrations of sodium (around 200 mM) are most appetitive to animals, while higher

salt concentrations (over 400 mM for monovalent salts) drive aversive behavior under salt-satiated conditions[34]. These two-opposing behavioral responses are mediated by molecularly and anatomically distinct pathways in the taste system. In mice, the epithelial sodium channel (ENaC) functions as the low salt receptor[33, 37], and knocking out of the gene encoding the ENaCα subunit abolishes behavioral attraction and taste nerve response to low salt without affecting high-salt aversive responses[33]. Functional ENaC is expressed in a unique set of TRCs that are distinct from those for other taste qualities. Interestingly, high salt does not activate its own taste population, but rather it appears to co-opt other taste pathways in mice[34]. In addition to the attractive ENaC pathway, higher concentrations of salt recruit additional pathways, including bitter and acid (sour)-sensing TRCs. Consequently, salt preference is regulated by attractive (ENaC) and aversive (mainly bitter) signals depending on salt concentration.

In Drosophila, recent studies suggested that Ir76b is involved in sodium attraction by forming a Na+ leak channel[32]. In addition, members of the ENaC family, ppk11 and ppk19, contribute to attractive salt responses in larvae[38]. However, it is still elusive how these putative channels functionally interact with each other in salt-sensitive GRNs. Analogous to the mammalian system, bitter GRNs have been shown to respond to high concentrations of salts[23].

Water Taste

Water is one of the well-established taste qualities in insects[39, 40, 41]. In Drosophila, water taste is mediated by a specific subset of GRNs expressing ppk28, a member of the Degenerin/epithelial sodium channel family (Deg/ENaC) family[41, 42]. Functional analyses in cell culture system revealed that ppk28 functions as a hypo-osmolality sensor[41]. While flies lacking ppk28 exhibit reduced water consumption, they retain normal water-seeking ability under thirsty conditions using hygrosensation (vapor detection)[43]. These data suggested that the taste system has a critical function for water detection, but can be compensated by additional water detection mechanisms.

Compared with insects, less is known about how water is sensed by the mammalian taste system. Electrophysiological studies since the 1940s have demonstrated that pure water can stimulate taste nerves in various vertebrate species, such as frogs, cats, and dogs[44]. However, the question of whether vertebrates can sense water as an independent taste quality has not yet been resolved. Some key issues in this context are that: (i) water does not evoke a unique taste sensation in humans; and (ii) no dedicated cells and molecules have been found. A recent study revisited this question using advanced genetic tools to address whether water is sensed by a specific type of TRCs[45]. Unexpectedly, the application of pure water on the tongue selectively stimulated acid-sensing taste cells expressing PKD2L1, a member of the TRP channel family. Moreover, optogenetic stimulation of PKD2L1-expressing TRCs triggered attractive licking behavior in thirsty mice, indicating that this population, at least in part, carries the information of external water. However, the molecular mechanisms of water detection in PKD2L1-expressing TRCs remain unclear. In addition, how water and acid (sour) tastes are encoded by the same TRC population needs to be addressed.

Sour Taste for Sensing Acidity

Sour is a unique taste quality evoked by protons in various acidic compounds. At the cellular level, acids are sensed by PKD2L1-expressing TRCs in mammals (Figure 1)[46, 47]. Silencing or ablating this population eliminates acid responses in taste nerves[45, 46]. By contrast, there are still several unsolved conundrums at the behavioral and molecular levels. First, eliminating acid taste responses does not affect acid aversion[45, 48]. These observations may indicate that 'sour' perception or aversion is a combination of taste and nontaste signals, for example via the trigeminal system[49]. Second, various candidate acid sensors have been proposed over the past decades, such as acid-sending ion channels (ASICs), Hyperpolarization-activated cyclic-nucleotide-gated (HCN) channels, and PKD2L1/1L3 [47, 50, 51, 52]. However, gene KO studies did not support the idea that these molecules are the main acid sensor in taste buds. Recently, an acid-sensitive potassium channel (KIR2.1) and

a H+ selective ion channel (Otopetrin 1) were shown to mediate acid responses in PKD2L1-expressing TRCs[53, 54]. Whether these channels are involved in behavioral aversion to acids remains to be tested.

In Drosophila, a subset of GRNs (sour GRNs) that express Ir76b and Ir25a mediate acid sensing[55]. In addition, low pH also affects the activity of bitter and sweet gustatory neurons [56], suggesting complex sour-sensing mechanisms in flies. It is notable that Ir76b appears to have diverse functions in multiple taste qualities, including salt (Ir76b[32]), sour (Ir76b+25a[55]), and amino acids (Ir76b+20a[31]). A caveat is that other IRs or channels are involved in processing of each of the tastes. For instance, ectopic expression of Ir20a in salt-sensitive (Ir76b+) cells is not sufficient to confer amino acid sensitivity[31], indicating that additional components may be required to form functional taste receptors or channels in GRNs.

Taken together, vertebrate and invertebrate species appear to use analogous taste-sensing strategies despite the molecular diversity of taste receptors. They have similar sets of basic taste qualities: bitter and sweet/umami for sensing the hedonic value of food; salt and water for body fluid homeostasis; and sour for detecting external acidity. Individual taste qualities are generally encoded by anatomically segregated cell populations in taste organs. It would be interesting to elucidate how the molecularly dissimilar taste receptors and channels have evolved to achieve similar functions across species.

CENTRAL MECHANISMS FOR SENSING INTERNAL WATER AND ENERGY BALANCE

The main function of the taste system is to detect environmental information and send it to the central nervous system. However, peripheral sensory information is intensely modulated by internal body state. Recent studies have pinpointed neurons that control appetite by sensing internal fluid and energy balance. These central interoceptive neurons are uniquely located outside the blood–brain barrier (BBB), and send their information to

downstream circuits to regulate ingestive behaviors. The neural basis of appetite regulation has been discussed by several recent reviews[1, 4, 7, 57, 58]. Here, I briefly describe current understanding of neurons and circuits for appetite regulation (Box 2).

Sensing Water Balance and Regulating Thirst

The lamina terminalis (LT) in the forebrain is the main brain structure that monitors internal water balance by detecting blood tonicity and dipsogenic hormones, such as angiotensin (ANGII)[1, 7, 59, 60]. This region contains three nuclei: the subfornical organ (SFO), vascular organ of lamina terminalis (OVLT), and median preoptic nucleus (MnPO), where the former two structures lack the normal BBB. It has been shown that stimulation of excitatory neurons in the SFO expressing neuronal nitric oxide synthase (nNOS) and a transcription factor, ETV1, rapidly drives drinking (within few seconds), while stimulation of the GABAergic population specifically suppresses thirst[61, 62]. More recently, additional genetic markers for thirst neurons in individual LT nuclei have been found[63, 64]. It has also been shown that the excitatory neurons within the LT form a hierarchical neural architecture, with the MnPO being its final output[65]. At the molecular level, changes in blood osmolality and ANGII are stimulators of SFO^{nNOS} and OVLT neurons. It has been demonstrated that an ANGII receptor, Agtr1a is highly enriched in the LT, likely mediating ANGII-induced drinking[1, 62, 64]. By contrast, the molecular basis of osmotic and/or sodium sensing in the LT remains unsolved. Multiple ion channels have been proposed as candidate osmolality sensors, including TRPV1 and TRPV4[66, 67]. For example, OVLT neurons in TRPV1 KO mice exhibit compromised responses to hypertonic stimuli in acute brain slice preparations. However, a study in TRPV1/TRPV4 double KO animals showed normal water intake and neural activity (measured by c-Fos expression) in the LT following a hyperosmotic challenge in vivo[68]. These findings indicate the existence of redundant mechanisms for osmolality sensing in the LT, which may compensate for the absence of TRPV1/TRPV4 channels.

Sensing Energy Balance and Hunger Regulation

Two distinct neural populations in the arcuate nucleus (Arc) have critical roles in regulating energy balance and feeding behavior: one population expressing Agouti-related protein (AgRP) and another population expressing proopiomelanocortin (POMC)-derived peptide[4]. A recent study demonstrated that most AgRP neurons but not POMC neurons are located outside the BBB and exposed to the bloodstream[69], showing that the AgRP population is the primary sensor of internal energy state in the Arc. Both ablation and neural manipulation studies have established that the activity of AgRP neurons is necessary and sufficient to orchestrate normal eating behavior[70, 71, 72, 73]. AgRP neurons sense various hunger-related blood-borne factors. One such factor is ghrelin, which is a hunger-inducing hormone secreted from the stomach when it is empty[74, 75]. Under hungry conditions, this peptide activates AgRP neurons through the ghrelin receptor, GHS-R, driving animals to eating behavior[75, 76, 77]. Recent studies demonstrated that many other factors, such as insulin, leptin, and glucose, affect the activity of AgRP and POMC neurons[78, 79, 80, 81].

Anticipatory Nature of Hunger and Thirst

Classical models of homeostasis posited a passive feedback loop: internal energy and water deficit drives ingestive behavior, and the behavior ceases when internal state recovers. In addition to this classical scheme, recent studies have shed light on several 'active' feed-forward signals driven by peripheral sensory cues, highlighting their anticipatory nature (Figure 2A)[61, 65, 82, 83, 84, 85]. AgRP neurons rapidly decrease their activity both in response to nutrient ingestion 86, 87 and during anticipation of food reward in hungry mice[61, 82], while POMC neurons show an increased activity during ingestive behavior (Figure 2B)[82, 88]. Specific GABAergic neurons in the dorsomedial hypothalamic nucleus contribute to the rapid inhibition of AgRP neurons[89]. Somewhat analogously, thirst neurons in the LT and vasopressin neurons in the supraoptic nucleus are suppressed with drinking onset under thirsty conditions (Figure 2C)[65, 84, 85, 90]. The former population is causally linked to drinking behavior, while the latter population is involved in thirst-associated vasopressin release (direct involvement in drinking has not been tested). It was recently found that drinking action itself stimulates a specific inhibitory population of the MnPO, marked by

the glucagon-like peptide-1 receptor (GLP1R), which in turn sends monosynaptic inhibition to thirst driving SFO^{nNOS} neurons[65]. This neural circuit appears to mediate drinking-induced rapid thirst alleviation before systemic fluid recovery. These rapid feed forward signals are proposed to help animals match their intake to the homeostatic need on a real-time basis.

POTENTIAL NEURAL MECHANISMS OF TOP-DOWN CONTROL OF SENSORY VALENCE

Putative Pathways from Interoceptive Neurons to the Cortex

According to the incentive motivation theory, the valence of sensory stimuli is dependent on the internal state[91, 92, 93]. However, the neural mechanisms underlying such internal state-dependent valence shifts are still largely unclear and remain an active research area (Box 3). Here, I summarize evidence on neural pathways that process appetite and sensory signals, and describe potential mechanisms of top-down control of the representation and valence of sensory stimuli.

Thirst

Anatomical tracing from the LT in rodents revealed that the LT sends information to the insular (InsCtx) and cingulate cortex via the mid-thalamus[94]. Reciprocal connections also exist between the mid-thalamus and the cortical sites, forming a thalamocortical loop that modulates viscerosensory reflexes and behavior[95]. Consistently, optogenetic stimulation of the excitatory projection from the MnPO to the paraventricular thalamic nucleus (PVT) elicited robust water intake[64, 90]. These results suggest that the thalamus serves as a key relay point of the signals from the LT to the cortex. In rhesus monkeys, the electrical stimulation of the anterior-mid cingulate cortex (ACC) elicited time-locked water intake[96]. Neuroimaging (fMRI and PET) studies in humans have also revealed a strong correlation between the subjective perception of thirst and the cortical activity (ACC, posterior

cingulate cortex, and InsCtx)[97, 98, 99, 100]. Collectively, studies from rodents to primates indicate potential information flow: the LT detects deviations from the homeostatic set-point, which is relayed to higher cortical areas through the mid-thalamic nuclei (interoceptive LT → thalamus → ACC/InsCtx), where the subjective feeling of thirst is likely encoded (Figure 3A).

Hunger

Human fMRI studies demonstrated that various brain areas, including the prefrontal cortex, thalamus, and InsCtx, are activated in response to food-associated cues under hungry conditions[101]. These functional data are supported by anatomical studies in mice using virus tracing from AgRP neurons in the Arc[102]. Among afferent projections from AgRP neurons, inputs to the bed nucleus of the stria terminalis, paraventricular hypothalamic nucleus, lateral hypothalamus (LH), and PVT are individually sufficient to drive voracious feeding[103]. Therefore, this study suggested a model in which feeding behavior is regulated by a parallel-circuit architecture in the brain. Further genetically defined circuit mapping has revealed that information from AgRP neurons is transmitted to the InsCtx via the PVT and basolateral amygdala (BLA) (AgRP → PVT → BLA → InsCtx; Figure 3B)[104]. Taken together, studies in the thirst and hunger circuits point to a model where the thalamus has a pivotal role in transmitting information from brain interoceptive neurons to the cortex[1, 4]. It would be interesting to explore whether separate neural substrates in the thalamus process distinct appetites.

Modulation of Sensory Valence by Appetite Circuits

The valence of sensory stimuli, such as visual and taste cues, is modulated by internal state[45, 105, 106]. Among these cues, taste is a particularly important one for animals to assess the palatability of a substance. All taste signals are relayed via sensory ganglia to the rostral and lateral nucleus tractus solitaris (NTS)[6, 107]. The lateral parabrachial nucleus (PBN) receives input from the NTS[108] and relays it to the ventroposteromedial nucleus of the

thalamus, from where it is conveyed onto higher cortical structures, such as ACC and InsCtx[6, 107, 109, 110]. As mentioned above, the ACC and InsCtx also receive indirect inputs from interoceptive neurons of the Arc and the LT. In addition, these regions integrate inputs from reward-related areas. such as BLA, LHA, and the ventral tegmental area[111]. Therefore, ACC and InsCtx are best suited to integrate peripheral taste, central interoceptive, and reward signals[112]. Consistently, recent studies have shown that the neural representation of food-associated cues in the InsCtx dynamically changes under sated and food-deprived conditions[4, 104, 105]. A key next step would be to dissect the neural mechanisms underlying internal state-dependent plasticity of sensory representation at the cortical level.

INTERACTION BETWEEN DIFFERENT MOTIVATIONAL DRIVES

Based on the availability of resources, environmental conditions, and internal state, animals need to choose a particular behavior over others, a principle known as 'singleness of action'[113]. How different motivational drives interact to give rise to a single behavioral output remains unsolved[114]. Recent studies focused on two distinct appetites, thirst and hunger, to tackle this question. In flies, genetically defined four interoceptive neurons in the subesophageal zone are activated under hunger states and inhibited under thirst states[115]. Interestingly, stimulation of this neural population promoted sugar consumption and suppressed water consumption. Thus, these neurons represent a key neural substrate for processing the motivational competition between eating and drinking. In mice, equivalent neural substrates have not yet been identified. However, activation of AgRP neurons has been shown to suppress competing drives, including thirst, pain, fear, and territory marking[116, 117, 118, 119]. Interestingly, projections from AgRP neurons to the PBN mediate the suppression of inflammatory pain, providing a neural basis for competing motivational drives between hunger and pain[116]. Whether the similar logic applies to thirst neurons in the LT remains unknown. Besides the PBN, AgRP neurons[103], MnPO neurons[63, 65, 90], and aggression-related neurons in the ventromedial hypothalamus[120] all have dense projections to the periaqueductal gray (PAG). Since this brain region processes both ascending and

descending sensory information[121], it may also be involved in the integration of multiple drives. However, some key questions remain, including: (i) which neurons receive distinct motivational signals; and (ii) how does the PBN/PAG integrate and process these inputs? Future work using cell type-specific imaging and manipulation should help unravel the neural logic for processing competing motivational drives.

CONCLUDING REMARKS

The main function of the peripheral sensory system is to create an internal representation of the external environment. Taste is a key modality for assessing nutrient and regulating appetite. Although taste qualities and their receptors are still being discovered, and many of the specific receptors vary among species, there is a striking similarity in the overall cellular logic of tastes across organisms. Central processing of taste information is currently being explored in both vertebrates and invertebrates. These studies continue to reveal similarities across various species in the coding logic of taste in the brain.

Hunger and thirst are primordial and innate drives, and impairments in these functions significantly impact the overall functioning of the organism. Pathological conditions involving appetite dysregulation include obesity, anorexia, and polydipsia. Using contemporary neural manipulation and mapping tools, recent studies have shown that brain appetite circuits are regulated by internal state as well as by real-time ingestive behaviors, such as eating and drinking. One of the important next goals for the field would be to unveil in greater detail the neural pathways that integrate sensory and enteric signals with brain appetite circuits (see Outstanding Questions).

Sensory valence is influenced by appetite signals originating from interoceptive neurons in the brain. Accumulating evidence suggests that the thalamus and cortex are potential areas that process peripheral and central signals to control sensory valence of food and water. A ripe area of future research would be to dissect micro- and macro-circuits underlying internal state-dependent valence shifts.

Outstanding Questions

How are taste signals encoded and processed at the periphery and in higher brain areas? How does the valence of tastes change under different conditions, for instance varying degrees of depletion?

Acid-sensing taste cells may contribute to water taste detection. How are acid and water detected and perceived by the taste system?

How do various nodes of the hunger and thirst circuits interact to produce specific motivational drives? Are there dedicated cortical circuits for the processing of distinct appetites?

What are the functional roles for each of the AgRP projection fields in hunger regulation?

Feeding and drinking are intrinsically rewarding under deprived states. How does the reward circuitry modulate the hunger and thirst circuits to regulate consumption?

What are the neural substrates underlying the feed-forward regulation of hunger and thirst? What is the physiological role of this regulation?

What are the genetic identities of circuits in higher brain centers for integrating peripheral sensory signals and internal state information? How do peripheral taste signals shape appetite?

Which neural circuits are critical for processing competing motivational drives?

Box 1

Peripheral Signals Regulating Appetite in Mammals

Peripheral signals originating from the oral cavity, oropharynx, and gastrointestinal tract have an important role in the regulation of appetite[5]. For example, several circulating factors, such as leptin and insulin, act on the hypothalamus and hindbrain to regulate feeding. The vagal afferent neurons (VANs) from the gut also convey enteric information to the NTS via the nodose ganglia[5]. A recent notable study showed that there are genetically distinct subsets of vagal afferent neurons each responding to different aspects of nutrient ingestion. The stomach and intestine are innervated by GLP1R-expressing neurons that detect gastric distension and relay this information to the medial NTS. By contrast, GPR65-expressing neurons detect nutrients in the intestinal villi, and synapse onto the NTS subcommisural zone[122]. The hindbrain has several receptors for feeding-related neuropeptides. The direct injection of GLP1[123] and leptin[124] into the NTS suppresses feeding. The PBN, one of the major downstream targets of the NTS, appears to integrate the taste, hormonal signals (e.g., GLP1 and leptin), and visceral malaise[108, 125, 126, 127]. Two studies have shown that the intragastric infusion of nutrients as well as hormones, such as CCK, PYY, and serotonin, rapidly modulates interoceptive AgRP neurons[86, 87]. Thirst neurons are also rapidly modulated by oral temperature change and ingestion of fluid[65, 85]. Taken together, peripheral signals from different sites regulate appetite-related circuits at varying time-scales.

Box 2

Neural Circuits Involved in Sodium Appetite

Sodium appetite is modulated by the 'synergy' of two hormones, angiotensin II (ANGII) and aldosterone[128]. The detection of sodium depletion and the regulation of sodium appetite is mediated by two main brain sites: the LT (mainly ANGII related) and the NTS (mainly aldosterone related). In the NTS, multiple studies have demonstrated that 11β-hydroxysteroid dehydrogenase 2 (HSD2)-expressing neurons are activated under sodium-depleted conditions, and artificial stimulation of this population promotes sodium intake[129, 130]. A recent study suggested that HSD2 neurons require concurrent ANG signals to fully drive sodium intake[130]. In addition to the NTS, the LT has also been suggested to contribute

to sodium appetite via a subset of Agtr1a-expressing neurons in the SFO. Knocking out Agtr1a in the SFO, and optogenetic inhibition of SFO glutamatergic neurons that project to the ventral lateral bed nucleus of the stria terminalis (BNST) suppress sodium appetite[131]. A caveat is that sodium appetite in these studies required additional motivational drives such as thirst, suggesting that there are more factors and/or circuits to be discovered. Interestingly, both NTS and SFO neurons that promote sodium appetite project to the BNST[129, 131]. Identification of specific neurons and circuitry in the BNST underlying sodium appetite should be a focus for future investigations.

Box 3

The Valence Encoded by Appetite Circuits

The behavioral definition of positive and negative valence is the willingness of an animal to work for access to a specific stimulus. Recent studies have begun to uncover the valence encoded by central appetite circuits. Context and state modulation appear to be crucial with regards to valence encoding. For instance, animals will work to receive stimulation of AgRP neurons (i.e., self-optogenetic stimulation of AgRP neurons) when food is available, and will continue doing so even if the food is taken away[132]. By contrast, in the absence of food, animals will avoid stimulation of AgRP neurons[61] or will fail to learn to self-stimulate during training[132]. The lateral hypothalamus (LH) appears to be another node involved in valence encoding related to appetite. Excitatory and inhibitory neurons of the LH have orthogonal effects on feeding and motivation. Stimulation of LH excitatory neurons inhibits feeding and drives aversion[133], whereas LH inhibitory stimulation is rewarding and induces feeding[134, 135]. A review by Rossi and Stuber[58] covers these in detail. Thirst is negatively reinforcing and the stimulation of thirst neurons in the LT appears to encode negative valence[61, 64, 90]. The MnPO dissociates the behavioral, cardiovascular, and affective outputs of the LT with photostimulation of the excitatory projections to the PVH and LH driving aversion[64].

Acknowledgments
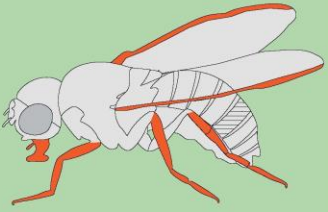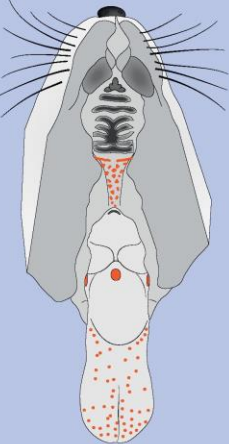
		Labellum, legs, and anterior wing margin	Fungiform (front), circumvallate (back), foliate (side), and soft palate
Sweet		Gr5, Gr61a, Gr64, etc. (~15 genes)	T1R2/T1R3
Umami		Ir76b + Ir20a (+ other Irs?)	T1R1/T1R3
Bitter		Gr66a, Gr32a, etc. (~30 genes)	T2Rs (~40 genes)
Salty		Ir76 ppk11 and 19 (larvae)	ENaC
Water		ppk28	PKD2L1+ TRCs
Sour		Ir76b + Ir25a (+ other Irs?)	PKD2L1+ TRCs (otopetrin 1?)

Figure 1

Figure 1. Taste Detection in Insects and Mammals. Taste organs in Drosophila melanogaster and mouse. In flies, taste stimuli are detected by gustatory receptor neurons (GRNs) in labella of the proboscis, legs, and wings (left, highlighted in orange). These taste organs express distinct but partially overlapping subsets of taste receptors. In mammals, taste buds are distributed in different regions of the tongue, including fungiform (front), foliate (side), and circumvallate (back) papilla, as well as soft palate (right, highlighted in orange). Most taste receptors are expressed in all papilla on the tongue, but functional epithelial sodium channel (ENaC) is expressed only in fungiform or palate buds. Each basic taste quality is mediated by a unique subset of gustatory receptors (GRs), ionotoropic receptors (IRs) or pickpocket (PPK) channels in flies. In mammals, taste receptors (T1Rs and T2Rs) and ion channels are responsible for basic taste detection. Vertebrates and invertebrates share similar cellular organization for taste detection in that different taste qualities are generally encoded by anatomically distinct neural populations.

(A)

Sensory cues | Interoception | Behavior

Feed-forward regulation

Food cues
Water → Hunger
Thirst → Feeding
Drinking

Feed-back inhibition

(B)

ARC^AgRP

DMH^LepR

Feeding

Gustatory cues?
Oropharyngeal cues?
Hormones?
Visual cues?
Olfactory cues?

???

(C)

SFO^nNOS

OVLT^nNOS → MnPO^nNOS
?

MnPO^GLP1R

Drinking

Gustatory cues?
Oropharyngeal cues?
Hormones?
Gastrointestinal cues?
Thermosensory cues?

???

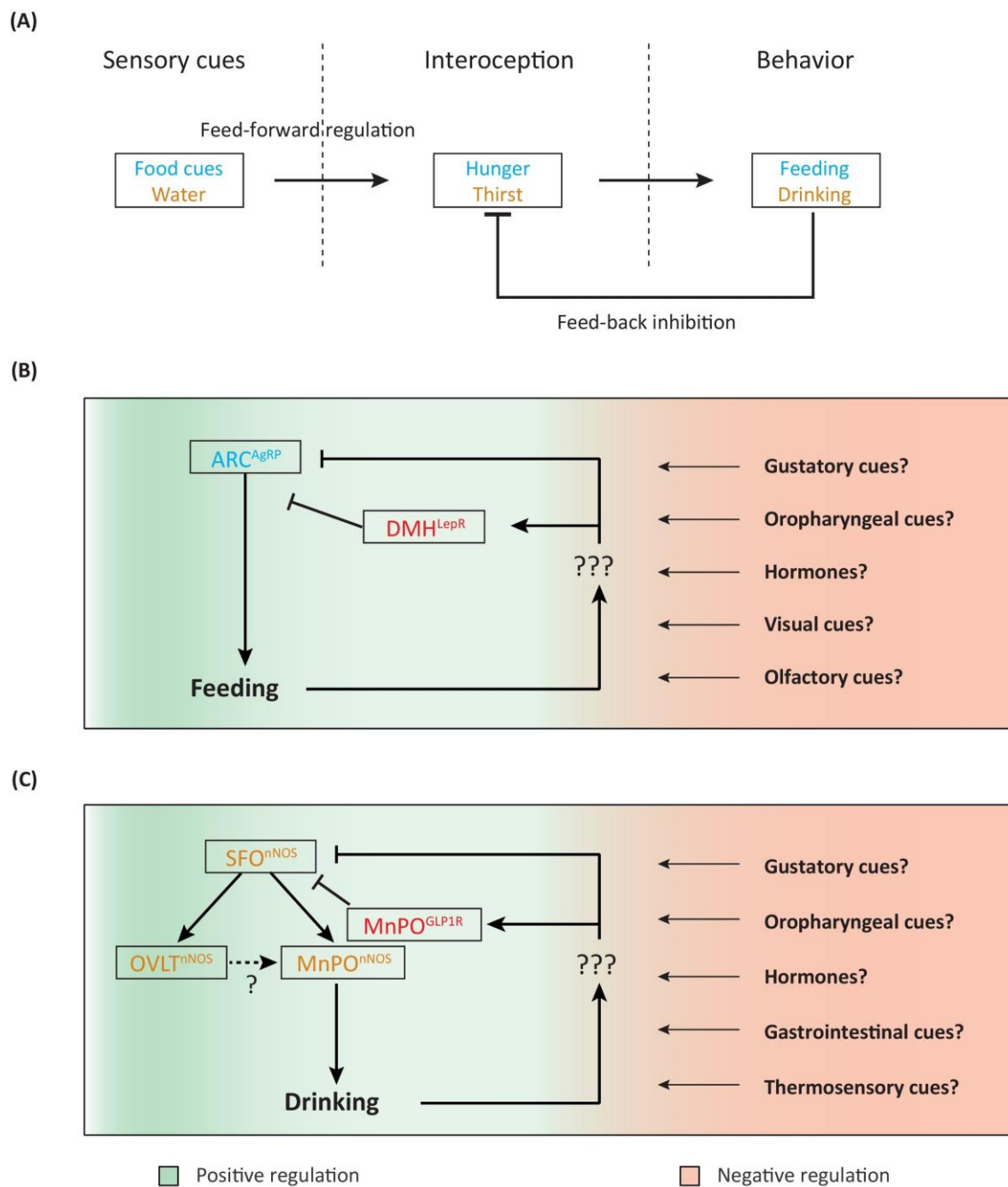Positive regulation | Negative regulation

Figure 2

Figure 2. Anticipatory Nature of Hunger and Thirst Regulation. (A) A schematic of feed-forward–feed-back regulation of thirst and hunger. Sensory cues and food ingestion (for hunger), or liquid drinking (for thirst) directly modulate the interoceptive circuits. Feed-back and feed-forward signals help optimize the amount and timing of ingestion on a real-time basis. **(B)** Hunger interoceptive neurons in the arcuate nucleus (AgRP neurons) detect energy deficits and drive feeding. Several peripheral signals modulate the activity of AgRP neurons. Leptin receptor-expressing neurons in the DMH are the only known neurons underlying this feed-forward regulation. **(C)** The excitatory neurons of the lamina terminalis (comprising the SFO, MnPO, and OVLT), marked by nNOS, form a hierarchical circuit to process thirst. Thirst interoceptive neurons (SFO^{nNOS} and $OVLT^{nNOS}$) respond to deviations in body fluid balance and convey this information to $MnPO^{nNOS}$ neurons. SFO^{nNOS} neurons are also rapidly modulated upon water intake. Inhibitory $MnPO^{GLP1R}$ neurons are activated by drinking (gulping) actions, which monosynaptically inhibit SFO^{nNOS} neurons of the SFO. Abbreviations: AgRP, Agouti-related peptide; Arc, arcuate nucleus; DMH, dorsomedial hypothalamic nucleus; GLP1r, glucagon-like peptide 1 receptor; LepR, leptin receptor; MnPO, median preoptic nucleus; nNOS, neuronal nitric oxide synthase; OVLT, vascular organ of lamina terminalis; SFO, subfornical organ.
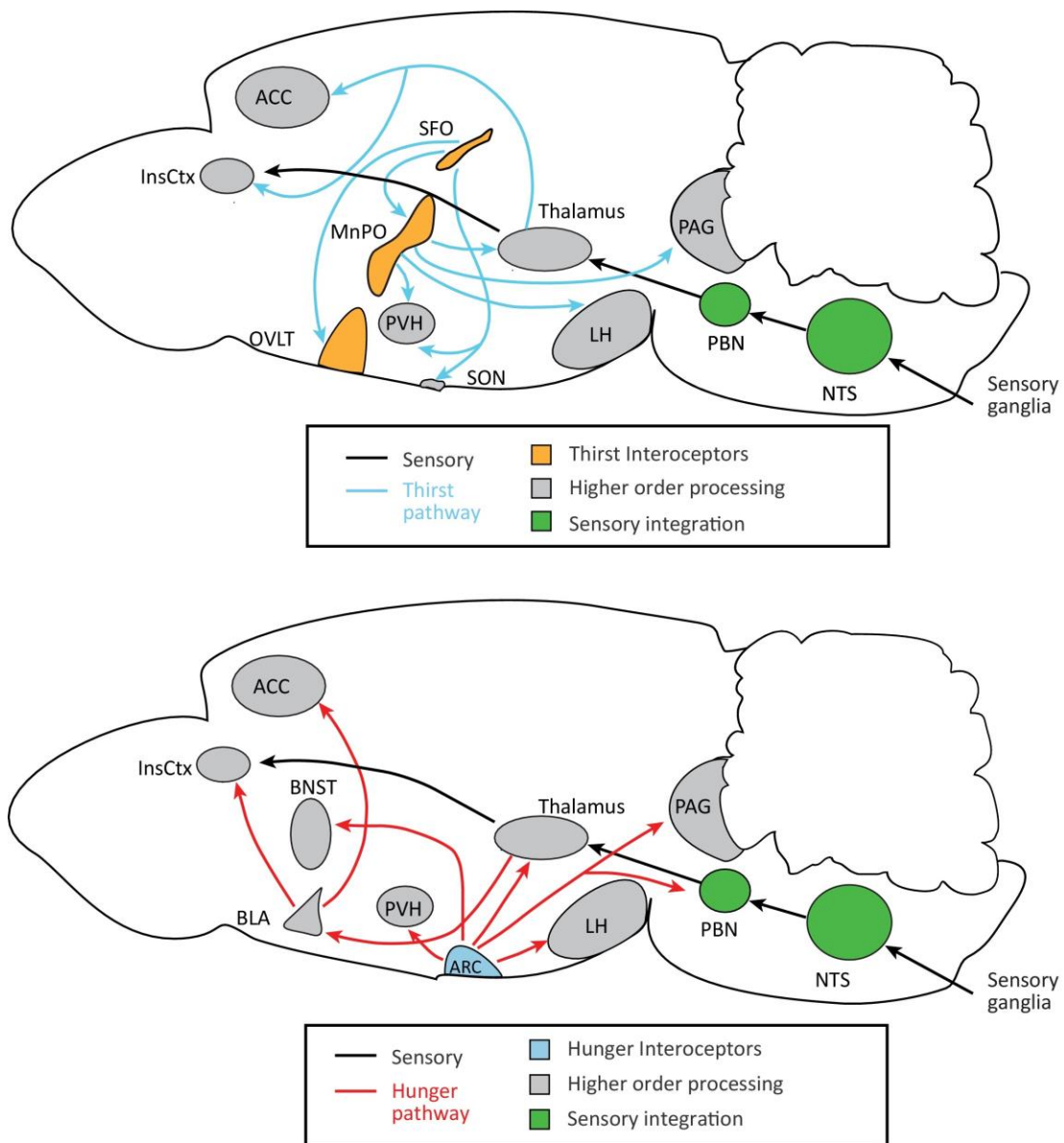
Figure 3

Figure 3. Neural Pathways for Sensory and Interoceptive Processing of Thirst and Hunger Signals. Schematics showing the sensory and interoceptive pathways in the mammalian brain. The NTS and PBN are potential sites that integrate peripheral and visceral signals. **(A)** Thirst: black arrows indicate sensory ascending pathways, while blue arrows show thirst-related circuits. **(B)** Hunger: red arrows show hunger-related circuits. Abbreviations: ACC, anterior cingulate cortex; Arc, arcuate nucleus; BLA, basolateral amygdala; BNST, bed nucleus of the stria terminalis; InsCtx, insular cortex; LH, lateral hypothalamus; MnPO, median preoptic nucleus; NTS, nucleus tractus solitarius; OVLT, vascular organ of lamina terminalis; PAG, periaqueductal gray; PBN, parabrachial nucleus; PVH, paraventricular hypothalamic nucleus; SFO, subfornical organ; SON, supraoptic nucleus.

REFERENCES

1   Gizowski, C. & Bourque, C. W. The neural basis of homeostatic and anticipatory thirst. *Nature Reviews Nephrology*, nrneph. 2017.2149 (2017).

2   Saper, C. B., Chou, T. C. & Elmquist, J. K. The need to feed: homeostatic and hedonic control of eating. *Neuron* **36**, 199-211 (2002).

3   Weigle, D. S. Appetite and the regulation of body composition. *The FASEB Journal* **8**, 302-310 (1994).

4   Andermann, M. L. & Lowell, B. B. Toward a wiring diagram understanding of appetite control. *Neuron* **95**, 757-778 (2017).

5   Kim, K.-S., Seeley, R. J. & Sandoval, D. A. Signalling from the periphery to the brain that regulates energy homeostasis. *Nature Reviews Neuroscience* (2018).

6   Yarmolinsky, D. A., Zuker, C. S. & Ryba, N. J. Common sense about taste: from mammals to insects. *Cell* **139**, 234-244 (2009).

7   Zimmerman, C. A., Leib, D. E. & Knight, Z. A. Neural circuits underlying thirst and fluid homeostasis. *Nature Reviews Neuroscience* **18**, 459-469 (2017).

8   Roper, S. D. & Chaudhari, N. Taste buds: cells, signals and synapses. *Nat Rev Neurosci* **18**, 485-497, doi:10.1038/nrn.2017.68 (2017).

9   Nelson, G. *et al.* An amino-acid taste receptor. *Nature* **416**, 199-202 (2002).

10   Nelson, G. *et al.* Mammalian sweet taste receptors. *Cell* **106**, 381-390 (2001).

11   Li, X. *et al.* Human receptors for sweet and umami taste. *Proceedings of the National Academy of Sciences* **99**, 4692-4696 (2002).

12   Zhao, G. Q. *et al.* The receptors for mammalian sweet and umami taste. *Cell* **115**, 255-266 (2003).

13   Matsunami, H., Montmayeur, J.-P. & Buck, L. B. A family of candidate taste receptors in human and mouse. *Nature* **404**, 601-604 (2000).

14   Pronin, A. N., Tang, H., Connor, J. & Keung, W. Identification of ligands for two human bitter T2R receptors. *Chemical Senses* **29**, 583-593 (2004).

15   Pronin, A. N. *et al.* Specific alleles of bitter receptor genes influence human sensitivity to the bitterness of aloin and saccharin. *Current Biology* **17**, 1403-1408 (2007).

16   Mueller, K. L. *et al.* The receptors and coding logic for bitter taste. *Nature* **434**, 225-229 (2005).

17   Chandrashekar, J. *et al.* T2Rs function as bitter taste receptors. *Cell* **100**, 703-711 (2000).

18   Li, X. *et al.* Pseudogenization of a sweet-receptor gene accounts for cats' indifference toward sugar. *PLoS genetics* **1**, e3 (2005).

19   Jiang, P. *et al.* Major taste loss in carnivorous mammals. *Proceedings of the National Academy of Sciences* **109**, 4956-4961 (2012).

20   Feng, P., Zheng, J., Rossiter, S. J., Wang, D. & Zhao, H. Massive losses of taste receptor genes in toothed and baleen whales. *Genome biology and evolution* **6**, 1254-1265 (2014).

21   Chandrashekar, J., Hoon, M. A., Ryba, N. J. & Zuker, C. S. The receptors and cells for mammalian taste. *Nature* **444**, 288-294 (2006).

22   Hallem, E. A., Dahanukar, A. & Carlson, J. R. Insect odor and taste receptors. *Annu. Rev. Entomol.* **51**, 113-135 (2006).

23   Scott, K. Taste recognition: food for thought. *Neuron* **48**, 455-464 (2005).

24   Freeman, E. G. & Dahanukar, A. Molecular neurobiology of Drosophila taste. *Current opinion in neurobiology* **34**, 140-148 (2015).

25   Joseph, R. M. & Carlson, J. R. Drosophila chemoreceptors: a molecular interface between the chemical world and the brain. *Trends in Genetics* **31**, 683-695 (2015).

26   Benton, R., Vannice, K. S., Gomez-Diaz, C. & Vosshall, L. B. Variant ionotropic glutamate receptors as chemosensory receptors in Drosophila. *Cell* **136**, 149-162 (2009).

27   Rytz, R., Croset, V. & Benton, R. Ionotropic receptors (IRs): chemosensory ionotropic glutamate receptors in Drosophila and beyond. *Insect Biochem Mol Biol* **43**, 888-897, doi:10.1016/j.ibmb.2013.02.007 (2013).

28 Dahanukar, A., Lei, Y. T., Kwon, J. Y. & Carlson, J. R. Two Gr genes underlie sugar reception in Drosophila. *Neuron* **56**, 503-516, doi:10.1016/j.neuron.2007.10.024 (2007).

29 Inagaki, H. K. *et al.* Optogenetic control of Drosophila using a red-shifted channelrhodopsin reveals experience-dependent influences on courtship. *Nature methods* **11**, 325-332 (2014).

30 Marella, S. *et al.* Imaging taste responses in the fly brain reveals a functional map of taste category and behavior. *Neuron* **49**, 285-295, doi:10.1016/j.neuron.2005.11.037 (2006).

31 Ganguly, A. *et al.* A molecular and cellular context-dependent role for Ir76b in detection of amino acid taste. *Cell reports* **18**, 737-750 (2017).

32 Zhang, Y. V., Ni, J. & Montell, C. The molecular basis for attractive salt-taste coding in Drosophila. *Science* **340**, 1334-1338 (2013).

33 Chandrashekar, J. *et al.* The cells and peripheral representation of sodium taste in mice. *Nature* **464**, 297-301 (2010).

34 Oka, Y., Butnaru, M., von Buchholtz, L., Ryba, N. J. & Zuker, C. S. High salt recruits aversive taste pathways. *Nature* **494**, 472-475 (2013).

35 Duncan, C. Salt preferences of birds and mammals. *Physiological Zoology* **35**, 120-132 (1962).

36 Geerling, J. C. & Loewy, A. D. Central regulation of sodium appetite. *Exp Physiol* **93**, 177-209, doi:10.1113/expphysiol.2007.039891 (2008).

37 Shigemura, N. *et al.* Amiloride-sensitive NaCl taste responses are associated with genetic variation of ENaC α-subunit in mice. *American Journal of Physiology-Regulatory, Integrative and Comparative Physiology* **294**, R66-R75 (2008).

38 Liu, L. *et al.* Contribution of Drosophila DEG/ENaC genes to salt taste. *Neuron* **39**, 133-146 (2003).

39 Wolbarsht, M. L. Water Taste in Phormia. *Science (New York, NY)* **125**, 1248-1248 (1957).

40   Evans, D. R. & Mellon, D. Electrophysiological studies of a water receptor associated with the taste sensilla of the blowfly. *The Journal of general physiology* **45**, 487-500 (1962).

41   Cameron, P., Hiroi, M., Ngai, J. & Scott, K. The molecular basis for water taste in Drosophila. *Nature* **465**, 91-95 (2010).

42   Chen, Z., Wang, Q. & Wang, Z. The amiloride-sensitive epithelial Na+ channel PPK28 is essential for Drosophila gustatory water reception. *Journal of Neuroscience* **30**, 6247-6252 (2010).

43   Lin, S. *et al.* Neural correlates of water reward in thirsty Drosophila. *Nature neuroscience* **17**, 1536-1542 (2014).

44   Zotterman, Y. Species differences in the water taste. *Acta Physiologica* **37**, 60-70 (1956).

45   Zocchi, D., Wennemuth, G. & Oka, Y. The cellular mechanism for water detection in the mammalian taste system. *Nature neuroscience* (2017).

46   Huang, A. L. *et al.* The cells and logic for mammalian sour taste detection. *Nature* **442**, 934-938 (2006).

47   Ishimaru, Y. *et al.* Transient receptor potential family members PKD1L3 and PKD2L1 form a candidate sour taste receptor. *Proceedings of the National Academy of Sciences* **103**, 12569-12574 (2006).

48   Finger, T. E. *et al.* ATP signaling is crucial for communication from taste buds to gustatory nerves. *Science* **310**, 1495-1499 (2005).

49   Julius, D. TRP channels and pain. *Annu Rev Cell Dev Biol* **29**, 355-384, doi:10.1146/annurev-cellbio-101011-155833 (2013).

50   Horio, N. *et al.* Sour taste responses in mice lacking PKD channels. *PLoS One* **6**, e20007 (2011).

51   Richter, T. A., Dvoryanchikov, G. A., Roper, S. D. & Chaudhari, N. Acid-sensing ion channel-2 is not necessary for sour taste in mice. *J Neurosci* **24**, 4088-4091, doi:10.1523/JNEUROSCI.0653-04.2004 (2004).

52   Stevens, D. R. *et al.* Hyperpolarization-activated channels HCN1 and HCN4 mediate responses to sour stimuli. *Nature* **413**, 631-635 (2001).

53   Tu, Y. H. *et al.* An evolutionarily conserved gene family encodes proton-selective ion channels. *Science* **359**, 1047-1050, doi:10.1126/science.aao3264 (2018).

54   Ye, W. *et al.* The K+ channel KIR2. 1 functions in tandem with proton influx to mediate sour taste transduction. *Proceedings of the National Academy of Sciences* **113**, E229-E238 (2016).

55   Chen, Y. & Amrein, H. Ionotropic Receptors Mediate Drosophila Oviposition Preference through Sour Gustatory Receptor Neurons. *Current Biology* **27**, 2741-2750. e2744 (2017).

56   Charlu, S., Wisotsky, Z., Medina, A. & Dahanukar, A. Acid sensing by sweet and bitter taste neurons in Drosophila melanogaster. *Nat Commun* **4**, 2042, doi:10.1038/ncomms3042 (2013).

57   Sternson, S. M. & Eiselt, A.-K. Three Pillars for the Neural Control of Appetite. *Annual review of physiology* **79**, 401-423 (2017).

58   Rossi, M. A. & Stuber, G. D. Overlapping Brain Circuits for Homeostatic and Hedonic Feeding. *Cell metabolism* (2017).

59   Bourque, C. W. Central mechanisms of osmosensation and systemic osmoregulation. *Nature Reviews Neuroscience* **9**, 519-531 (2008).

60   McKinley, M. *et al.* The median preoptic nucleus: front and centre for the regulation of body fluid, sodium, temperature, sleep and cardiovascular homeostasis. *Acta Physiologica* **214**, 8-32 (2015).

61   Betley, J. N. *et al.* Neurons for hunger and thirst transmit a negative-valence teaching signal. *Nature* **521**, 180-185 (2015).

62   Oka, Y., Ye, M. & Zuker, C. S. Thirst driving and suppressing signals encoded by distinct neural populations in the brain. *Nature* **520**, 349-352 (2015).

63   Abbott, S. B., Machado, N. L., Geerling, J. C. & Saper, C. B. Reciprocal control of drinking behavior by median preoptic neurons in mice. *Journal of Neuroscience* **36**, 8228-8237 (2016).

64   Leib, D. E. *et al.* The Forebrain Thirst Circuit Drives Drinking through Negative Reinforcement. *Neuron* **96**, 1272-1281. e1274 (2017).

65   Augustine, V. *et al.* Hierarchical neural architecture underlying thirst regulation. *Nature* (2018).

66   Ciura, S. & Bourque, C. W. Transient receptor potential vanilloid 1 is required for intrinsic osmoreception in organum vasculosum lamina terminalis neurons and for normal thirst responses to systemic hyperosmolality. *Journal of Neuroscience* **26**, 9069-9075 (2006).

67   Liedtke, W. & Friedman, J. M. Abnormal osmotic regulation in trpv4-/-mice. *Proceedings of the National Academy of Sciences* **100**, 13698-13703 (2003).

68   Kinsman, B. *et al.* Osmoregulatory thirst in mice lacking the transient receptor potential vanilloid type 1 (TRPV1) and/or type 4 (TRPV4) receptor. *American Journal of Physiology-Regulatory, Integrative and Comparative Physiology* **307**, R1092-R1100 (2014).

69   Yulyaningsih, E. *et al.* Acute Lesioning and Rapid Repair of Hypothalamic Neurons outside the Blood-Brain Barrier. *Cell reports* **19**, 2257-2271 (2017).

70   Aponte, Y., Atasoy, D. & Sternson, S. M. AGRP neurons are sufficient to orchestrate feeding behavior rapidly and without training. *Nature neuroscience* **14**, 351-355 (2011).

71   Atasoy, D., Betley, J. N., Su, H. H. & Sternson, S. M. Deconstruction of a neural circuit for hunger. *Nature* **488**, 172-177 (2012).

72   Krashes, M. J., Shah, B. P., Koda, S. & Lowell, B. B. Rapid versus delayed stimulation of feeding by the endogenously released AgRP neuron mediators GABA, NPY, and AgRP. *Cell metabolism* **18**, 588-595 (2013).

73   Luquet, S., Perez, F. A., Hnasko, T. S. & Palmiter, R. D. NPY/AgRP neurons are essential for feeding in adult mice but can be ablated in neonates. *Science* **310**, 683-685, doi:10.1126/science.1115524 (2005).

74   Kojima, M. *et al.* Ghrelin is a growth-hormone-releasing acylated peptide from stomach. *Nature* **402**, 656-660 (1999).

75   Nakazato, M. *et al.* A role for ghrelin in the central regulation of feeding. *Nature* **409**, 194-198 (2001).

76   Andrews, Z. B. *et al.* UCP2 mediates ghrelin's action on NPY/AgRP neurons by lowering free radicals. *Nature* **454**, 846-851 (2008).

77   Cowley, M. A. *et al.* The distribution and mechanism of action of ghrelin in the CNS demonstrates a novel hypothalamic circuit regulating energy homeostasis. *Neuron* **37**, 649-661 (2003).

78   Könner, A. C. *et al.* Insulin action in AgRP-expressing neurons is required for suppression of hepatic glucose production. *Cell metabolism* **5**, 438-449 (2007).

79   van den Top, M., Lee, K., Whyment, A. D., Blanks, A. M. & Spanswick, D. Orexigen-sensitive NPY/AgRP pacemaker neurons in the hypothalamic arcuate nucleus. *Nature neuroscience* **7**, 493 (2004).

80   Belgardt, B. F., Okamura, T. & Brüning, J. C. Hormone and glucose signalling in POMC and AgRP neurons. *The Journal of physiology* **587**, 5305-5314 (2009).

81   Blouet, C. & Schwartz, G. J. Hypothalamic nutrient sensing in the control of energy homeostasis. *Behavioural brain research* **209**, 1-12 (2010).

82   Chen, Y., Lin, Y.-C., Kuo, T.-W. & Knight, Z. A. Sensory detection of food rapidly modulates arcuate feeding circuits. *Cell* **160**, 829-841 (2015).

83   Gizowski, C., Zaelzer, C. & Bourque, C. Clock-driven vasopressin neurotransmission mediates anticipatory thirst prior to sleep. *Nature* **537**, 685-688 (2016).

84   Mandelblat-Cerf, Y. *et al.* Bidirectional Anticipation of Future Osmotic Challenges by Vasopressin Neurons. *Neuron* **93**, 57-65 (2017).

85   Zimmerman, C. A. *et al.* Thirst neurons anticipate the homeostatic consequences of eating and drinking. *Nature* **537**, 680-684 (2016).

86   Beutler, L. R. *et al.* Dynamics of Gut-Brain Communication Underlying Hunger. *Neuron* **96**, 461-475. e465 (2017).

87   Su, Z., Alhadeff, A. L. & Betley, J. N. Nutritive, Post-ingestive Signals Are the Primary Regulators of AgRP Neuron Activity. *Cell reports* **21**, 2724-2736 (2017).

88   Mandelblat-Cerf, Y. *et al.* Arcuate hypothalamic AgRP and putative POMC neurons show opposite changes in spiking across multiple timescales. *Elife* **4**, e07122 (2015).

89   Garfield, A. S. *et al.* Dynamic GABAergic afferent modulation of AgRP neurons. *Nature neuroscience* (2016).

90   Allen, W. E. *et al.* Thirst-associated preoptic neurons encode an aversive motivational drive. *Science* **357**, 1149-1155 (2017).

91   Berridge, K. C. Motivation concepts in behavioral neuroscience. *Physiology & behavior* **81**, 179-209 (2004).

92   Olds, J. Self-stimulation of the brain: Its use to study local effects of hunger, sex, and drugs. *Science* **127**, 315-324 (1958).

93   Toates, F. M. *Motivational systems*. (CUP Archive, 1986).

94   Hollis, J. H., McKinley, M. J., D'Souza, M., Kampe, J. & Oldfield, B. J. The trajectory of sensory pathways from the lamina terminalis to the insular and cingulate cortex: a neuroanatomical framework for the generation of thirst. *American Journal of Physiology-Regulatory, Integrative and Comparative Physiology* **294**, R1390-R1401 (2008).

95   Craig, A. D. How do you feel? Interoception: the sense of the physiological condition of the body. *Nat Rev Neurosci* **3**, 655-666, doi:10.1038/nrn894 (2002).

96   Robinson, B. W. & Mishkin, M. Alimentary responses to forebrain stimulation in monkeys. *Experimental brain research* **4**, 330-366 (1968).

97   Denton, D. *et al.* Correlation of regional cerebral blood flow and change of plasma sodium concentration during genesis and satiation of thirst. *Proceedings of the National Academy of Sciences* **96**, 2532-2537 (1999).

98   Denton, D. *et al.* Neuroimaging of genesis and satiation of thirst and an interoceptor-driven theory of origins of primary consciousness. *Proceedings of the National Academy of Sciences* **96**, 5304-5309 (1999).

99   Farrell, M. J. *et al.* Cortical activation and lamina terminalis functional connectivity during thirst and drinking in humans. *American Journal of Physiology-Regulatory, Integrative and Comparative Physiology* **301**, R623-R631 (2011).

100   Saker, P. *et al.* Regional brain responses associated with drinking water during thirst and after its satiation. *Proceedings of the National Academy of Sciences* **111**, 5379-5384 (2014).

101   Fuhrer, D., Zysset, S. & Stumvoll, M. Brain activity in hunger and satiety: an exploratory visually stimulated FMRI study. *Obesity (Silver Spring)* **16**, 945-950, doi:10.1038/oby.2008.33 (2008).

102   Wang, D. *et al.* Whole-brain mapping of the direct inputs and axonal projections of POMC and AgRP neurons. *Frontiers in neuroanatomy* **9**, 40 (2015).

103   Betley, J. N., Cao, Z. F. H., Ritola, K. D. & Sternson, S. M. Parallel, redundant circuit organization for homeostatic control of feeding behavior. *Cell* **155**, 1337-1350 (2013).

104   Livneh, Y. *et al.* Homeostatic circuits selectively gate food cue responses in insular cortex. *Nature* (2017).

105   Accolla, R. & Carleton, A. Internal body state influences topographical plasticity of sensory representations in the rat gustatory cortex. *Proc Natl Acad Sci U S A* **105**, 4010-4015, doi:10.1073/pnas.0708927105 (2008).

106   Burgess, C. R., Livneh, Y., Ramesh, R. N. & Andermann, M. L. Gating of visual processing by physiological need. *Curr Opin Neurobiol* **49**, 16-23, doi:10.1016/j.conb.2017.10.020 (2017).

107   Carleton, A., Accolla, R. & Simon, S. A. Coding in the mammalian gustatory system. *Trends in neurosciences* **33**, 326-334 (2010).

108   Palmiter, R. D. The Parabrachial Nucleus: CGRP Neurons Function as a General Alarm. *Trends in Neurosciences* **41**, 280-293 (2018).

109   Tokita, K., Inoue, T. & Boughter, J. Afferent connections of the parabrachial nucleus in C57BL/6J mice. *Neuroscience* **161**, 475-488 (2009).

110   Chen, X., Gabitto, M., Peng, Y., Ryba, N. J. & Zuker, C. S. A gustotopic map of taste qualities in the mammalian brain. *Science* **333**, 1262-1266 (2011).

111   Shackman, A. J. *et al.* The integration of negative affect, pain and cognitive control in the cingulate cortex. *Nat Rev Neurosci* **12**, 154-167, doi:10.1038/nrn2994 (2011).

112   de Araujo, I. E. & Simon, S. A. The gustatory cortex and multisensory integration. *Int J Obes (Lond)* **33 Suppl 2**, S34-43, doi:10.1038/ijo.2009.70 (2009).

113   Sherrington, C. *The integrative action of the nervous system*. (CUP Archive, 1910).

114   McFarland, D. & Sibly, R. The behavioural final common path. *Philosophical Transactions of the Royal Society of London B: Biological Sciences* **270**, 265-293 (1975).

115   Jourjine, N., Mullaney, B. C., Mann, K. & Scott, K. Coupled sensing of hunger and thirst signals balances sugar and water consumption. *Cell* **166**, 855-866 (2016).

116   Amber L. Alhadeff, Z. S., Elen Hernandez, Michelle L. Klima, Sophie Z. Phillips, Ruby A. Holland, Caiying Guo, Adam W. Hantman, Bart C. De Jonghe, J. Nicholas Betley4,'Correspondence information about the author J. Nicholas Betley. A Neural Circuit for the Suppression of Pain by a Competing Need State. *Cell* **173**, 140-152 (2018).

117   Burnett, C. J. *et al.* Hunger-driven motivational state competition. *Neuron* **92**, 187-201 (2016).

118   Jikomes, N., Ramesh, R. N., Mandelblat-Cerf, Y. & Andermann, M. L. Preemptive stimulation of AgRP neurons in fed mice enables conditioned food seeking under threat. *Current Biology* **26**, 2500-2507 (2016).

119   Padilla, S. L. *et al.* Agouti-related peptide neural circuits mediate adaptive behaviors in the starved state. *Nature neuroscience* **19**, 734-741 (2016).

120   Wang, L., Chen, I. Z. & Lin, D. Collateral pathways from the ventromedial hypothalamus mediate defensive behaviors. *Neuron* **85**, 1344-1358 (2015).

121   Behbehani, M. M. Functional characteristics of the midbrain periaqueductal gray. *Progress in neurobiology* **46**, 575-605 (1995).

122   Williams, E. K. *et al.* Sensory neurons that detect stretch and nutrients in the digestive system. *Cell* **166**, 209-221 (2016).

123   Hayes, M. R. *et al.* Intracellular signals mediating the food intake-suppressive effects of hindbrain glucagon-like peptide-1 receptor activation. *Cell metabolism* **13**, 320-330 (2011).

124   Grill, H. J. *et al.* Evidence that the caudal brainstem is a target for the inhibitory effect of leptin on food intake. *Endocrinology* **143**, 239-246 (2002).

125   Alhadeff, A. L., Baird, J.-P., Swick, J. C., Hayes, M. R. & Grill, H. J. Glucagon-like peptide-1 receptor signaling in the lateral parabrachial nucleus contributes to the control of food intake and motivation to feed. *Neuropsychopharmacology* **39**, 2233 (2014).

126   Alhadeff, A. L., Hayes, M. R. & Grill, H. J. Leptin receptor signaling in the lateral parabrachial nucleus contributes to the control of food intake. *American Journal of Physiology-Regulatory, Integrative and Comparative Physiology* **307**, R1338-R1344 (2014).

127   Carter, M. E., Han, S. & Palmiter, R. D. Parabrachial calcitonin gene-related peptide neurons mediate conditioned taste aversion. *J Neurosci* **35**, 4582-4586, doi:10.1523/JNEUROSCI.3729-14.2015 (2015).

128   Sakai, R. R., Nicolaidis, S. & Epstein, A. N. Salt appetite is suppressed by interference with angiotensin II and aldosterone. *American Journal of Physiology-Regulatory, Integrative and Comparative Physiology* **251**, R762-R768 (1986).

129   Jarvie, B. C. & Palmiter, R. D. HSD2 neurons in the hindbrain drive sodium appetite. *Nature neuroscience* **20**, 167 (2017).

130   Resch, J. M. *et al.* Aldosterone-Sensing Neurons in the NTS Exhibit State-Dependent Pacemaker Activity and Drive Sodium Appetite via Synergy with Angiotensin II Signaling. *Neuron* **96**, 190-206. e197 (2017).

131   Matsuda, T. *et al.* Distinct neural mechanisms for the control of thirst and salt appetite in the subfornical organ. *Nature neuroscience* **20**, 230 (2017).

132   Chen, Y., Lin, Y.-C., Zimmerman, C. A., Essner, R. A. & Knight, Z. A. Hunger neurons drive feeding through a sustained, positive reinforcement signal. *Elife* **5** (2016).

133   Jennings, J. H., Rizzi, G., Stamatakis, A. M., Ung, R. L. & Stuber, G. D. The inhibitory circuit architecture of the lateral hypothalamus orchestrates feeding. *Science* **341**, 1517-1521 (2013).

134   Jennings, J. H. *et al.* Visualizing hypothalamic network dynamics for appetitive and consummatory behaviors. *Cell* **160**, 516-527 (2015).

135   Navarro, M. *et al.* Lateral hypothalamus GABAergic neurons modulate consummatory behaviors regardless of the caloric content or biological relevance of the consumed stimuli. *Neuropsychopharmacology* **41**, 1505 (2016).

Chapter 3

TEMPORALLY AND SPATIALLY DISTINCT THIRST SATIATION SIGNALS IN THE BRAIN

SUMMARY

For thirsty animals, fluid intake provides both satiation and pleasure of drinking. How the brain processes these factors is currently unknown. Here, we identified neural circuits underlying thirst satiation and examined their contribution to reward signals. We show that thirst-driving neurons receive temporally distinct satiation signals by liquid-gulping-induced oropharyngeal stimuli and gut osmolality sensing. We demonstrate that individual thirst satiation signals are mediated by anatomically distinct inhibitory neural circuits in the lamina terminalis. Moreover, we used an ultrafast dopamine (DA) sensor to examine whether thirst satiation itself stimulates the reward-related circuits. Interestingly, spontaneous drinking behavior but not thirst drive reduction triggered DA release. Importantly, chemogenetic stimulation of thirst satiation neurons did not activate DA neurons under water-restricted conditions. Together, this study dissected the thirst satiation circuit, the activity of which is functionally separable from reward-related brain activity.

Augustine, V. et al. (2019). "Temporally and Spatially Distinct Thirst Satiation Signals,". In: *Neuron*. doi: 10.1016/ j.neuron.2019.04.039.

INTRODUCTION

The timing and amount of water intake is strictly regulated by the brain for maintaining body fluid homeostasis (Augustine et al., 2018b; Gizowski and Bourque, 2018; Ichiki et al., 2019; McKinley and Johnson, 2004). Fluid imbalance, such as dehydration, is mainly detected by a forebrain structure, lamina terminalis (LT). Recent studies have pinpointed neural populations and the circuit organization in the LT that process the internal fluid information (Abbott et al., 2016; Allen et al., 2017; Augustine et al., 2018a; Betley et al., 2015; Leib et al., 2017; Matsuda et al., 2017; Nation et al., 2016; Oka et al., 2015). Emerging evidence suggests that drinking behavior rapidly affects the activity of thirst circuits prior to water absorption into the systemic circulation (Allen et al., 2017; Augustine et al., 2018a; Gizowski et al., 2016; Mandelblat-Cerf et al., 2015; Thrasher et al., 1981; Zimmerman et al., 2016). For example, thirst-related neurons in the LT receive rapid inhibitory signals with the onset of fluid ingestion. We have reported that an inhibitory circuit, involving MnPO neurons that express glucagon-like peptide 1 receptor (MnPO^{GLP1r} neurons), is activated by liquid gulping behavior (Augustine et al., 2018a). Once activated, these neurons monosynaptically inhibit thirst neurons in the subfornical organ (SFO). In addition to these gulping-induced signals, thirst neurons receive another satiation signal by postoral osmolality (hypotonicity) sensing, the neural basis of which remains unknown. Besides satiation factors, water serves as reward for dehydrated animals and reinforces motivated ingestive behavior (Berridge, 2004; Epstein, 1982). Previous studies demonstrated that water intake activates the reward circuits in an internal-statedependent manner (Bayer and Glimcher, 2005; Fortin and Roitman, 2018;

Lin et al., 2014). Although reward and satiation are key factors that control ingestive

behaviors, how these signals interact in the brain is unknown. In this study, we use

optical recording of neural activity and dopamine (DA) release to examine the

representation of thirst satiation signals in the reward-related circuit.

LIQUID GULPING AND GUT OSMOLALITY SENSING TRANSMIT TEMPORALLY DISTINCT THIRST SATIATION SIGNALS TO THE BRAIN

Thirst neurons in the LT receive inhibitory signals from both oropharyngeal and

gastrointestinal areas associated with water intake (Augustine et al., 2018a; Zimmerman

et al., 2019). To characterize individual thirst satiation signals, we combined calcium

recording in vivo with intragastric (IG) infusion in awake-behaving animals. We first

transduced adeno-associated virus (AAV) encoding Cre-dependent GCaMP6s in neuronal

nitric oxide synthase (nNOS)-positive SFO neurons (SFO^{nNOS}) using nNOS-Cre

transgenic mice (Figure S1A). This procedure was followed by intragastric surgery to

implant a gastric cannula for fluid infusion (Ueno et al., 2012; Figures 1A and S1B). Oral

consumption of water rapidly quenched the activity of SFO^{nNOS} neurons (50 s; Figures

1B and 1C). These results indicate that oropharyngeal and gastrointestinal signals

transmit independent inhibitory inputs to the thirst circuit. We next examined the effect of

fluid tonicity on the inhibitory signals. Oral intake of water or isotonic saline suppressed

SFO^{nNOS} neural activity, whereas the inhibition by saline was transient. By contrast, IG

infusion of isotonic fluids exhibited no inhibitory effect (Figures 1D, 1E, and S1C–S1F).

Importantly, IG water infusion drastically suppressed SFO^{nNOS} neurons as well as

subsequent water consumption (Figures 1D–1F). Collectively, these data show that (1) gut osmolality changes induce persistent pre-absorptive thirst satiation and (2) oropharyngeal stimulation by drinking action is not required for osmolality-induced satiation signals.

GLP1R-POSITIVE SFO NEURONS MEDIATE THIRST SATIATION SIGNALS BY GUT OSMOLALITY CHANGE

We have recently shown that GLP1r-positive MnPO neurons (MnPO^{GLP1r}) mediate rapid inhibitory signals evoked by liquid gulping action regardless of osmolality (Augustine et al., 2018a). However, the neural substrates that encode osmolality-induced satiation have not been characterized. Because optogenetic activation of the SFO GABAergic population strongly suppressed water intake in thirsty animals (Oka et al., 2015), we suspected that these inhibitory neurons may be involved in osmolality-induced satiation signals. Histological analysis revealed that a majority of GABAergic SFO neurons expressed GLP1r (SFO^{GLP1r}; Figures 2A and S2A). Consistent with previous publication (Oka et al., 2015), SFO^{GLP1r} neurons were distinct from thirst-driving SFO^{nNOS} neurons, and optogenetic activation of ChR2-expressing SFO^{GLP1r} neurons drastically suppressed water intake in water-deprived animals (Figures 2B and S2B–S2D). Our electrophysiological experiments confirmed that SFO^{GLP1r} neurons send monosynaptic inhibitory inputs to SFO$^{GLP1r-negative}$ (presumably SFO^{nNOS}) neurons (Figures 2C and S2E), suggesting direct local inhibition within the SFO. We note that the application of a GLP1r agonist did not change acute firing rate (Figure S2F). We next tested whether SFO^{GLP1r} neurons are involved in osmolality-induced inhibition of thirst neurons using

fiber photometry. Similar to MnPO^{GLP1r} neurons (Augustine et al., 2018a), SFO^{GLP1r} neurons were strongly activated upon water ingestion (Figure 2D). However, compared to MnPO^{GLP1r} neurons, SFO^{GLP1r} neurons showed significantly slower calcium dynamics (Figure 2D). Indeed, the activation of SFO^{GLP1r} neurons was observed toward the end of licking episodes and lasted for several minutes. Because ingested water stimulates oropharyngeal and gastrointestinal areas in a sequential manner, our results suggest that MnPO^{GLP1r} neurons transmit oropharyngeal-induced satiation, and SFO^{GLP1r} neurons mediate satiation signals originated from gut osmolality sensing (Figure 2E). If this model is correct, we expect that SFO^{GLP1r} neurons should be selectively activated by hypo-osmotic stimuli in the gut. To directly test this, we recorded neural activity of SFO^{GLP1r} neurons upon fluid administration via the oral or IG route. These neurons were strongly activated by oral water intake, but not by silicone oil or isotonic saline (Figures 3A, 3B, and S3A–S3C). Similarly, ingestion of Ensure under hungry conditions did not activate this population (Figure 3B, right). Moreover, this activation did not require oropharyngeal stimulation because IG infusion of water induced similar activation of SFO^{GLP1r} neurons (Figures 3C and S3D). Together, these results demonstrate that SFO^{GLP1r} neurons represent gut osmolality changes, which in turn transmit satiation signals to SFO$^{nNOS-positive}$ thirst neurons through monosynaptic inhibition. We next examined the significance of SFO^{GLP1r} neurons in regulating water intake using an inhibitory opsin, stGtACR2 (Mahn et al., 2018). In the presence of blue light, neural firing was strongly inhibited (Figure S3E) and animals drank significantly more water compared to no-light conditions (Figure 3D). By contrast, saline intake was not affected

by photoinhibition. These results support our model that SFO^{GLP1r} neurons transmit osmolality signals to SFO^{nNOS} neurons.

THIRST SATIATION IS FUNCTIONALLY SEPARABLE FROM DRINKING-ASSOCIATED DOPAMINE RELEASE

For thirsty animals, water intake is both satiating and rewarding. According to drive-reduction theory, satiation should be the driving factor for drinking. It is, however, unknown whether thirst satiation directly serves as reward signals. Recent development of genetically encoded neuromodulator sensors allows us to examine real-time activity of the reward circuit during ingestive behaviors (Patriarchi et al., 2018; Sun et al., 2018). Given the neural basis of thirst satiation, we next employed a dopamine sensor, dLight (Patriarchi et al., 2018), to ask how the reward circuit responds to thirst satiation signals. We injected AAV-hSyndLight1.3 in the dorsal part of the nucleus accumbens medial shell (NAc) and implanted an optic fiber (400 mm diameter) for recording DA release as fluorescence changes (Figures 4A and S4A). In accordance with recent studies (Brischoux et al., 2009; Cohen et al., 2012; Patriarchi et al., 2018), DA release rapidly increased in the NAc upon a rewarding stimulus (Ensure intake) and decreased upon an aversive stimulus (footshock; Figure 4B). During spontaneous drinking, rapid and sustained DA release in the NAc was observed for both water and saline (Figures 4C, 4D, left, and S4B). In sharp contrast, IG infusion of water, saline, or air had no effect on DA release (Figures 4C, 4D, and S4B). We observed similar results from presynaptic activity of tyrosine hydroxylase (TH)-positive neurons of the ventral tegmental area (VTA) or DA release in the dorsal striatum (Figures S4C–S4E). These results demonstrate that

quenching thirst neurons (and thus, thirst drive reduction) is not sufficient to activate the reward circuit. We further examined whether stimulation of thirst satiation signals evokes DA release. To this end, we expressed an excitatory designer receptor exclusively activated by designer drugs (DREADD; hM3Dq) in SFO^{GLP1r}/MnPO^{GLP1r} neurons while infecting dLight1.3 in NAc neurons. This experimental setting allowed us to activate thirst satiation neurons chemogenetically while recording DA release in the same animals (Figure 4E). As a behavioral control, we confirmed that activation of hM3Dq-expressing SFO^{GLP1r}/MnPO^{GLP1r} neurons by clozapine-N-oxide (CNO) drastically inhibited water intake in water deprived animals (Figure 4F). In these animals, CNO injection had no effect on DA release (Figure 4G). Importantly, consistent with optical recording above, IG water infusion failed to reinforce the lever-press behavior in water-deprived animals (Figures 4H and S4F). Taken together, this study provides important functional implications for satiation and reward processing in the mammalian brain. First, thirst satiation signals mediated by MnPO^{GLP1r} and SFO^{GLP1r} neurons are functionally separable from DA release. Second, DA release is equally induced by water and saline drinking regardless of the homeostatic outcome.

DISCUSSION

Recent studies revealed genetically defined appetite circuits that regulate initiation of ingestive behaviors (Andermann and Lowell, 2017; Augustine et al., 2018b; Sternson and Eiselt, 2017). Conversely, the mechanisms underlying ingestive termination are not well understood. In this study, we demonstrated that osmolality sensing in the gut induces persistent inhibition of thirst neurons in the SFO. We further show that gut osmolality

change is mediated at least in part by a specific inhibitory population of the SFO: SFO^{GLP1r} neurons. We have shown that another inhibitory population, MnPO^{GLP1r}, transmits gulping-induced transient inhibition to thirst neurons. Thus, despite the lack of single-cell information in photometry recording, our results indicate that the LT contains two distinct thirst satiation pathways that are activated at distinct kinetics after the drinking onset. What is the functional significance of redundant thirst satiation signals? Interestingly, silencing SFO^{GLP1r} neurons increased hypo-osmotic fluid intake (Figures 3D and S3E), and silencing MnPO^{GLP1r} neurons augmented intake of non-hypo-osmotic liquid (Augustine et al., 2018a). A potential model is that the initial thirst satiation signals by MnPO^{GLP1r} neurons prevent animals from excessive fluid intake in general, and the slower satiation by SFO^{GLP1r} neurons ensures that animals have drunk hypo-osmotic fluids that are rehydrating (Booth, 1991; Figure 2E). How thirst satiation signals are transmitted from the periphery to the brain is currently unclear (Kim et al., 2018). The gut-to-brain signaling may require afferent neural pathways (Zimmerman et al., 2019) or hormonal signaling. Nutrient ingestion induces both satiation and satisfaction (Lee et al., 2019; Rossi and Stuber, 2018). It has been shown that postingestive nutrient signals after feeding stimulate DA release in the brain (Figure S4G; Han et al., 2018; Ren et al., 2010). But few studies to date have investigated the interaction of satiation and reward processing for thirst regulation. We have shown that DA release is exclusively induced by drinking behavior regardless of liquid type. Notably, suppression of thirst neurons by IG water infusion or stimulation of GLP1r-positive LT neurons did not induce robust DA release. These results explain the previous findings that non-oral water ingestion (e.g., IG or intravenous water infusion) is much less rewarding as compared to oral drinking

(McFarland, 1969; Nicolaıdis and Rowland, 1974). From the functional perspective of DA neurons, this study demonstrates that reinforcement learning for water intake requires peripheral signals associated with drinking, but not the reduction of appetite per se. Nevertheless, the valence of water is highly affected by internal state, suggesting that homeostatic signals modulate reward processing. Identifying neural substrates that integrate interoceptive and reward signals will provide insights into appetite and behavioral regulations in the brain.

EXPERIMENTAL MODEL AND METHOD DETAILS

Animals

All procedures followed animal care guidelines from NIH for the care and use of laboratory animals and California Institute of Technology Institutional Animal Care and Use Committee (1694–14). Animals used for experiments were at least 8 weeks of age. The following mice were purchased from the Jackson Laboratory: C57BL/6J, stock number 000664; Nos1-cre, stock number 017526; Ai75D, stock number 025106; Ai3, stock number 007903; Ai9, stock number 007909; GLP1r-cre and TH-Cre lines were provided by Dr. F. Gribble (Cambridge) and Dr. V. Gradinaru (Caltech), respectively. Mice were housed in temperature- and humiditycontrolled rooms with a 13 h: 11h light: dark cycle with ad llbitum access to food and water except for specific depletion experiments (water, food). Male and female mice were used for experiments, and randomly assigned before surgery. Animals that underwent gastric catheter implantation surgery were singly-housed.

Surgery

Mice were anaesthetized with a mixture of ketamine (1 mg/mL) and xylazine (10 mg/mL) in isotonic saline, intraperitoneally (ip) injected at 10 mL/g body weight. Ketoprofen was administered at 5 mL/g body weight subcutaneously. The animal was then placed in a stereotaxic apparatus (Narishige Apparatus) with a heating pad. Surgery was performed as previously described (Augustine et al., 2018a; Oka et al., 2015). In brief, the three-dimensional MRI coordinate system was used as a reference for the injection site coordinates. Viral constructs were injected using a microprocessor-controlled injection system (Nanoliter 2000, WPI) at 100 nL/min. The coordinates for SFO are AP: -4030, ML: 0, DV: -2550 (150-300 nL injection), MnPO are AP: -3100, ML: 0, DV: -4080 (100 nL injection) and -3800 (50 nL injection), dorsal part of the nucleus accumbens medial shell are AP: -2100, ML: +700, DV: -4000 (500 nL injection), dorsal striatum are AP: -2400, ML: +1800, DV: -4200 (500 nL injection), ventral tegmental area (VTA) are AP: -6000, ML: +1000, DV: -4400 (200 nL injection). For optogenetic experiments, implants were made with a 200 mm fiber bundle (FT200EMT, Thorlabs) glued to a ceramic ferrule (CF230, Thorlabs). For photometry, a 400 mm fiber bundle (FT400UMT, Thorlabs) and a ceramic ferrule (CF440, Thorlabs) were used. A fiber was implanted 300 mm above (for optogenetic experiments) or inside the SFO, the dorsal part of the nucleus accumbens medial shell or the dorsal striatum (for photometry). Virus expression and implant position was verified after data collection. For intragastric (IG) infusion, catheter construction and implantation closely followed as described previously (Ueno et al., 2012). IG catheters were custom made using silastic tubing (Dow

Corning, 508-002), tygon tubing (Instech, BTPE-25) and pinport (Instech, PNP3F25-50) with a dead volume of approximately 13 mL. IG surgery was performed after animals recovered from the initial optogenetic or photometry surgeries. After surgery, animals were placed in a clean cage placed on a heating pad overnight. Animals were given at least 7 days postsurgery on antibiotics and Ibuprofen with ad lib food and water to allow complete recovery. Behavioral and histological experiments were then performed.

Optogenetic manipulation

For ChR2 photostimulation, 473 nm laser pulses (20ms, 20Hz) were delivered via an optic cable (MFP-FC-ZF, Doric Lenses) using a pulse generator (SYS-A310, WPI). The laser intensity was maintained at 10 mW at the tip of the fiber. For photoinhibition experiments, 473 nm light was continuously turned on with 7 mW intensity at the fiber tip.

Chemogenetic manipulation

For acute activation experiments, CNO dissolved in PBS was injected at 1 mg/kg body weight.

Behavioral assays

For water-restriction experiments, mice were provided with 1 mL of water daily. For food-restriction experiments, mice were provided with 0.5 pellets per 20 g of body weight daily. All assays were performed in home cages, an operant chamber or a modified lickometer as described previously (Augustine et al., 2018a; Oka et al., 2015). In foot shock experiments (Figure 4B) animals were given a foot shock (0.3 mA) for 30 s.

Long-term access assays

After 24 h of water or food restriction, animals were acclimatized to the behavior chamber for 10-15 min. Animals were then given access to a bottle filled with water, isotonic saline, Ensure, or silicone oil for 2 min (Figures 1D, 1E, S1C, S1D, and S1F), or the entire session (other data). For Figure 3D, no light was illuminated for the first 90 s of access. In the case of IG infusion experiments (Figures 1, 3C, 4C, S1, S3D, and S4B–S4E), animals were infused with water, isotonic saline, or isotonic mannitol for 2 min (0.5 mL/min) via gastric catheter using an infusion syringe pump (NE-300, New Era Pump Systems Inc). For Figure S4G, 45% glucose, 20% intralipid, isotonic saline, or water was infused at 50 mL/min for 20 mins. For Figure 1F, after 15 min of acclimatization, animals were given oral or IG administration of water or isotonic saline at 0.5 mL/min for 2 min. 3 min after administration, water consumption was measured for 10 min by a lickometer. Animals without fluid administration before the lick measurement were treated as controls. For Figure 4F, 30 min after CNO/PBS (1 mg/kg) ip injection, water consumption was measured for 30 min by a lickometer after 24 h of water-restriction.

Brief access assays

Animals were subjected to water restriction, or food-deprivation (Figures 2B and S2D) for 24 h before behavioral experiments. In each 60 s trial, stimulation was started 10 s before water or Ensure presentation, and maintained until the end of the trial. The number of licks in a 5 s window following the first lick was analyzed. Animals were tested for six trials (3 each with light on/off) each, and the number of licks was averaged across trials.

Lever-pressing for water reward

The experimental method is adapted from a previous report (Gipson et al., 2013; McFarland, 1969). Mice were subjected to water deprivation for 24 h before each session. Sessions were done in an operant chamber equipped with two levers (active and inactive) and a lickometer (Med Associates). Animals were trained on FR1, followed by FR3 schedules to obtain water reward for 1 s from the lickometer (average 20 mL/sec). After training was completed, animals were tested under sated (control) and water-deprived conditions on FR3 schedule for 15 min. These test paradigms were followed by four extinction sessions for 15 min each. An empty water bottle was presented to animals during the extinction sessions. Animals were then subjected to FR3 reinstatement paradigms. As a reinforcer (reward), water was provided through the IG route (20 mL) via a gastric catheter by a peristaltic pump (Minipuls 3, Gilson), or oral access. We analyzed whether IG or oral water intake reinforce lever press behavior after three training sessions for 15 min each (Figures 4H and S4F).

Fiber photometry

For all photometry assays, animals were acclimatized for 5-15 min in the chamber before stimuli were presented. Bulk fluorescence signals were collected using fiber photometry as previously described (Augustine et al., 2018a; Patriarchi et al., 2018). Signals were then extracted and subjected to a low-pass filter at 1.8 and 25 Hz for GCaMP and dLight respectively. A linear function was used to scale up the 405-nm channel signal to the 490-nm channel signal to obtain the fitted 405-nm signal. The resultant $\Delta F/F$ was calculated as (raw 490 nm signal – fitted 405 nm signal)/ (fitted 405 nm signal). $\Delta F/F$ was then

time-binned by a factor of 2.5 times the sampling frequency and down-sampled to 1 Hz. Data were detrended to account for photo-bleaching. For all sessions, the mean fluorescence for 4-5 min before the first lick, intragastric infusion start or CNO/saline ip injection was calculated and subtracted from the entire session. The licks from the lickometer were simultaneously recorded. The area under the curve (AUC) was quantified by integrating the baseline-subtracted fluorescence signals for 1 (for dLight) or 5 (for GCaMP of SFO^{GLP1r}) min after the start of the bout. For SFO^{nNOS} neurons (Figures 1E, S1D, and S1E), AUCs were calculated for 50 s at two time points; after the start of administration (transient inhibition) and 80 s after the end of administration (persistent inhibition). Z-scores (Figure S4G) were calculated from the $\Delta F/F$ time-series signal (for 20 min after the start of intragastric infusion) by subtraction of mean and division by mean standard deviation of $\Delta F/F$ during saline intragastric infusion, calculated from all animals. This was to account for the signal variation for different stimuli infusion across animals.

dLight1.3b sensitivity experiments

For Figure S4A, AAV-cag-dLight1.3b was transfected in HEK293T cells. 48 h later, 293 cells were imaged continuously in HBSS while sequentially perfusing with 0.9% saline, 10 nM dopamine, HBSS washout, 10 nM dopamine and 5 nM DRD1 antagonist SCH 23390 as indicated.

Histology

Mice were anaesthetized with CO2 and then transcardially perfused with PBS followed by 4% PFA in PBS (pH 7.4). The brain was dissected and fixed in 4% PFA at 4C for overnight. Fixed brains were sectioned into 100 mm coronal sections using a vibratome (Leica, VT-1000 s). For immunohistochemistry (IHC), brain sections were incubated in a blocking buffer (10% Donkey serum, 0.2% Triton-X) for 1-2 h. Sections were then incubated overnight with the following primary antibodies: rabbit anti-GAD65+GAD67 (1:500, Abcam, ab183999), rabbit anti-NOS1 (1:500, Santa Cruz, sc-648), chicken anti-GFP (1:1000, Abcam, ab13970). Sections were washed three times with PBS, and then were incubated with secondary antibodies (1:500 dilutions, Jackson laboratory) in blocking buffer for 4 h. GAD65+GAD67 staining was performed without Triton-X.

Plasma osmolality measurements

After water deprivation for 24 h, trunk blood was collected in an EDTA coated tube, from wild-type mice before or 5 min after the water drinking onset. Plasma was then separated by centrifugation at 1500 g for 20 min. Plasma osmolality was measured using a vapor pressure osmometer (Vapro 5520).

Slice electrophysiology

Coronal sections containing SFO were obtained using a vibratome (VT-1000s, Leica) in ice-cold sucrose-aCSF (artificial cerebrospinal fluid) solution (in mM: Sucrose 213, KCl 2.5, NaH2PO4 1.2, NaHCO3 25, glucose 10, MgSO4 7, CaCl2 1, at pH 7.3), and then incubated in normal aCSF (in mM: NaCl 124, KCl 2.5, NaH2PO4 1.2, NaHCO3 24,

glucose 25, MgSO4 1, CaCl2 2, bubbled with 95% O2/5% CO2) at 34.5C for 30 min.

After that slices were held at room temperature until use. For patch-clamp recording, slices were perfused with normal aCSF on an upright microscope (Examiner.D1, Zeiss). Electrical signals were filtered at 3kHz with Axon MultiClamp 700B (Molecular Devices) and collected at 20 kHz with Axon Digidata 1550A (Molecular Devices). For current clamp recordings, intracellular solution containing (in mM) K-gluconate 145, NaCl 2, KCl 4, HEPES 10, EGTA 0.2, Mg-ATP 4, Na-GTP 0.3 (pH 7.25) was used, while for voltage clamp whole-cell recordings, intracellular solution contained (in mM) CsCl 145, NaCl 2, HEPES 10, EGTA 0.2, QX-314 bromide 5, Mg-ATP 4, Na-GTP 0.3 (pH 7.25). In some experiments (Figures S2E and S2F), cell-attached loose-patch recordings (seal resistance, 20-80 MΩ) were performed. For optogenetics experiments, light beam from an LED light source (X-Cite 120LED, Excelitas Technologies) was delivered through an optical filter (475/30). Light pulses (1-2 ms) were given 5 times at 1 Hz for 4 cycles in connectivity experiment (Figure 2C). To verify GABAergic connections, picrotoxin (100 μM) was applied through perfusion. Light was applied at 20 Hz for 5 s to show ChR2-induced neuronal firing in GLP1r+ cells (Figure S2C) and applied at 10 Hz for 20-30 s to verify the monosynaptic inhibition from GLP1r+ to GLP1r- cells (Figure S2E). To show inhibition by stGtACR2 (Figure S3E), light was continuously illuminated for 4.5 min to show the light-induced inhibition of GLP1r+ cells.

Quantification and statistical analysis

All statistical analyses were done using Prism (GraphPad). We either used a two-tailed paired/unpaired t test, one/two-way ANOVA depending on the experimental paradigm. $*p < 0.05$, $**p < 0.01$, $***p < 0.001$, $****p < 0.0001$. Data sheets with the analysis of statistical tests from Prism reporting estimates of variance within each group, comparison of variances across groups are available on reasonable request. Viral expression and implant placement was verified by histology before animals were included in the analysis. While recording calcium dynamics of SFO^{nNOS} neurons, animals with DF/F less than 10% by ip injection of 300 mL 2M NaCl were excluded from data analysis. These criteria were pre-established. No statistics to determine sample size, blinding, or randomization methods were used. Data are presented as mean ± sem unless otherwise mentioned.
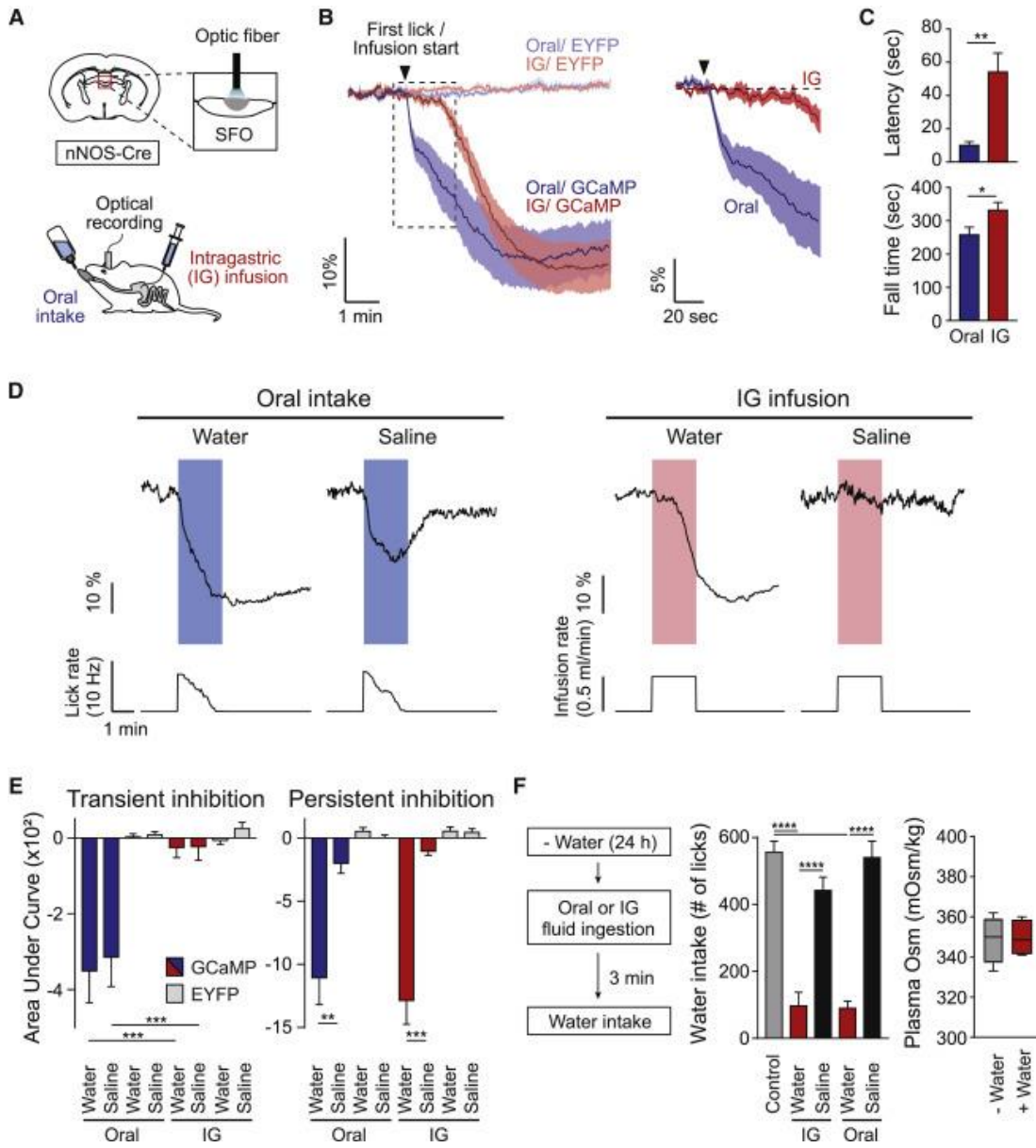
Figure 1

Figure 1. Thirst Circuits Receive Temporally Distinct Inhibitory Signals after Water Intake (A) A diagram of optical recording of GCaMP6s signals from SFO^{nNOS} neurons. Fluid was given either orally or via IG infusion. (B) Temporally distinct inhibition of SFO^{nNOS} neurons by ad lib oral intake or IG infusion of water (0.5 mL/min for 2 min; n = 8 mice for GCaMP6s; n = 4 and 6 mice for enhanced yellow fluorescent protein (EYFP) for oral and IG administration, respectively). (C) IG water infusion induced significantly slower onset of inhibition compared to oral water intake (latency). Fall time is defined as the time to maximum inhibition from first lick or infusion onset (n = 8 mice for GCaMP6s). (D) Representative traces of calcium dynamics during oral intake or IG infusion of water and saline (1 out of 8 mice). Lick and infusion rates are indicated below calcium traces. (E) Quantified responses of SFO^{nNOS} neurons. Signals were quantified during (transient) and after (persistent) liquid ingestion or infusion; n = 8 mice for GCaMP6s; n = 6 mice for EYFP). (F) Drinking-induced satiation after oral or IG water administration. Animals were given access to water after oral intake or IG infusion (0.5 mL/min) of fluid for 2 min. Water consumption was measured for 10 min (left, n = 11 mice for control [no pre-ingestion] and for pre-IG; n = 7 mice for pre-oral). Note that the systemic osmolality was unchanged after oral water intake (right, n = 4 mice). $*p < 0.05$, $**p < 0.01$, $***p < 0.001$, and $****p < 0.0001$ by two-tailed paired t test; two-way repeated-measures ANOVA (Bonferroni's multiple comparisons) or oneway ANOVA (Tukey's multiple comparisons). Data are presented as mean ± SEM. Boxplots show median, quartiles (boxes), and range (whiskers). See also Figure S1.
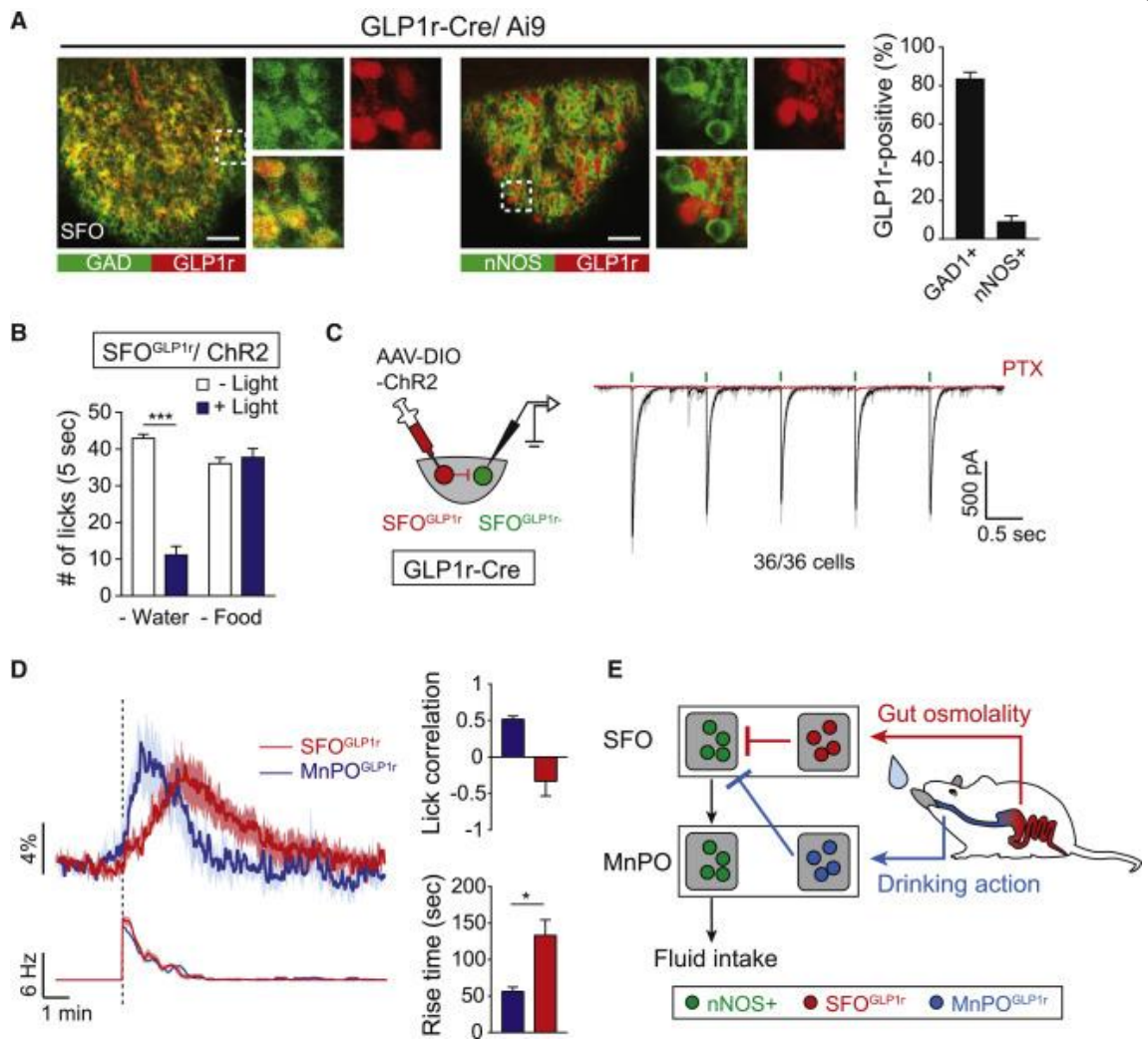
Figure 2

Figure 2. GLP1r-Positive SFO Neurons Monosynaptically Inhibit Thirst-Driving Neurons (A) GLP1r is specifically expressed in GABAergic neurons of the SFO. Immunohistological staining shows that a majority of GLP1r-positive neurons (labeled by Ai9) overlapped with glutamic acid decarboxylase (GAD; left panels). These neurons did not overlap with glutamatergic nNOS-positive neurons (middle panels). Quantification of the percentage of GLP1r-positive neurons that coexpressed GAD or nNOS is shown (n = 3 mice; representative images are from 1 out of 3 mice). (B) Optogenetic stimulation of SFO^{GLP1r} neurons selectively suppresses water intake, but not liquid food intake (n = 5 mice). (C) The SFO^{GLP1r} / $SFO^{non-GLP1r}$ monosynaptic connections. All GLP1r-negative neurons (36/36 cells) in the SFO received monosynaptic inhibitory inputs from SFO^{GLP1r} neurons. (D) Two inhibitory populations in the LT exhibit temporally distinct response to drinking behavior. Calcium dynamics of SFO^{GLP1r} and $MnPO^{GLP1r}$ neurons upon water drinking and lick rate (left) is shown. Quantification of calcium dynamics is shown. $MnPO^{GLP1r}$ neurons have significantly faster activation kinetics compared to SFO^{GLP1r} neurons (right). $MnPO^{GLP1r}$, but not SFO^{GLP1r}, neurons have a positive correlation with lick timing (n = 6 mice). Rise time is defined as the time to maximum excitation from first lick. For $MnPO^{GLP1r}$ neurons, we re-analyzed the data from the previous report (Augustine et al., 2018a). (E) A possible model of thirst-quenching signals. Liquid gulping signals are mediated by $MnPO^{GLP1r}$ neurons, which provide rapid and transient suppression of SFO^{nNOS} neurons. Subsequently, SFO^{GLP1r} neurons are activated by gastrointestinal hypo-osmotic stimuli to mediate slower inhibitory signals. *p < 0.05; ***p < 0.001 by two-tailed paired or unpaired (Welch's correction) t test. Data are presented as mean ± SEM. Scale bars, 50 mm. See also Figure S2.
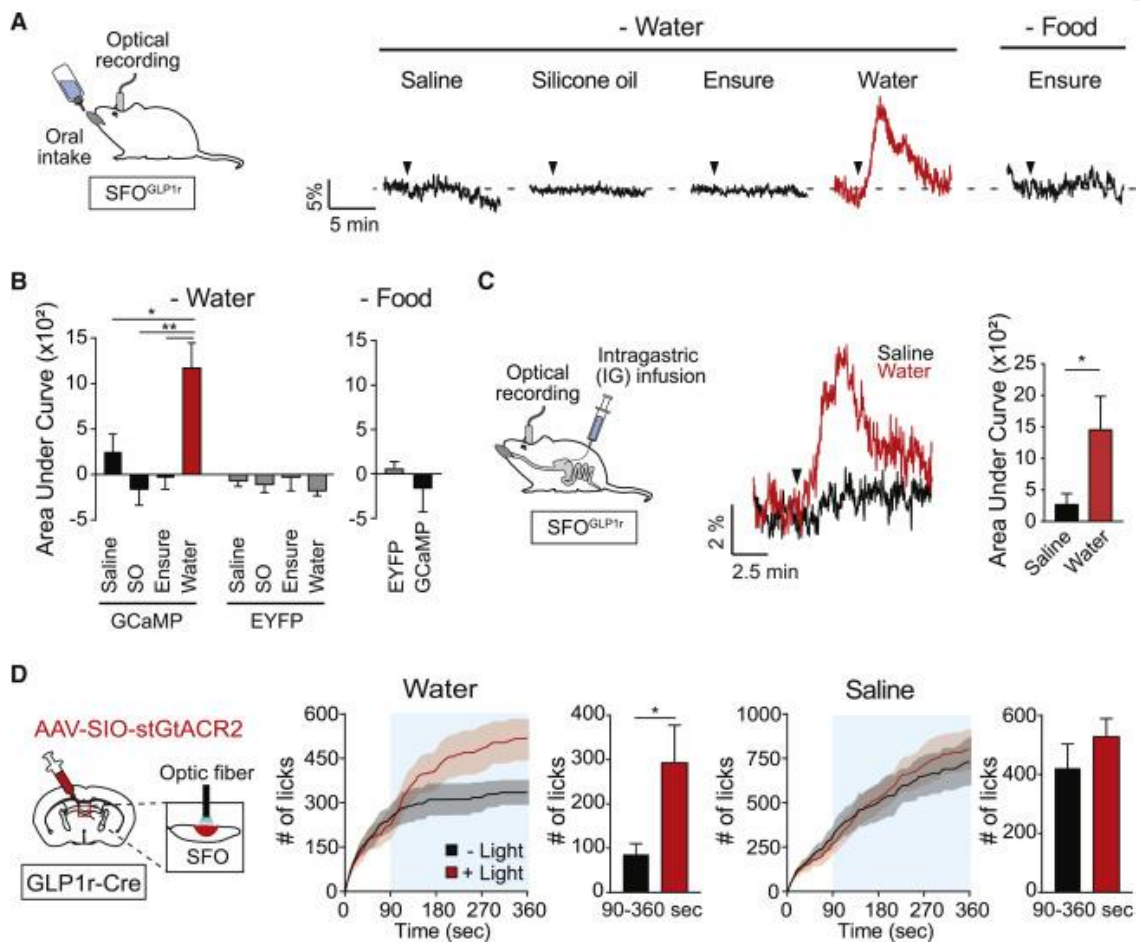
Figure 3

Figure 3. SFO^{GLP1r} Neurons Are Activated by Hypo-osmotic Stimuli in the Gut

(A) Representative traces showing calcium responses of SFO^{GLP1r} neurons upon ingestion of different fluids. SFO^{GLP1r} neurons were selectively activated by water, but not by other fluids. Black triangles indicate the onset of licking (1 out of 6 mice). (B) Quantification of responses of GCaMP6s and EYFP signals during 5 min after the first lick (n = 6 and 3 mice for GCaMP6s for water and food restriction, respectively, and n = 6 mice for EYFP). SO, silicone oil. (C) Responses of SFO^{GLP1r} neurons upon intragastric fluid infusion. A diagram of IG infusion and fiber photometry is shown (left panel). Representative traces are shown for IG water (red) or isotonic saline (black) infusion. A total of 1 mL (0.5 mL/min) of water or saline was infused. Black triangle indicates the onset of infusion (middle panel, traces are from 1 of 5 mice). Quantification of calcium responses to water or isotonic saline is shown (right panel, n = 5 mice). (D) Optogenetic inhibition of SFO^{GLP1r} neurons selectively increases water intake, but not isotonic saline intake. SFO neurons of GLP1r-Cre mice were infected with AAV-SIO-stGtACR2. Continuous illumination was performed from 90 to 360 s (blue shaded area; n = 5 mice). *p < 0.05 and **p < 0.01 by two-tailed paired t test or one-way repeated-measures ANOVA (Dunnett's multiple comparisons). Data are presented as mean ± SEM. See also Figure S3.
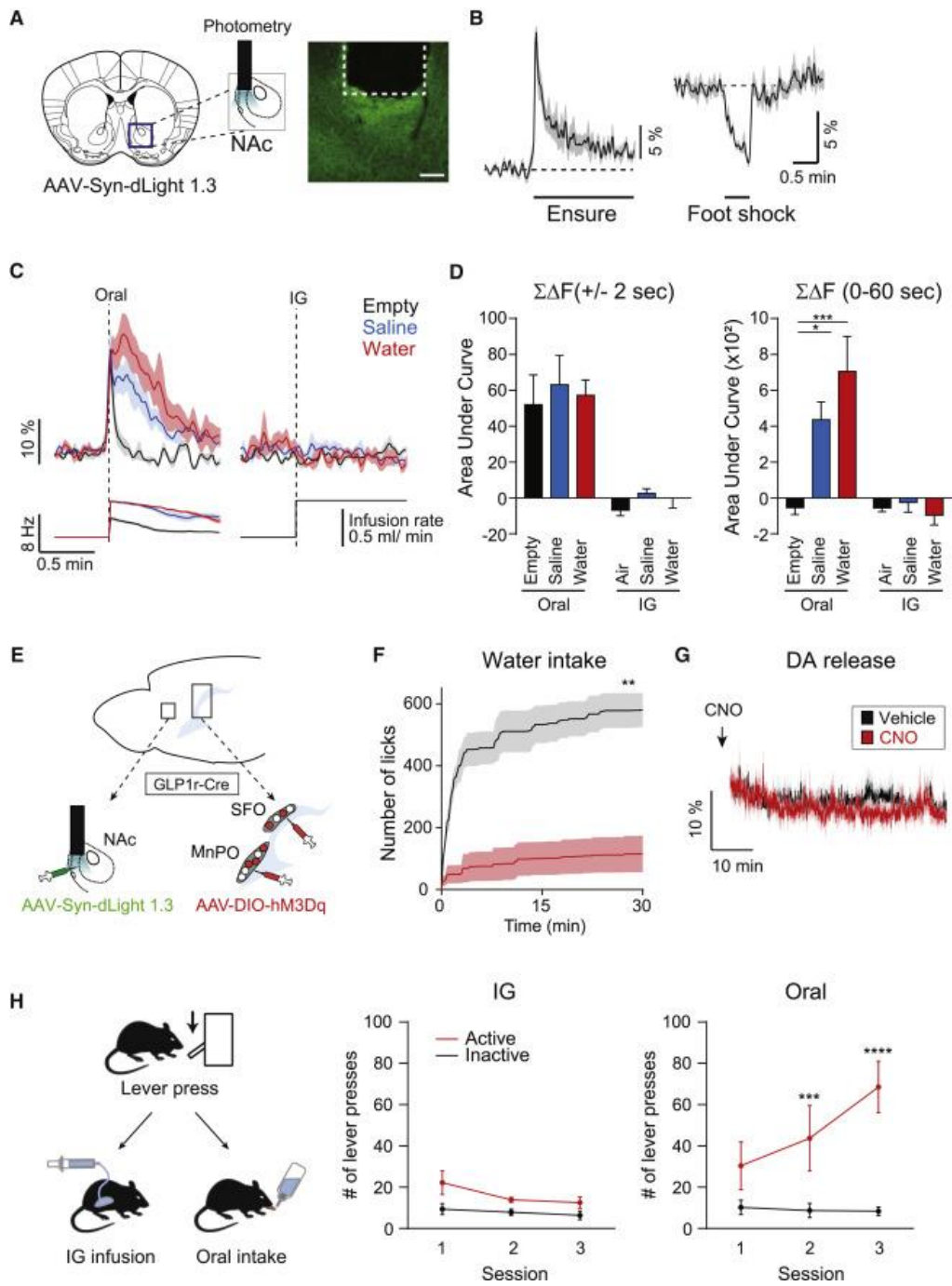
A Photometry
AAV-Syn-dLight 1.3
NAc

B Ensure   Foot shock
5 %
5 %
0.5 min

C Oral   IG
Empty
Saline
Water
10 %
8 Hz
Infusion rate
0.5 ml/ min
0.5 min

D ΣΔF(+/- 2 sec)   ΣΔF (0-60 sec)
Area Under Curve
Area Under Curve (x10²)
Empty Saline Water | Air Saline Water
Oral | IG

E GLP1r-Cre
SFO
MnPO
NAc
AAV-Syn-dLight 1.3
AAV-DIO-hM3Dq

F Water intake
Number of licks
Time (min)
**

G DA release
CNO
Vehicle
CNO
10 %
10 min

H Lever press
IG infusion   Oral intake
IG   Oral
Active
Inactive
# of lever presses
Session
***   ****

Figure 4

Figure 4. Activity of the Reward Circuits Is Separable from Thirst Satiation Signals (A) A diagram of optical recording of DA release by dLight1.3. A representative image of dLight expression is shown. (B) DA release is induced by appetitive (Ensure) stimulus and suppressed by aversive (footshock) stimulus (n = 7 mice). (C) dLight fluorescence changes are shown during oral ad lib intake and IG infusion (n = 7 mice). Spontaneous drinking induced robust DA release in the NAc compared to empty control regardless of liquid type (left). For empty control experiments, DA release was observed transiently prior to lick due to reward expectation. By contrast, IG infusion of fluid had no effect on DA release (right, n = 7 mice). (D) Quantified data of dLight responses during 4 s around the first lick (left) or 60 s (right) after the first lick or IG infusion (n = 7 mice). (E) A schematic for activating thirst satiation circuits in the LT by hM3Dq while measuring DA release in the NAc by dLight1.3. (F) Chemogenetic stimulation of SFO^{GLP1r} and MnPO^{GLP1r} neurons attenuates water intake under dehydrated conditions (n = 6 mice). (G) By contrast, the same stimulation paradigm did not induce DA release (n = 6 mice). (H) A diagram of operant task. Mice were initially trained to associate lever press and water reward. After extinction sessions (see Figure S4F), animals were subjected to reinstatement paradigms with either IG or oral water reward (left). In IG sessions, animals received water through a gastric catheter on an FR3 schedule (middle). In oral sessions, the same amount of water reward was provided through a spout (right, n = 6 mice). Only oral water intake efficiently reinforced lever press behavior. *p < 0.05, **p < 0.01, ***p < 0.001, and ****p < 0.0001 by two-tailed paired t test; one-way repeated-measures ANOVA (Dunnett's multiple comparisons) or twoway repeated-measures ANOVA (Bonferroni's multiple comparisons). Data are presented as mean ± SEM. Scale bar, 50 mm. See also Figure S4.
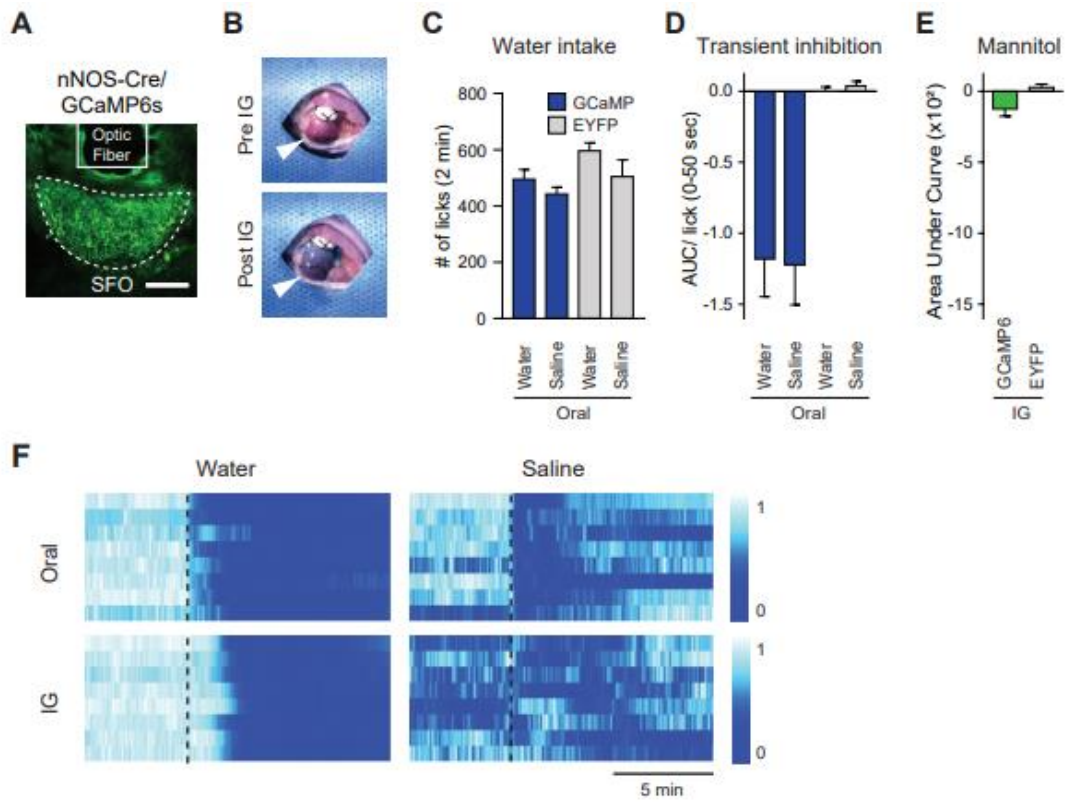
Figure S1

Figure S1. Characterization of SFOnNOS neurons after oral or IG administration of fluid, related to Figure 1. A, A representative image of GCaMP6s expression and optic fiber placement in the SFO. B, Confirmation of IG surgery. Blue dye was infused into the stomach to ensure successful IG surgery. Before (top) and after (bottom) IG infusion from the same animal are shown. C, The number of licks for Figures 1D and 1E. Liquid intake for 2 min was quantified while recording calcium dynamics of SFO^{nNOS} neurons. D, Activity change per lick for SFO^{nNOS} neurons (n = 8 mice for GCaMP6s, n = 6 mice for EYFP). All data were reanalyzed from Figure 1E. E, Hypoosmotic stimulus is required for persistent inhibition of SFO^{nNOS} neurons. IG infusion of isotonic mannitol (308 mM) had no effect on the activity of SFO^{nNOS} neurons (n = 8 mice for GCaMP6s, n = 4 mice for EYFP). F, Normalized fluorescence changes of SFO^{nNOS} neurons from individual mice during oral ad lib drinking or IG infusion. Data presented as mean ± s.e.m. Scale bar, 100 μm.
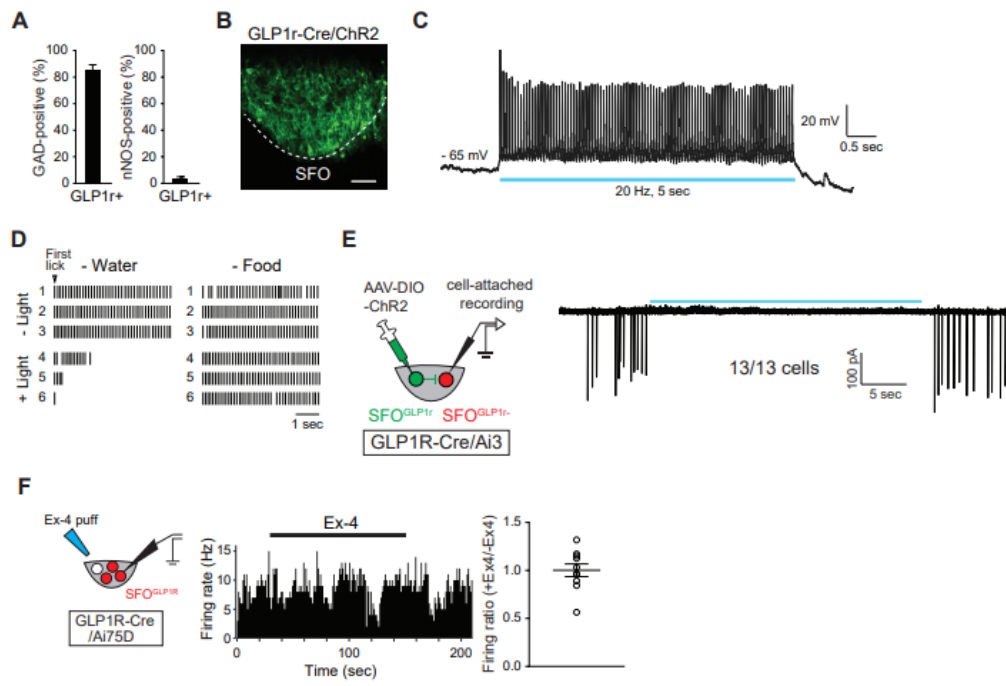
Figure S2

Figure S2. Gain-of-function of SFOGLP1r neurons, related to Figure 2. A, Cell count for Figure 2A. Quantification of the percentage of GAD- or nNOS-positive neurons that coexpressed GLP1r. B, A representative image of ChR2-expressing SFO^{GLP1r} neurons (1 out of 5 mice). C, Electrophysiological recording in fresh brain slices. Illumination of 475 nm light at 20 Hz activates SFOGLP1r neurons infected with AAV-DIO-ChR2-EYFP (8 out of 8 neurons from 2 mice). D, Photostimulation of SFO^{GLP1r} neurons inhibited water intake under water-restricted conditions. However, the same stimulation did not affect Ensure intake under food-restricted conditions. Each black bar indicates a lick event. Representative raster plots from 1 out of 5 mice are shown. E, The SFO^{GLP1r} → SFO$^{non\text{-}GLP1r}$ monosynaptic connection. Spontaneous firing of all GLP1r-negative neurons tested (13/13 cells) were suppressed by optogenetic activation of SFO^{GLP1r} neurons under cell-attached recording conditions. F, Application of an agonist for GLP1r did not induce firing. Electrophysiological recording in SFO^{GLP1r} neurons upon brief application of Exendin-4, a GLP1r-agonist (20 μM), did not affect the firing rate (10/10 cells). Data presented as mean ± s.e.m. Scale bar, 50 μm.
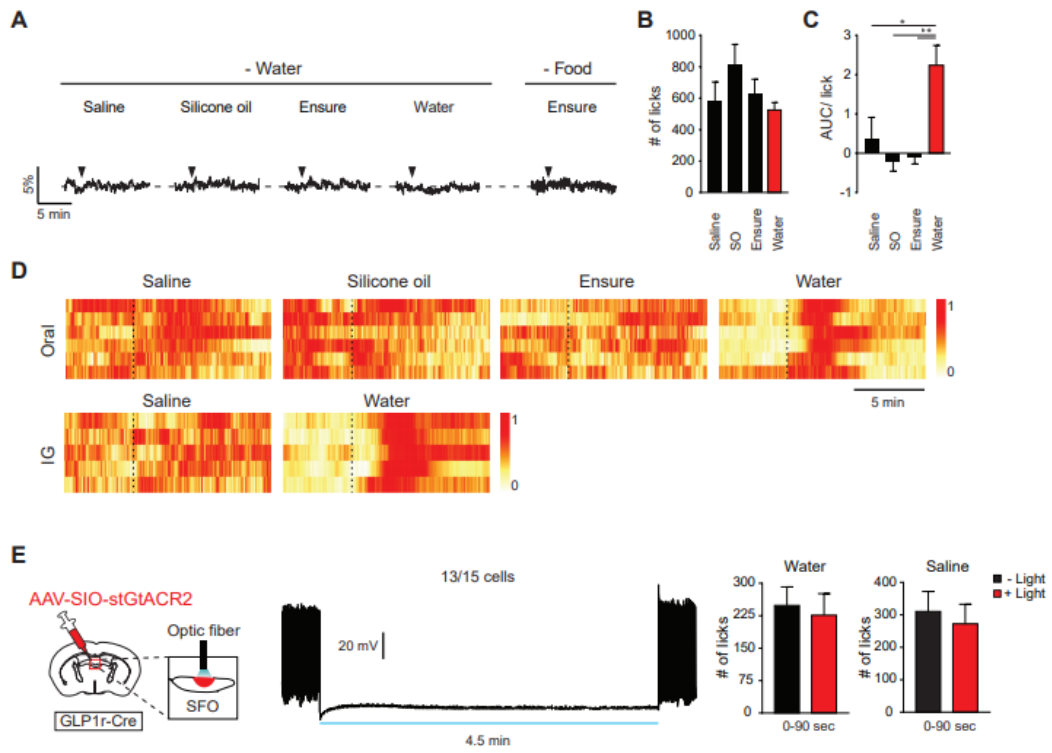
Figure S3

Figure S3. SFO^{GLP1r} neurons are activated by hypoosmotic stimuli in the gut, related to Figure 3. A, Control experiments for Figure 3A. Representative responses of SFO^{GLP1r} neurons infected with AAV-DIO-EYFP to different fluids. B, The amount of liquid intake for the first 5 min was quantified for Figure 3B. C, Fluorescence change per lick for SFO^{GLP1r} neurons (n = 6 mice for GCaMP6s). All data were reanalyzed from Figure 3B. D, Normalized fluorescence change of SFO^{GLP1r} neurons from individual mice during oral ad lib drinking or IG infusion. E, A diagram for optogenetic inhibition of SFO^{GLP1r} neurons (left). Electrophysiological recording in brain slices. Illumination of 475 nm light inhibits action potential firing in SFOGLP1r neurons infected with AAV-SIO-stGtACR2 (middle, 13 out of 15 neurons). Number of licks before optogenetic inhibition of SFOGLP1r neurons (right, 0-90 sec, Figure 3D). *P<0.05 and **P<0.01 by one-way repeated measures ANOVA (Dunnett's multiple comparisons). Data presented as mean ± s.e.m.

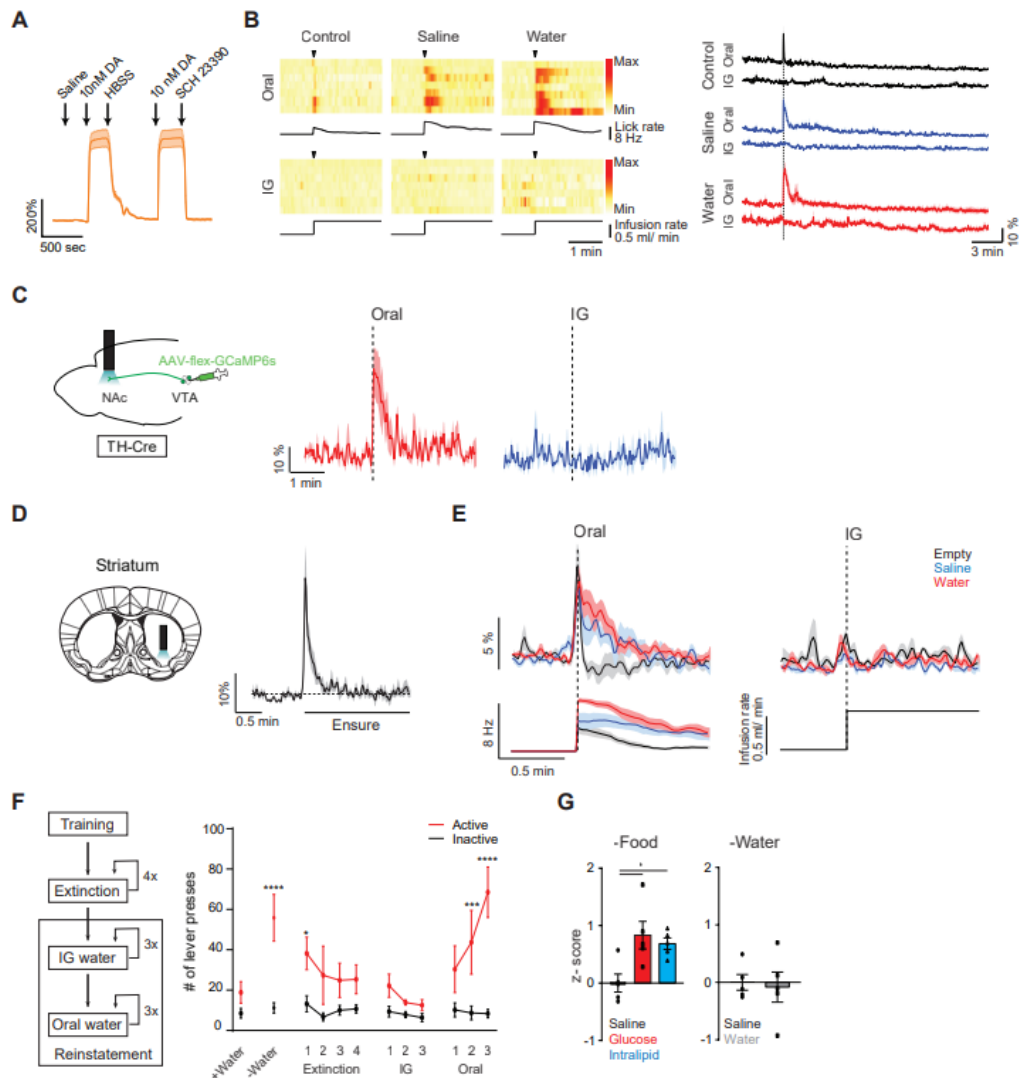Figure S4

Figure S4. dLight fluorescence change upon fluid administration, related to Figure 4. A, dLight is sensitive and photostable in response to low concentration of dopamine during continuous imaging (~30mins, n = 5 cells). dLight did not respond to saline but showed increased fluorescence to 10 nM dopamine before the signal was abolished by DRD1 specific antagonist SCH 23390 (right, 5nM). B, dLight fluorescence changes from individual mice are shown during oral ad lib intake and IG infusion (left, n = 7 mice). For oral access, animals were given an empty bottle (control), isotonic saline, or water. For IG infusion, air, isotonic saline, or water was infused at a speed of 0.5 mL/min for 2 min. Mean traces of dLight fluorescent signals during oral ad-lib drinking or IG infusion (right, n = 7 mice). C, A diagram of GCaMP6s recording from the projections of VTATH neurons in the NAc. Water was given either orally or via IG infusion. Spontaneous drinking induced robust activation in the NAc when the animal drank water (middle) compared to IG infusion of water (right, n = 3 mice). D, A diagram of optical recording of dLight fluorescence in the dorsal striatum. DA release is induced by rewarding stimulus (Ensure, n = 6 mice). E, Peristimulus time histogram of dLight responses to empty, saline, and water. Similar to the NAc, only spontaneous drinking induced DA release in the dorsal striatum (n = 6 mice). F, A training paradigm for operant conditioning. Mice underwent training and extinction sessions, followed by reinstatement sessions. In reinstatement sessions, animals were first subjected to IG sessions followed by oral sessions. The data for IG and oral reinstatement sessions are from Figure 4H (n=6 mice). G, Quantified data of dLight responses to intragastric infusion of nutrients or water (n = 5 mice). Isotonic saline, 45% glucose or 20% Intralipid was infused into food-deprived mice. Saline or water was infused into water-deprived mice. Post infusion DA release was observed in food-deprived animals (left), but not in water deprived animals (middle). *P<0.05, ***P<0.001 and ****P<0.0001 by one-way repeated measures ANOVA (Dunnett's multiple comparisons) or two-way repeated measures ANOVA (Bonferroni's multiple comparisons). Data presented as mean ± s.e.m.

References

1. ABBOTT, S. B., MACHADO, N. L., GEERLING, J. C. & SAPER, C. B. 2016. Reciprocal Control of Drinking Behavior by Median Preoptic Neurons in Mice. *J Neurosci,* 36**,** 8228-37.

2. ALLEN, W. E., DENARDO, L. A., CHEN, M. Z., LIU, C. D., LOH, K. M., FENNO, L. E., RAMAKRISHNAN, C., DEISSEROTH, K. & LUO, L. 2017. Thirst-associated preoptic neurons encode an aversive motivational drive. *Science,* 357**,** 1149-1155.

3. ANDERMANN, M. L. & LOWELL, B. B. 2017. Toward a Wiring Diagram Understanding of Appetite Control. *Neuron,* 95**,** 757-778.

4. AUGUSTINE, V., GOKCE, S. K., LEE, S., WANG, B., DAVIDSON, T. J., REIMANN, F., GRIBBLE, F., DEISSEROTH, K., LOIS, C. & OKA, Y. 2018a. Hierarchical neural architecture underlying thirst regulation. *Nature,* 555**,** 204-209.

5. AUGUSTINE, V., GOKCE, S. K. & OKA, Y. 2018b. Peripheral and Central Nutrient Sensing Underlying Appetite Regulation. *Trends Neurosci,* 41**,** 526-539.

6. BAYER, H. M. & GLIMCHER, P. W. 2005. Midbrain dopamine neurons encode a quantitative reward prediction error signal. *Neuron,* 47**,** 129-41.

7. BERRIDGE, K. C. 2004. Motivation concepts in behavioral neuroscience. *Physiol Behav,* 81**,** 179-209.

8. BETLEY, J. N., XU, S., CAO, Z. F., GONG, R., MAGNUS, C. J., YU, Y. & STERNSON, S. M. 2015. Neurons for hunger and thirst transmit a negative-valence teaching signal. *Nature,* 521**,** 180-5.

9. BOOTH, D. J. R. A. D. 1991. *Thirst: Physiological and Psychological Aspects*, Springer-Verlog.

10. BRISCHOUX, F., CHAKRABORTY, S., BRIERLEY, D. I. & UNGLESS, M. A. 2009. Phasic excitation of dopamine neurons in ventral VTA by noxious stimuli. *Proc Natl Acad Sci U S A,* 106**,** 4894-9.

11. COHEN, J. Y., HAESLER, S., VONG, L., LOWELL, B. B. & UCHIDA, N. 2012. Neuron-type-specific signals for reward and punishment in the ventral tegmental area. *Nature,* 482**,** 85-8.

12. EPSTEIN, A. N. 1982. The Physiology of Thirst. *In:* PFAFF, D. W. (ed.) *The Physiological Mechanisms of Motivation.* New York, NY: Springer New York.

13. FORTIN, S. M. & ROITMAN, M. F. 2018. Challenges to Body Fluid Homeostasis Differentially Recruit Phasic Dopamine Signaling in a Taste-Selective Manner. *J Neurosci,* 38**,** 6841-6853.

14. GIPSON, C. D., REISSNER, K. J., KUPCHIK, Y. M., SMITH, A. C., STANKEVICIUTE, N., HENSLEY-SIMON, M. E. & KALIVAS, P. W. 2013. Reinstatement of nicotine seeking is mediated by glutamatergic plasticity. *Proc Natl Acad Sci U S A,* 110**,** 9124-9.

15. GIZOWSKI, C. & BOURQUE, C. W. 2018. The neural basis of homeostatic and anticipatory thirst. *Nat Rev Nephrol,* 14**,** 11-25.

16. GIZOWSKI, C., ZAELZER, C. & BOURQUE, C. W. 2016. Clock-driven vasopressin neurotransmission mediates anticipatory thirst prior to sleep. *Nature,* 537**,** 685-8.

17. HAN, W., TELLEZ, L. A., PERKINS, M. H., PEREZ, I. O., QU, T., FERREIRA, J., FERREIRA, T. L., QUINN, D., LIU, Z. W., GAO, X. B., KAELBERER, M. M., BOHORQUEZ, D. V., SHAMMAH-LAGNADO, S. J., DE LARTIGUE, G. & DE ARAUJO, I. E. 2018. A Neural Circuit for Gut-Induced Reward. *Cell,* 175**,** 665-678 e23.

18. ICHIKI, T., AUGUSTINE, V. & OKA, Y. 2019. Neural populations for maintaining body fluid balance. *Curr Opin Neurobiol,* 57**,** 134-140.

19. KIM, K. S., SEELEY, R. J. & SANDOVAL, D. A. 2018. Signalling from the periphery to the brain that regulates energy homeostasis. *Nat Rev Neurosci,* 19**,** 185-196.

20. LEE, S., AUGUSTINE, V., ZHAO, Y., EBISU, H., HO, B., KONG, D. & OKA, Y. 2019. Chemosensory modulation of neural circuits for sodium appetite. *Nature,* 568**,** 93-97.

21. LEIB, D. E., ZIMMERMAN, C. A., POORMOGHADDAM, A., HUEY, E. L., AHN, J. S., LIN, Y. C., TAN, C. L., CHEN, Y. & KNIGHT, Z. A. 2017. The Forebrain Thirst Circuit Drives Drinking through Negative Reinforcement. *Neuron,* 96**,** 1272-1281 e4.

22. LIN, S., OWALD, D., CHANDRA, V., TALBOT, C., HUETTEROTH, W. & WADDELL, S. 2014. Neural correlates of water reward in thirsty Drosophila. *Nat Neurosci,* 17**,** 1536-42.

23. MAHN, M., GIBOR, L., PATIL, P., COHEN-KASHI MALINA, K., ORING, S., PRINTZ, Y., LEVY, R., LAMPL, I. & YIZHAR, O. 2018. High-efficiency optogenetic silencing with soma-targeted anion-conducting channelrhodopsins. *Nat Commun,* 9**,** 4125.

24. MANDELBLAT-CERF, Y., RAMESH, R. N., BURGESS, C. R., PATELLA, P., YANG, Z., LOWELL, B. B. & ANDERMANN, M. L. 2015. Arcuate hypothalamic AgRP and putative POMC neurons show opposite changes in spiking across multiple timescales. *Elife,* 4.

25. MATSUDA, T., HIYAMA, T. Y., NIIMURA, F., MATSUSAKA, T., FUKAMIZU, A., KOBAYASHI, K., KOBAYASHI, K. & NODA, M. 2017. Distinct neural mechanisms for the control of thirst and salt appetite in the subfornical organ. *Nat Neurosci,* 20**,** 230-241.

26. MCFARLAND, D. 1969. Separation of satiating and rewarding consequences of drinking. *Physiology & Behavior,* 4**,** 987-989.

27. MCKINLEY, M. J. & JOHNSON, A. K. 2004. The physiological regulation of thirst and fluid intake. *News Physiol Sci,* 19**,** 1-6.

28. NATION, H. L., NICOLEAU, M., KINSMAN, B. J., BROWNING, K. N. & STOCKER, S. D. 2016. DREADD-induced Activation of Subfornical Organ Neurons Stimulates Thirst and Salt Appetite. *J Neurophysiol***,** jn 00149 2016.

29. NICOLAIDIS, S. & ROWLAND, N. 1974. Long-term self-intravenous "drinking" in the rat. *J Comp Physiol Psychol,* 87**,** 1-15.

30. OKA, Y., YE, M. & ZUKER, C. S. 2015. Thirst driving and suppressing signals encoded by distinct neural populations in the brain. *Nature,* 520**,** 349-52.

31. PATRIARCHI, T., CHO, J. R., MERTEN, K., HOWE, M. W., MARLEY, A., XIONG, W. H., FOLK, R. W., BROUSSARD, G. J., LIANG, R., JANG, M. J., ZHONG, H., DOMBECK, D., VON ZASTROW, M., NIMMERJAHN, A., GRADINARU, V., WILLIAMS, J. T. & TIAN, L. 2018. Ultrafast neuronal imaging of dopamine dynamics with designed genetically encoded sensors. *Science,* 360.

32. REN, X., FERREIRA, J. G., ZHOU, L., SHAMMAH-LAGNADO, S. J., YECKEL, C. W. & DE ARAUJO, I. E. 2010. Nutrient selection in the absence of taste receptor signaling. *J Neurosci,* 30**,** 8012-23.

33. ROSSI, M. A. & STUBER, G. D. 2018. Overlapping Brain Circuits for Homeostatic and Hedonic Feeding. *Cell Metab,* 27**,** 42-56.

34. STERNSON, S. M. & EISELT, A. K. 2017. Three Pillars for the Neural Control of Appetite. *Annu Rev Physiol,* 79**,** 401-423.

35. SUN, F., ZENG, J., JING, M., ZHOU, J., FENG, J., OWEN, S. F., LUO, Y., LI, F., WANG, H., YAMAGUCHI, T., YONG, Z., GAO, Y., PENG, W., WANG, L., ZHANG, S., DU, J., LIN, D., XU, M., KREITZER, A. C., CUI, G. & LI, Y. 2018. A Genetically Encoded Fluorescent Sensor Enables Rapid and Specific Detection of Dopamine in Flies, Fish, and Mice. *Cell,* 174**,** 481-496 e19.

36. THRASHER, T. N., NISTAL-HERRERA, J. F., KEIL, L. C. & RAMSAY, D. J. 1981. Satiety and inhibition of vasopressin secretion after drinking in dehydrated dogs. *Am J Physiol,* 240**,** E394-401.

37. UENO, A., LAZARO, R., WANG, P. Y., HIGASHIYAMA, R., MACHIDA, K. & TSUKAMOTO, H. 2012. Mouse intragastric infusion (iG) model. *Nat Protoc,* 7**,** 771-81.

38. ZIMMERMAN, C. A., HUEY, E. L., AHN, J. S., BEUTLER, L. R., TAN, C. L., KOSAR, S., BAI, L., CHEN, Y., CORPUZ, T. V., MADISEN, L., ZENG, H. & KNIGHT, Z. A. 2019. A gut-to-brain signal of fluid osmolarity controls thirst satiation. *Nature,* 568**,** 98-102.

39. ZIMMERMAN, C. A., LIN, Y. C., LEIB, D. E., GUO, L., HUEY, E. L., DALY, G. E., CHEN, Y. & KNIGHT, Z. A. 2016. Thirst neurons anticipate the homeostatic consequences of eating and drinking. *Nature,* 537**,** 680-684.